8-27-2009

Control for an optically powered firing set using miniature photovoltaic arrays

Todd Plichta

Todd E. Plichta
Candidate

Electrical Engineering
Department

This thesis is approved, and it is acceptable in quality and form for publication on microfilm:

Approved by the Thesis Committee:

Chaouki T. Abdallah, Ph.D , Chairperson

Ramiro Jordan, Ph.D

Josh Schare, Ph.D

Accepted:

Dean, Graduate School

Date

CONTROL FOR AN OPTICALLY POWERED FIRING SET USING MINIATURE PHOTOVOLTAIC ARRAYS

BY

TODD EDWARD PLICHTA

BACHELOR OF SCIENCE IN ELECTRONICS ENGINEERING TECHNOLOGY 2002

THESIS

Submitted in Partial Fulfillment of the
Requirements for the Degree of

Master of Science
Electrical Engineering

The University of New Mexico
Albuquerque, New Mexico

May, 2009

DEDICATION

I dedicate this thesis to my family.

ACKNOWLEDGMENTS

I would like to acknowledge my UNM advisor Chaouki Abdallah and my Sandia advisor Josh Schare. They have both encouraged and supported me in the development of this thesis. Without their support, their suggestions in chapter content, and overall guidance, I could not have completed this thesis.

I am also grateful for the additional help that my Sandia colleagues have provided. Greg Lyons was instrumental in providing the thesis topic and is much appreciated. Jason Shelton was willing to help out in any way possible throughout the entire process and motivated me to continue on. His support is greatly appreciated. Kent Childs provided additional photocells when my only unit was damaged during characterization. Jeff Humphries also provided extra LCC packages and additional diode lasers. Dorothy Meister provided characterization data on the reflectivity of a component. Their help was instrumental in allowing me to collect all the data. Susan Esfahani supported and kept me on track throughout my thesis work and Jim Wilder provided me with the opportunity and support to work on this topic. Their assistance is also greatly appreciated.

I am also grateful to my editor and wife, Patricia Plichta. She has been understanding and supportive throughout this entire process. Without her love and guidance, this thesis would not have been complete.

This work was done in support of ongoing programs at Sandia National Laboratories.

Sandia is a multiprogram laboratory operated by Sandia Corporation, a Lockheed Martin Company, for the United States Department of Energy's National Nuclear Security Administration under Contract DE-AC04-94AL85000

CONTROL FOR AN OPTICALLY POWERED FIRING SET USING MINIATURE PHOTOVOLTAIC ARRAYS

BY

TODD EDWARD PLICHTA

THESIS

Submitted in Partial Fulfillment of the
Requirements for the Degree of

Master of Science
Electrical Engineering

The University of New Mexico
Albuquerque, New Mexico

May, 2009

CONTROL FOR AN OPTICALLY POWERED FIRING SET USING MINIATURE PHOTOVOLTAIC ARRAYS

by: Todd Edward Plichta

B.S., Electronics Engineering, DeVry Institute of Technology, 2002

M.S., Electrical Engineering, University of New Mexico, 2009

ABSTRACT

The optically powered firing set looks to revolutionize the design of future electrical firing sets. Optically powered devices have many features that make them attractive, such as immunity to noise problems from Electromagnetic Interference (EMI) and Electromagnetic Radiation (EMR). Also, optically powered devices provide additional safety to prevent unintended usage and are small in volume in comparison to their electrical equivalent. These advancements have led to the design of a prototype firing set developed at Sandia National Laboratories. The main components are comprised of a miniature photovoltaic array (MPA) that transforms light energy to electrical energy and a capacitive discharge unit (CDU) used to store and deliver the transformed electrical energy to a detonator. In order for this system to be further optimized for implementation into an actual firing set, the output voltage state needs to be controlled and the temperature of the MPA and illuminating source minimized. This thesis reports on the development of an optical firing set model that represents the electrical, optical, and thermal characteristics of the system. A closed loop feedback control system with a PI controller is then developed to control the output voltage state as well as minimizing the MPA and illuminating source temperature.

TABLE OF CONTENTS

LIST OF FIGURES

LIST OF TABLES

1. INTRODUCTION

1.1 Objective of Work

The objective of work is to develop a complete model of an optical powered firing set composed of a diode laser, Miniature Photovoltaic Array (MPA), current generator, and capacitive discharge unit (CDU). Each device will have an electrical model that is based on theoretical equations and experimental data. The diode laser and MPA will also include a thermal model based on the heat rate equation for each device. The model will be simulated in Simulink and verified to experimental data. The complete model will provide capability that will allow a designer to adjust design parameters and investigate their input. A control system will then be implemented to control the output voltage state and minimize the temperature states of the diode laser and MPA.

1.2 Background and Motivation

Sandia National Laboratories has developed an optically powered 1500 V firing set in a prototype configuration with the use of MPA's. An MPA is a silicon device that generates current when illuminated by a light source. It is constructed of an array of photocells that are connected together in series to provide high voltage output when connected to a high impedance load. The MPA is intended to charge capacitors to high voltages when illumined by a laser. This has led to the desire to design a compact optically powered firing set that could be used to replace the traditional transformer based firing set. Optically powered systems have many features that make them an attractive power conversion system for CDU's. Unlike electrical signals, optical signals are

immune to many noise problems such as Electromagnetic Interference (EMI) and Electromagnetic Radiation (EMR). Optically powered systems are also electrically isolated from the power source. This allows the currents generated from the power source to be separate from the CDU preventing ground loops and minimizing the common-mode (CM) current. CM current is a component of EMR energy and is the major cause of EMR emissions which cause EMI. Optical isolation can also serve to enhance the overall safety of the CDU since it prevents accidental use of the system. The MPA's high voltage output is generated without the use of DC-DC converters which translates to a possible reduction of volume. Specifically, a 5mm MPA is currently used which can generate about 1600 V when connected to a CDU.

Some disadvantages of the design include the longer charge times needed since the devices only generate a maximum of about 70 uA of short circuit current when illuminated with 3 W of optical power for the current design. For example, the optically powered firing set configuration of a 51.5 nF capacitor and 70 M ohm parallel resistor takes about 1.5 seconds to reach 1500 V. These devices also require an illumination and power source which add additional volume to the system. Mechanical disadvantages include keeping the illumination source and MPA in optical alignment which may be difficult to attain in certain environments. An MPA powered firing set offers some important positive features as well as some negative tradeoffs that will entirely depend on final requirements and application.

The current prototype optically powered firing set is a generic open-loop system. The system cannot compensate for any disturbances that may add to the controller's driving signal. In other words, the output is simply commanded by the input. This limitation affects the usefulness of the device since the output is dependant on the input signal and plant characteristics. The MPA is also operating in a constant "on" mode even when the high voltage capacitor is fully charged and little current is needed. This inefficiency is exploited when the temperature of the MPA device increases to a point where the output voltage begins to linearly decrease with temperature. The high voltage output also cannot be preset. The following figure illustrates the block diagram of the prototype optically powered firing set.

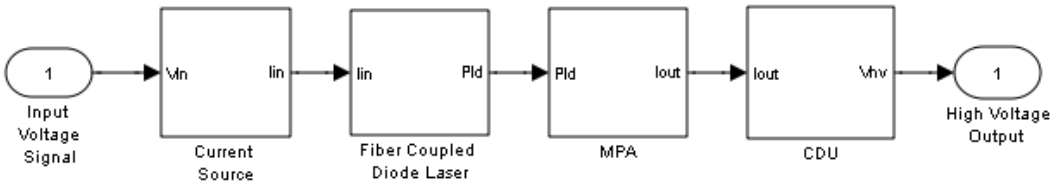

Figure 1: Block diagram of the prototype optical powered firing set.

Figure 1 shows a voltage signal being applied to the current source which provides an output current. This current drives the diode laser to produce light. The light illuminates the MPA and a current is generated. The output current is then fed to the CDU to charge a high voltage capacitor. Table 1 shows the subsystem breakdown with input and output signals for the optically powered firing set. Any disturbance to these signals will affect the output; therefore a closed-loop (feedback control) system needs to be implemented.

Subsystem	Input	Output
Diode Laser Driver (Current Source) LDX-3565	V_{in}: drive voltage (V)	I_{in}: current to diode laser (A)
3W Diode Laser	I_{in}: current from diode laser driver (A)	P_{ld}: illumination output (W)
MPA	P_{ld}: illumination output from diode laser (W)	I_{out}: output current from MPA when illuminated (A)
CDU	I_{out}: current from MPA (A)	V_{hv}: Output voltage across capacitor

Table 1: Subsystem Input/Output breakdown for the optically powered firing set.

1.3 Problem Statement and Control System Requirements

This thesis continues the design of the optical powered firing set that was previously reported in [9, 16] and seeks to add a controlling feature to the firing set. Specifically, this thesis will develop a control system that is designed to 1) control the output high voltage state, 2) minimize the temperature of the MPA, and 3) minimize the temperature of the 3 W fiber coupled diode laser. Electrical, optical, and thermal models will be developed so simulations can be compared to experimental data. The models will be validated with experimental data and a control solution will be presented.

The high voltage output of the optical powered firing set must be controlled to provide a consistent level regardless of the electrical and thermal disturbances of each firing set. The ability to adjust the output voltage is a desirable feature. Physical size can be controlled by reducing the heating of the optical components since cooling techniques

usually require additional volume. Thermal heating of the MPA is an area of concern since current and voltage output drops off at higher temperatures.

The main goal of this work is to develop a feedback control system for the optically powered firing set. This system will control the voltage level and the laser diode output state. The general requirements for the control problem include the following:

1. The system shall regulate the output voltage on a 50 nF capacitor to a predetermined level of 1500 V with 3% regulation ripple (1525 V– 1475 V) and a rise time of less then 5 seconds.
2. The system shall have the ability to adjust the output voltage level.
3. The system shall regulate for a minimum of 5 seconds and a maximum of 30 seconds.
4. The system shall minimize thermal heating of the MPA during regulation.
5. The system shall minimize thermal heating of the 3 W fiber coupled laser diode during regulation.
6. The number of electrical and mechanical components shall be minimized.

2. FIRING SET DESIGN

In general, firing sets are systems that are developed to deliver high-power signals to a detonator. As seen in Figure 2, a firing set typically receives its input power from an external power source and transforms it to the desired output that is required by the detonator. A trigger signal is usually used to initiate the high power output signal. Unique input and various output signals may exist depending on the design and requirements.

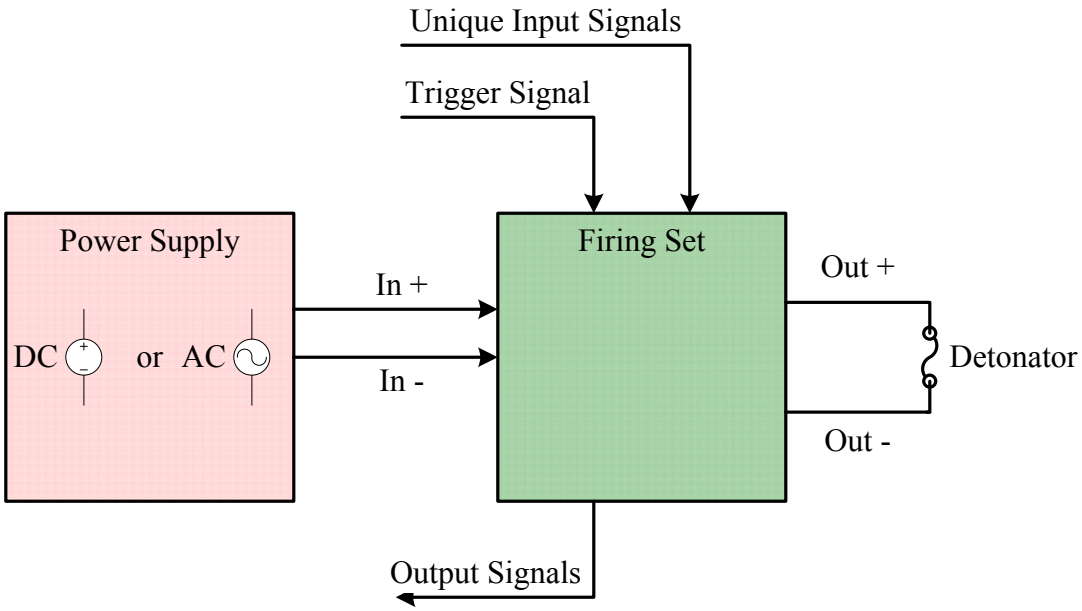

Figure 2: Block diagram of a general firing set.

Firing sets can be broken down into three main categories: 1) electrical firing sets, 2) explosive firing sets, and 3) optical firing sets. There are many different designs/technologies for each category and the primary focus of this work is on electrical/optical firing sets. More specifically, the CDU design will be examined.

2.1 Electrical Firing Sets – CDU Design

A CDU consists of a capacitor (C_{hv}), resistor (R), and switch. High voltage to a capacitor is used because it can efficiently generate the large amounts of current required by a detonator and they can generally be multiuse devices. All of the components must be able to handle the high stress caused by large voltages. Figure 3 shows a schematic representation of an electrical firing set with a CDU.

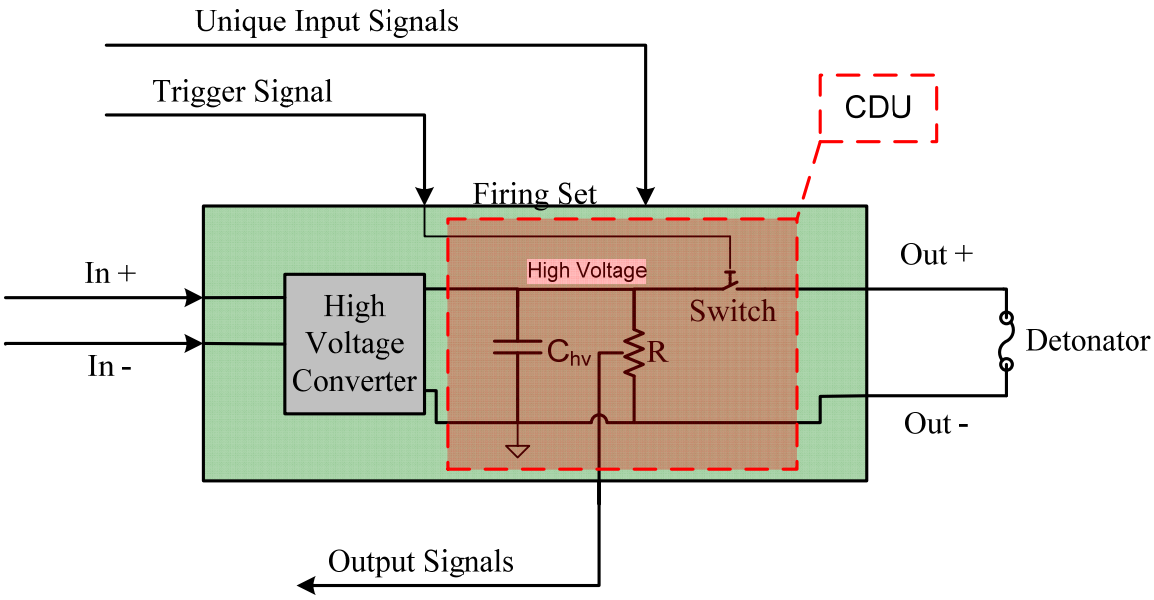

Figure 3: Electrical firing set with CDU components highlighted in the red shaded box.

The high voltage converter's primary function is to generate high voltage from input power. High voltage output can range from hundreds to thousands of volts. Various forms of input power that may be used include thermal batteries, battery packs, or utility power. The primary emphasis is on direct current (DC) power sources that are usually between 10 volts to 50 volts. There are many different circuit topologies of DC-to-DC converter design and usually the requirements of the design will narrow the search. Two common DC-to-DC designs are the push-pull and flyback converters. In use, these topologies require many components such as transformers, transistors, op-amps, and

other passive components that add to the overall volume of the firing set. The generated high voltage is then applied to the capacitor. The capacitor is used to store the energy from the power source and provide the large current discharge to the detonator. The capacitors are typically a few microfarads to tens and hundreds of nanofarads in value. These capacitors are specifically designed to handle high voltage/high current pulses and are usually the largest component of the firing set. The resistor functions to serve as a safety device to allow the capacitor's charge to bleed off when the CDU is charged but not used and for feedback monitors, if required. The resistors are typically a few megaohms depending on the desired bleed down and charge time. Once the capacitor is charged to the desired voltage a switch is used to transfer the built up charge directly to the detonator as efficiently as possible. The switch is designed to handle thousands of amps as well as to hold off high voltage.

The desire of future firing set architecture is to minimize the weight and volume of the system as well as increase the overall safety from unintended usage. The largest component, the capacitor, has offered volume savings when ceramic materials have been implemented. The next largest components include the transformer and control circuitry that is used in the high voltage converter design. Reductions in size and volume of the control circuitry have been modest but the size of the transformer is dependant on the circuit topology. Figure 4 shows the relative sizes of these components. The ability to decrease volume and weight of the high voltage converter and increasing the safety is the motivation for the development of the optically powered firing set.

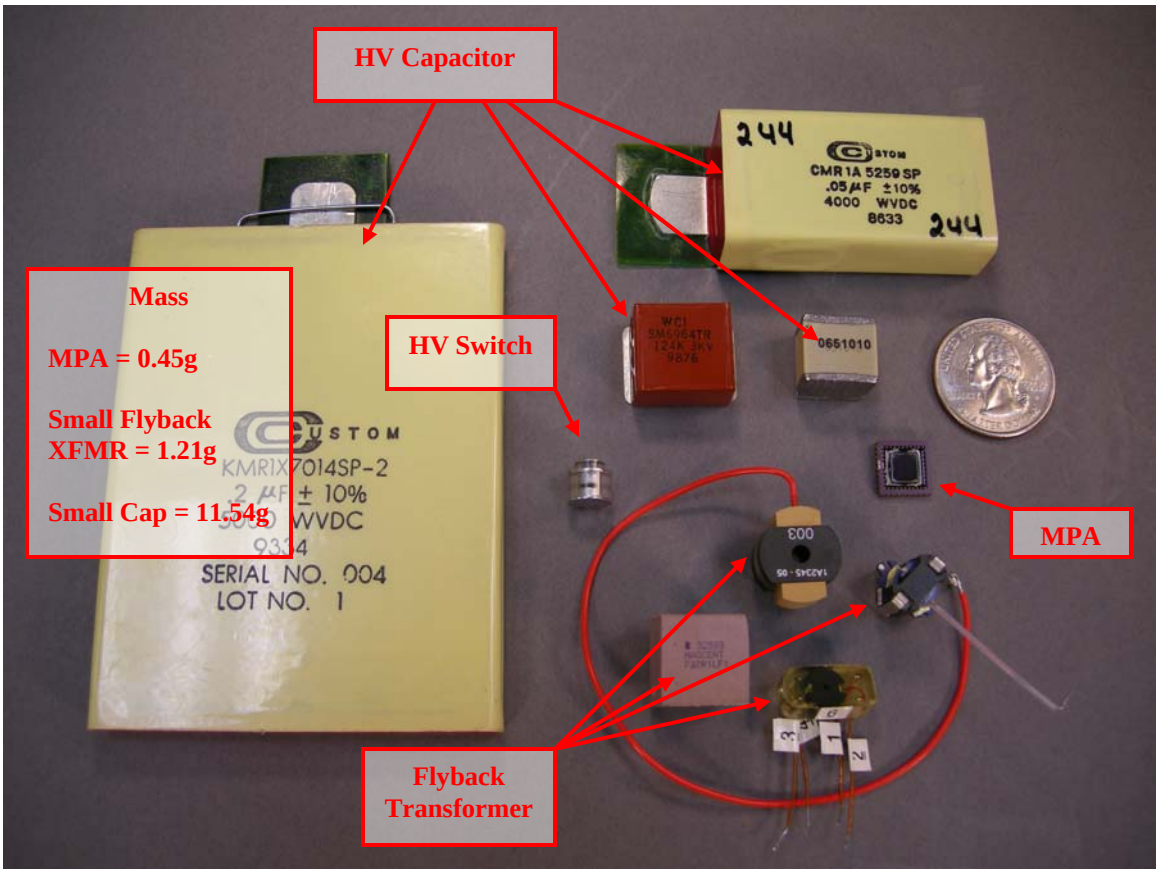

Figure 4: Comparison of component sizes that make up a typical electrical firing set. Note the difference in size of the MPA with respect to the flyback transformers.

2.2 Optically Powered Firing Sets

In the optically powered firing set, the high voltage converter is replaced by the MPA and the input power is replaced by an optical fiber as seen in Figure 5. The MPA functions to serve as the voltage converter by generating current from the light energy provided by the optical fiber. Since the device is a collection of series connected photovoltaic cells, high voltage output can be realized. The rest of the circuit operates identically to the electrical firing set.

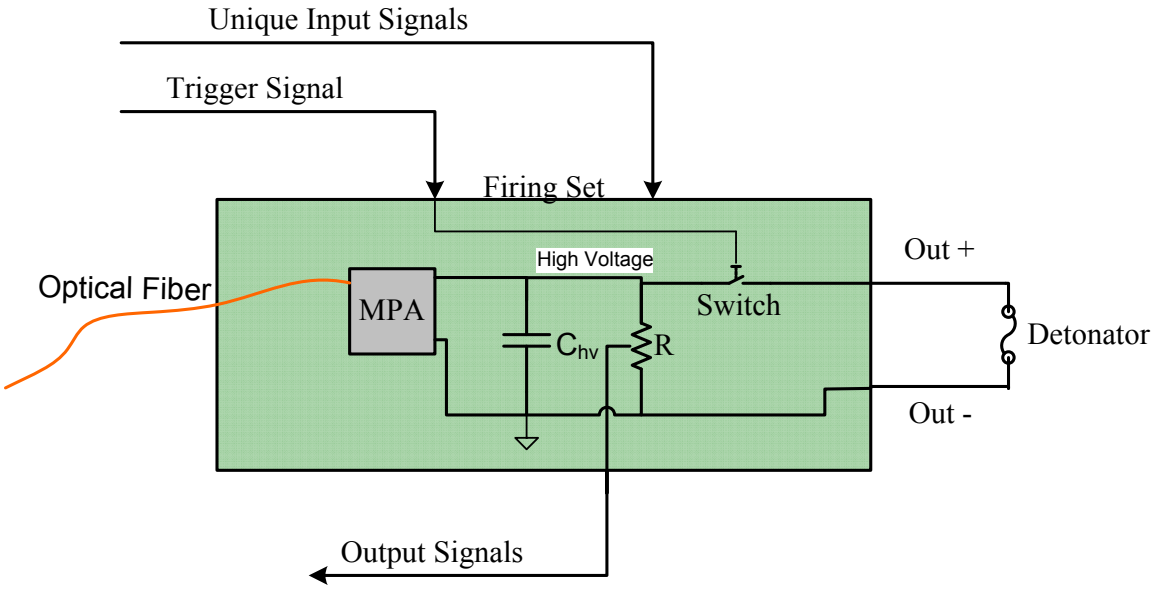

Figure 5: Schematic of optically powered firing set.

The uniqueness of this design is twofold: first the volume and weight of the MPA is quite a bit less than the electrical equivalent high voltage converter as shown in Figure 4, secondly the usage of the optical power source permits electrical isolation from external systems. Moreover, adding optical isolators to the input and output signals of the firing set will completely electrically isolate the firing set except for the connection to the detonator. The removal of all conductive electrical wires to the firing set will greatly enhance the overall safety of the device from unintended usage.

The prototype configuration of the optically powered firing set also includes the diode laser and current source as seen in Figure 6. Figure 6 shows all of the component parts in a breadboard configuration as tested.

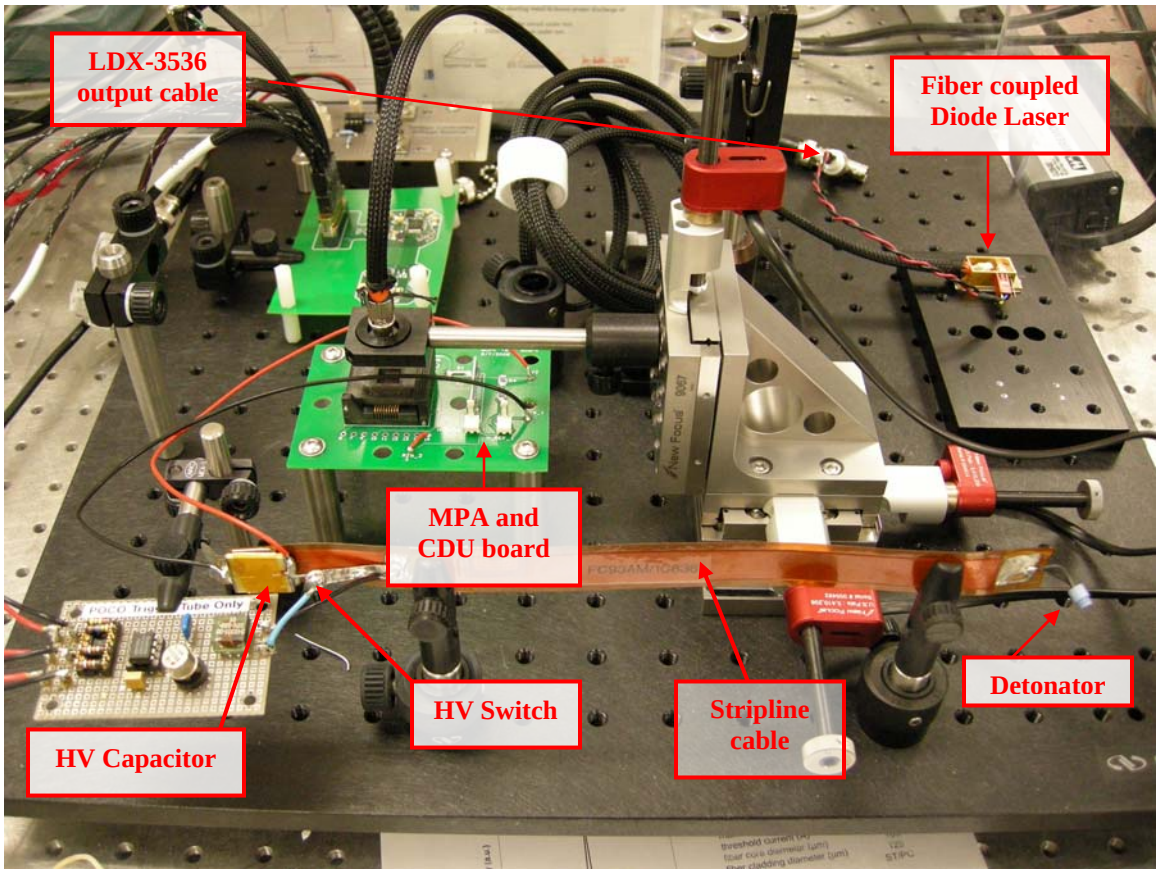

Figure 6: Photograph of the optically powered firing set experimental setup. The diode laser is driven by an ILX: LDX-3565 precision current source. The MPA is then illuminated by the diode laser and injects current to the HV capacitor. A HV switch is then used to discharge the capacitor into the detonator.

3. MODELING THE OPTICALLY POWERED FIRING SET

3.1 Semiconductor Physics

The characteristic equations that describe the diode laser operation are based on the photon and electron emission rates of semiconductor materials that make up the diode laser structure. Photon emissions take place due to the electronic transitions from conduction to valance bands in a semiconductor. Figure 7 shows both the radiative and non-radiative transitions that occur in a semiconductor material.

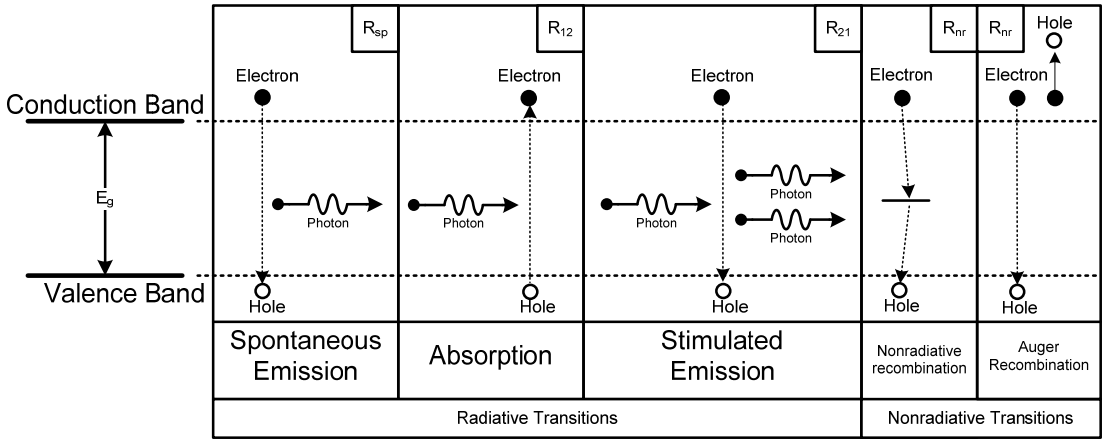

Figure 7: Band transitions in semiconductors.

Three radiative transitions occur: spontaneous emission (recombination), absorption (stimulated generation), and stimulated emission (recombination). Spontaneous emission transpires when the electron in the conduction band recombines spontaneously with a hole in the valence band, generating a photon. The emissions are incoherent due to their randomness in time, phase, and direction [10]. A Light Emitting Diode (LED) operates in this fashion. Absorption happens when a photon is absorbed in the semiconductor material. This stimulates the generation of an electron to the conduction band while leaving a hole in the valance band. Stimulated emission occurs when a photon disturbs

the system which stimulates the recombination of an electron and hole. This simultaneously generates a new photon which has the same phase and direction as the first photon. Figure 7 shows two photons that are generated during this process since the incident photon remains unchanged. This process is often referred to as "optical amplification" and is the emission process used by a laser. The term "laser" is an acronym for light amplification by stimulated emission of radiation.

Two types of nonradiative transitions also occur but do not generate any photons and energy is usually dissipated as heat. Nonradiative recombination happens at point defects, surfaces, and interfaces in the active region [8]. In Auger recombination, the electron-hole recombination energy is transferred to another electron or hole in the form of kinetic energy [8].

3.2 Heat Rate Equations

In order to develop the thermal model for the diode laser, a study of heat transfer was conducted. Heat transfer is the flow of thermal energy (q) that occurs in a medium or between media when a thermal difference is present. Heat flow is analogous to the flow of charge and temperature difference is analogous to the voltage potential difference in electrical circuits. There are three modes of heat transfer: conduction, convection, and radiation.

3.2.1 Conduction

Conduction occurs when there is a temperature difference in a conducting medium. The medium can be a solid or a stationary fluid. Heat transfer by conduction (q_{cond}) flows in

the direction of lower temperature ($T_{s,2}$) as seen in Figure 8. An example of conduction heating is when a metal rod is held in one hand and the opposite side is placed into a flame. The person holding the rod soon begins to feel the metal rod increase in temperature due to an increase of vibrations from the atoms and electrons of the metal [17]. The application of heat to the metal causes the atoms and electrons in the metal to begin to vibrate with larger and larger amplitudes. They in turn interact with their neighbors transferring some of their energy. This continues slowly down the bar and the temperature begins to increase.

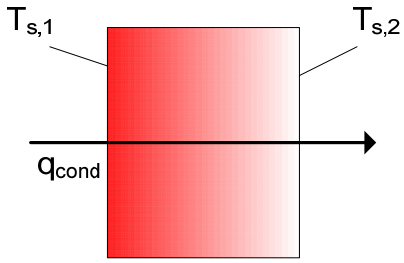

Figure 8: Conduction in a plane surface.

Rate equations are used to describe the heat transfer process. Fourier's Law states that for a 1-d plane wall having a temperature distribution of T(x), the heat flux (q''_x) in the x direction is [4].

$$q''_x = -k\frac{dT}{dx} \tag{3.1}$$

The term k is the thermal conductivity (W/m * K) and $\frac{dT}{dx}$ is the temperature gradient.

The heat flux is therefore proportional to the temperature gradient and thermal conductivity. In steady state conditions where the temperature distribution is linear, the temperature gradient can be simplified to [4]:

$$\frac{dT}{dx} = \frac{T_{s,2} - T_{s,1}}{L} \tag{3.2}$$

Eq. (3.1) can be rewritten as:

$$q''_x = -k\frac{T_{s,2} - T_{s,1}}{L} = k\frac{\Delta T}{L} \tag{3.3}$$

Since heat flux is the heat transfer rate (q_x) per unit area (A), the heat rate in Watts is then:

$$q''_x = \frac{q_x}{A} \tag{3.4}$$

Therefore by combining Eq. (3.1) and (3.4) the heat transfer rate is found in the following equation.

$$q_x = -kA\frac{dT}{dx} \tag{3.5}$$

Heat flux that has been defined in Eq. (3.5) is a directional quantity that is normal to the cross-sectional area A. Therefore, heat flux can further be extended to the y and z direction. One-dimensional, steady-state models can be used to accurately represent major systems [4]. In the case of the laser diode and the miniature photovoltaic array, the heat equation for conduction will be modeled in the x-dimension and Eq. (3.5) will be used.

3.2.2 Convection

Convection happens when thermal energy is transferred between a surface and a moving heated substance. An example of convection is the operation of a typical kitchen oven. Figure 9 illustrates this mode of heat transfer. In the example the surface temperature (T_s) is greater than the ambient temperature (T_{amb}).

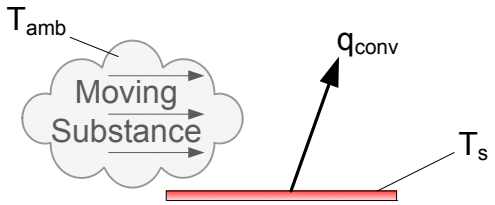

Figure 9: Convection from a surface.

The rate equation is obtained from Newton's law of cooling which states that the heat flux (W/m^2) is [4]:

$$q'' = h(T_s - T_{amb}) \tag{3.6}$$

The heat rate can then be found to be the following by using Eq. (3.4):

$$q_{conv} = hA(T_s - T_{amb}) \tag{3.7}$$

T_s is the temperature in Kelvin of the surface and T_{amb} is the temperature of the moving substance. T_{amb} can be ambient air, liquid, or gas temperature. The term h is defined as the convection heat transfer coefficient (W/m^2*K). This coefficient depends on the surface geometry, fluid thermodynamic and transport properties, as well as fluid motion [4].

3.2.3 Radiation

All objects radiate energy continuously in the form of electromagnetic waves. These waves make up the electromagnetic spectrum and they include, in decreasing energy, gamma rays, X rays, ultraviolet, visible, infrared, and microwaves. In the study of heat transfer, only the wavelength of 0.1 to 100 um which includes a portion of ultraviolet and all visible and infrared is significant. These electromagnetic waves are often lumped together and called thermal radiation. Thermal radiation is of two forms: emitted radiation (q_{rad1}) from a surface or incident radiation (q_{rad2}) from a special source to the

surface of interest. The emission is due to the changes in electron configurations of the atoms or molecules of the material [4]. Figure 10 illustrates the two forms of radiation.

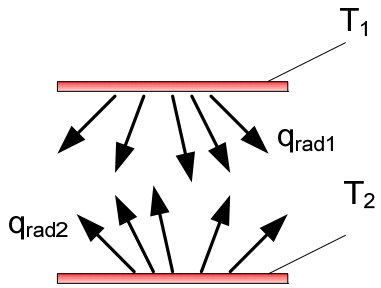

Figure 10: Radiation exchange between two surfaces.

In emitted $\left(q''_{rad\,2}\right)$ or incident $\left(q''_{rad1}\right)$ radiation, the heat flux from the thermal energy of matter is found to be:

$$q'' = \varepsilon\sigma T_s^4 \tag{3.8}$$

ε is the emissivity and σ is the Stefan-Boltzmann constant.

3.2.4 Thermal Resistance and Conductance for Conduction

The term resistance can be used to simplify analysis of a thermal model. Intuitively, we can imagine that a material possesses certain properties that will resist the flow of heat. These properties can be lumped together and called thermal resistance. This is the same concept of electrical resistance in which ohm's law gives the following relationship:

$$R_{elec} = \frac{V_{s,1} - V_{s,2}}{I} = \frac{L}{\sigma A} \tag{3.9}$$

Similarly, the thermal resistance is defined as:

$$R_{thermal} = \frac{T_{s,1} - T_{s,2}}{q} = \frac{L}{kA} \tag{3.10}$$

By developing the concept of thermal resistance, a thermal model can be simplified by transforming it into a thermal equivalent circuit. Thermal conductance can therefore be defined as the quantity of heat that can pass through a plate with given dimensions. Again this is analogous to electrical conduction. In equation form:

$$\lambda_{thermal} = \frac{1}{R_{thermal}} = \frac{kA}{L} \tag{3.11}$$

The conduction rate equation can then be written as:

$$q_x = \frac{\left(T_{s,1} - T_{s,2}\right)}{R_{cond}} = \lambda_{cond}\left(T_{s,1} - T_{s,2}\right) \tag{3.12}$$

3.2.5 Thermal Resistance and Conductance for Convection

Thermal resistance can also be used to simplify the heat rate equations for convection losses. In this mode of heat loss, thermal resistance is defined as:

$$R_{conv} = \frac{1}{hA} \tag{3.13}$$

It is important to note that the term L is not used in Eq. (3.13). Thermal conductance for convection is therefore

$$\lambda_{thermal} = \frac{1}{R_{thermal}} = hA \tag{3.14}$$

Therefore we can substitute the thermal resistance in the heat rate equation for convection and obtain the following:

$$q_x = \frac{\left(T_{s,2} - T_{s,1}\right)}{R_{conv}} = \lambda_{conv}\left(T_{s,2} - T_{s,1}\right) \tag{3.15}$$

3.2.4 Heat Analysis Summary

Thermal models will be developed for only the diode laser and MPA. The following table lists the equations that will be used for the thermal model analysis:

Mode	Heat Flux: $q''\left(\frac{W}{m^2}\right)$	Heat Rate: $q(W)$
Conduction	$q''_{cond} = k\frac{\Delta T}{L}$	$q_{cond} = \frac{kA}{L}(\Delta T) = \lambda_{cond}(\Delta T)$
Convection	$q''_{con} = h(T_{s,2} - T_{s,1})d$	$q_{conv} = hA(T_s - T_{amb}) = \lambda_{conv}(T_s - T_{amb})$
Radiation	$q''_{rad} = \varepsilon\sigma(T_s{}^4 - T_{sur}^4)$	$q_{rad} = h_r A(T_s - T_{sur})$

Table 2: Heat rate and heat flux equations.

The First Law of Thermodynamics (Law of Conservation of Energy) will be used to combine all the heat rate terms. It states that the total energy in a system is conserved and the only way that energy can change is if energy crosses its boundaries [4]. In equation form it states that the total stored energy is equal to the sum of the net heat (Q) transferred to a system and the net work (W) done by the system:

$$\Delta E_{st}^{tot} = Q - W \tag{3.16}$$

The increase in the amount of energy stored in a control volume must equal the difference between the amount of energy that enters the control volume and the amount that leaves the control volume at some time (t). Figure 11 illustrates this concept.

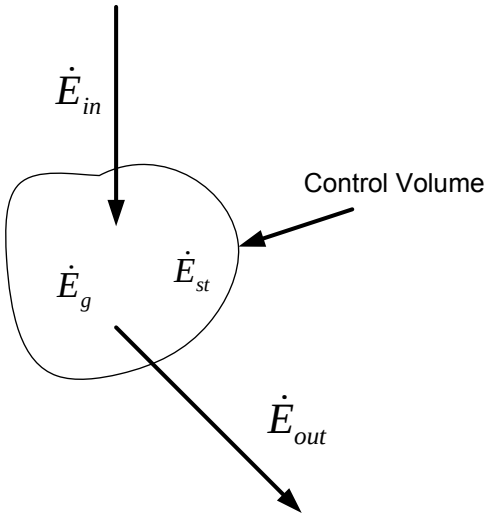

Figure 11: Conservation of Energy.

In equation form, the Conservation of Energy is:

$$\dot{E}_{st} = \dot{E}_{in} - \dot{E}_{out} + \dot{E}_g \tag{3.17}$$

The stored energy is the term (E_{st}). The dot over this term is used to indicate a rate. The term $\dot{E}_{st}$ is then the rate of increase of energy stored within a control volume and the units are in Watts. The terms $\dot{E}_{out}$ and $\dot{E}_{in}$ are the rate of energy transfer out of and into a control volume respectively. These terms occur at the control surface and are usually proportional to the surface area. They include heat transfer and work interactions. $\dot{E}_g$ is the rate of energy generation that occurs from chemical, electrical, electromagnetic, or nuclear to thermal energy. The above equation will be used in conjunction with the thermal heat rates as summarized in Table 1. When a system is made up of multiple junctions or layers, Eq. (3.17) can be applied as separate nodes.

3.3 Semiconductor Diode Laser

A 3 Watt Jenoptik (Part No. JUM3000/105/20) and a Unique Mode (Part No. JOLD-3-BAFC-11) broad area edge-emitting fiber coupled diode laser is used to illuminate the MPA. This diode was selected for its compact size, 808 nm emitting wavelength, and high optical output power capability. The fiber pigtail uses an ST/PC-connector that is attached to a Fiberguide[sm] AFS105/125Y optical fiber. The optical output power during normal operation is 3 W at 4.3 A input current.

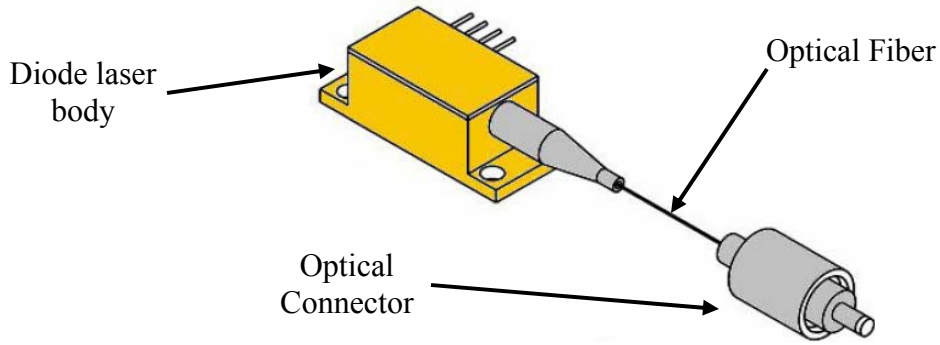

Figure 12: Picture of a JUM3000/105/20 and JOLD-3-BAFC-11 diode laser. It is made up of a body that serves as a heat sink, an optical fiber, and an optical connector.

The structure of a diode laser is made up of 4 basic elements. They are optical gain medium, optical waveguide, resonator, and lateral confinement. The optical gain medium provides optical gain by stimulated emission. The optical medium is composed of layers of P-type and N-type material separated by an active layer. When doped with certain materials, a semiconductor becomes either N-type or P-type. N-type material has an incidence of free electrons whereas P-type material has free holes. It is commonly referred to as P-i-N junction as shown in Figure 13. When this junction is forward-biased due to an applied electrical field, a potential well is formed at the active layer. The holes and electrons are pushed towards the well and at a point they will recombine with each other. Radiative and nonradiative emissions will begin to occur and then photons are

emitted. In the case of edge emitting diode lasers, the photons leave the semiconductor perpendicular to the edge surface as illustrated in Figure 13.

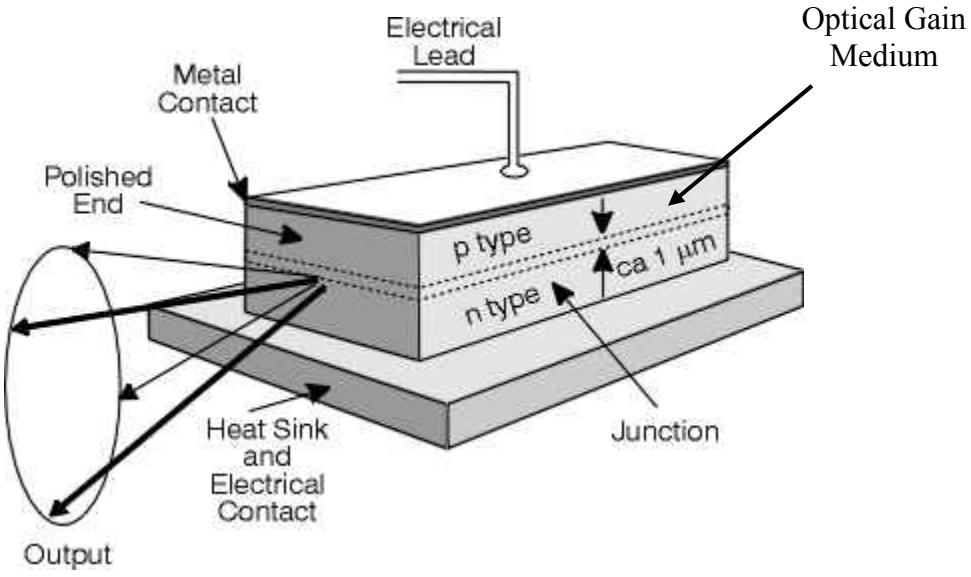

Figure 13: Edge emitting diode laser structure.

The optical waveguide is used to guide the generated photons. It is made of a dielectric material that has two components; core and cladding as shown in Figure 14. The core is made up of a high refractive index material and the cladding surrounds the core and is made up of a lower refractive index material. This combination allows the photons to travel within the core material by reflection off the core wall.

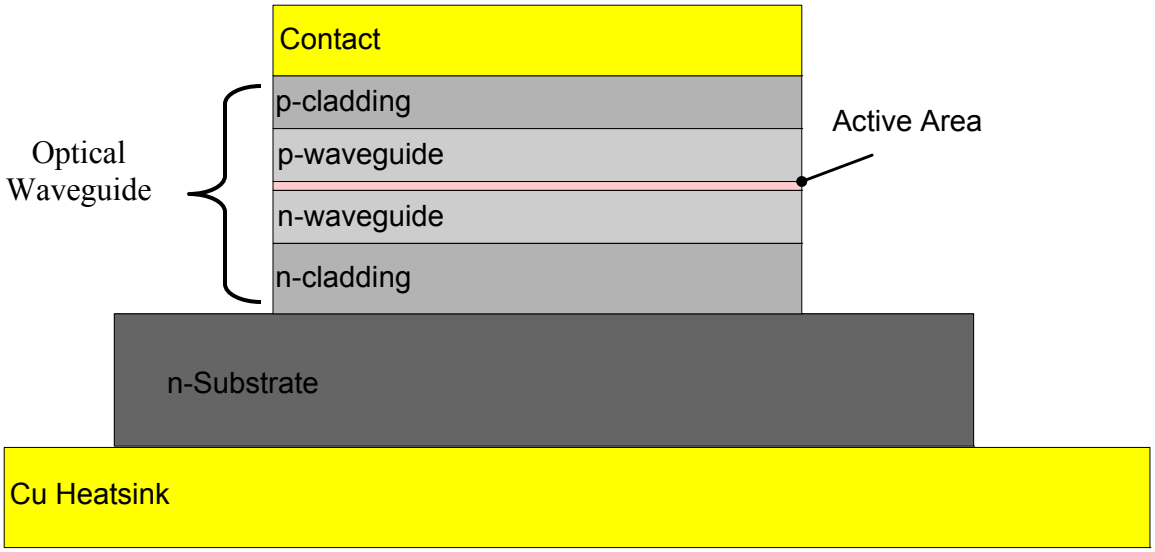

Figure 14: Side View of a Broad area diode laser to show the optical waveguide.

A resonator, or optical cavity, is a collection of mirrors to form a standing wave cavity resonator for optical feedback. Some common types of resonators include Fabry-Perot, Distributed Feedback, and Distributed Bragg Reflector.

The lateral confinement of current, carriers, and photons are needed to allow the system of components to operate as effectively and efficiently as a diode laser. Three basic types of confinement are current, optical, and carrier confinement. The diode laser structure determines the type of confinement.

Figure 15 is a photograph of the Jenoptik diode laser after the lid is removed. As current enters the anode it travels through bond wires to the diode laser bar. Stimulated emission begins and the photons are sent to the ball lens. The ball lens then focuses the emitted light to the fiber optic. From Figure 15, the diode laser bar is attached to the substrate material. The substrate material is a fairly large conductive block that is then attached to the heat-sink body. A photodiode was built-in to measure the output power during

normal operation. The photodiode outputs a voltage that is proportional to the output power in a narrow range. The photodiode was not used.

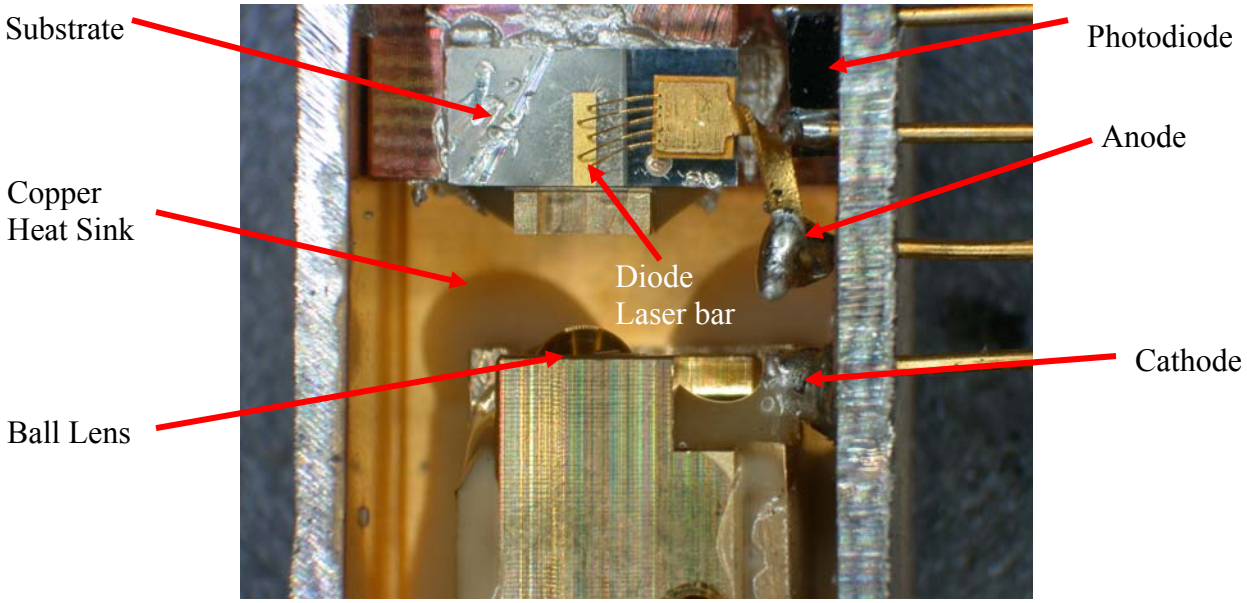

Figure 15: Photograph of internal components of Jenoptik diode laser. The internal structure of the Unique Mode diode laser is identical.

The size of the diode laser bar is an important characteristic of the device and used in the electrical model. Figure 16 is a zoomed photograph of the diode laser bar. Height was difficult to measure so it was estimated from a side view.

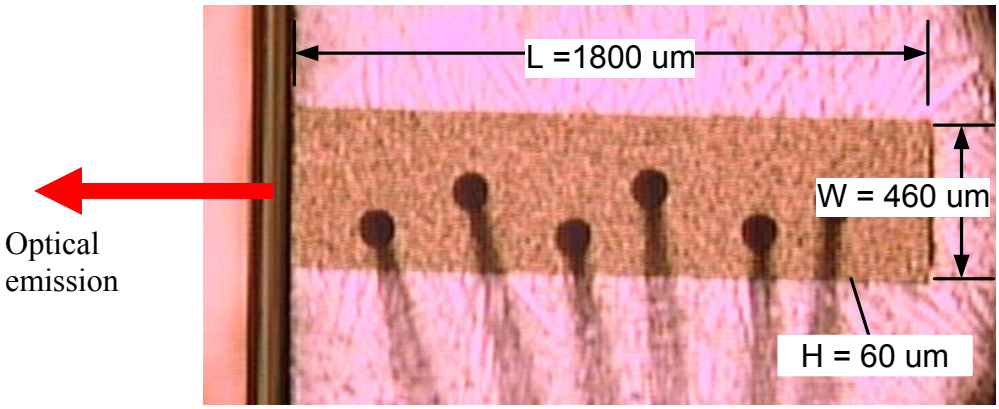

Figure 16: Photograph of the dimensions of diode laser bar.

3.3.1 Electrical Model

A set of rate equations are used to describe the behavior of diode lasers and LEDs. These equations describe the time variations in the carrier density (N) and the photon density (N_p). Carrier density is the number of charge carriers per volume and photon density is the number of photons in the volume of the resonator. Figure 17 shows a reservoir model that is used to develop the rate equations.

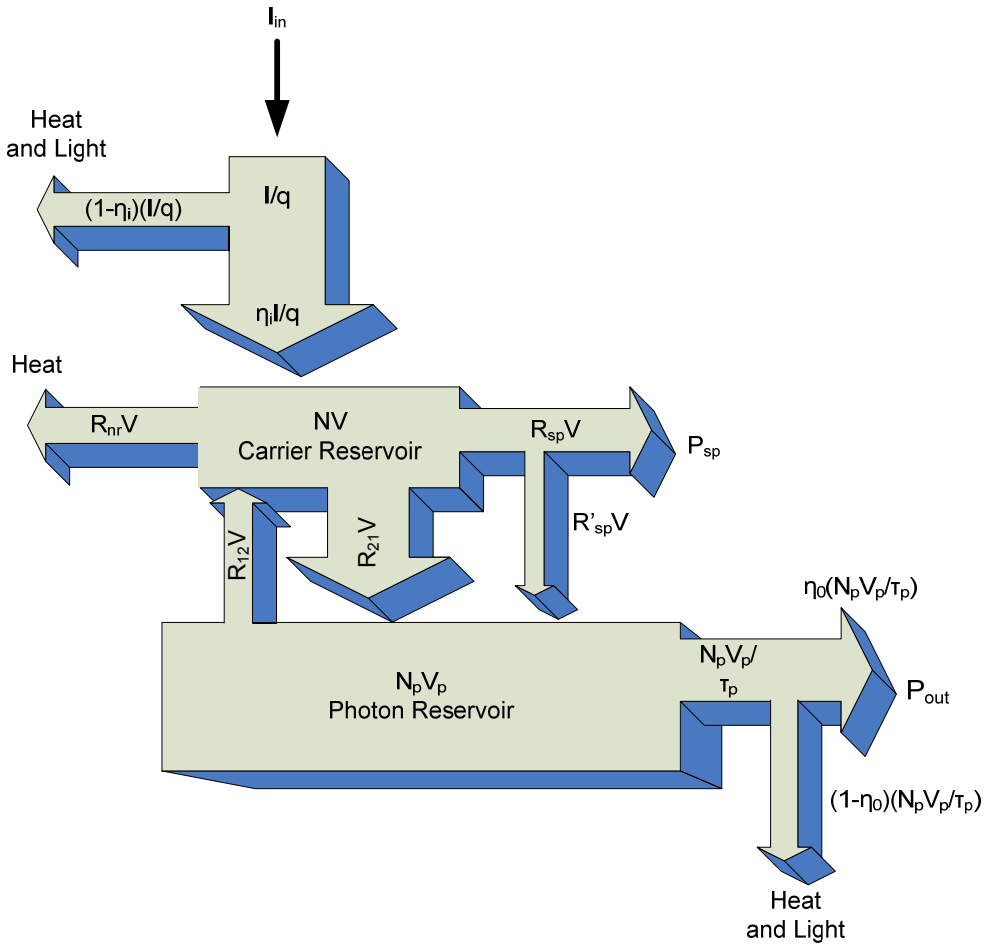

Figure 17: Reservoir Model of diode laser.

A carrier and photon rate equation can be realized by setting the time rate of change to equal the rates going into each reservoir minus the rate leaving the reservoir. The carrier and photon number rate equation is then:

$$V\frac{dN}{dt} = \frac{\eta_i I_{in}}{q} - (R_{sp} + R_{nr})V - (R_{21} - R_{12})V \tag{3.18a}$$

$$V_p\frac{dN_p}{dt} = (R_{21} - R_{12})V - \frac{N_p V_p}{\tau_p} + R'_{sp}V \tag{3.18b}$$

Table 1 lists the parameters used in the above equations. These equations show that carrier density is the amount of carrier injection that reaches the active area less the nonradiative transitions that leave as heat and the radiative transitions of spontaneous emission, absorption, and emission. The photon density is the amount from stimulated emission and spontaneous emission less the absorption and amount of photons leaving the active area.

These equations can be further simplified by dividing out the volume and approximating a few terms. For the carrier rate equation, the spontaneous and nonradiative emission can be approximated by [4]:

$$(R_{sp} + R_{nr}) \approx \frac{N}{\tau} \tag{3.19}$$

These two terms can be lumped together as a natural carrier decay process which is described by the carrier lifetime (τ) constant and only depends on carrier density. Stimulated emission and absorption for both rate equations can also be approximated by:

$$R_{21} - R_{12} \approx v_g g N_p \tag{3.20}$$

The number of photons generated in the active material is the carrier loss by stimulated emission [8]. The photon density from stimulated emission exponentially increases with optical gain (g) when light travels through a material with thickness of Δz as seen in the following equation.

$$N_p(z) = N_p(0) * e^{gz} \tag{3.21}$$

$N_p(0)$ is the incoming or initial density of photons. The solution to $\frac{dN_p}{dz}$ is the exponential function. Converting the differential equation to time results in,

$$\frac{dN_p}{dt} = N_p v_g g = R_{21} - R_{12} \tag{3.22}$$

v_g is the group velocity of the photons in the active area. In Eq. (3.20) the term g is the non-linear material gain which is a function of the carrier and photon density ($g(N,N_p)$). This term can be approximated by a logarithmic function such that:

$$g_o \ln\left(\frac{N + N_s}{N_{tr} + N_s}\right) \tag{3.23}$$

g_o is the gain coefficient, N_{tr} is the transparency carrier density, and N_s is the gain linearity factor [8]. These parameters are obtained from a curve fit to the gain curves. The spontaneous emission rate is sometimes approximated by $R'_{sp} \approx \beta_{sp} R_{sp}$ [8]. For many high power laser diodes, this term does not affect the output since the spontaneous emission factor β_{sp} is very small. With these assumptions, the differential equations that model the diode laser carrier and photon density for a single-mode model are now:

$$\frac{dN}{dt} = \frac{\eta_i I_{in}}{qV} - \frac{N}{\tau} - v_g g(N, N_p) N_p \tag{3.24a}$$

$$\frac{dN_p}{dt} = \left[\Gamma v_g g(N, N_p) - \frac{1}{\tau_p} \right] N_p + \Gamma R'_{sp} \qquad (3.24b)$$

Parameter	Description	Value	Units
η_i	injection efficiency	<1	none
q	electron charge	1.60E-19	C
V	volume of carrier reservoir (active area)		cm^3
τ	differential carrier lifetime		s
v_g	group velocity		cm/s
Γ	confinement factor		none
V_p	volume of photon reservoir		cm^3
τ_p	differential photon lifetime		s
η_o	optical efficiency of laser	<1	none
R'_{sp}	spontaneous emission rate into 1 optical mode		cm^{-3}/s
g_o	empirical gain coefficient		1/cm
N_s	gain linearity parameter		$1/cm^3$
N_{tr}	transparency carrier density		$1/cm^3$
hv	energy per photon at desired wavelength	2.03E-10	J/photon
d	thickness		m
w	width		m
L_a	Active section length		m
L	Length for photons		m

Table 3: List of parameters pertaining to a diode laser that are used in the differential equations, Eq.(3.24).

Parameter	Description	Units
I_{ld}	Input Current	W
N	carrier density	cm^{-3}
N_p	photon density	cm^{-3}
g	material gain $g(N,N_p)$	

Table 4: List of dynamic variables pertaining to a diode laser that are used in the differential equations, Eq. (3.24).

Tables 3 and 4 list the common parameters that make up the differential equation. It should also be noted that the third term in Eq. (3.24a) and the first term in Eq. (3.24b) make this set of equations nonlinear since the state variables must be linearly independent. The additional constant term $\Gamma R'_{sp}$ in Eq. (3.24b) also limits the ability to form these equations into the state space representation.

The optical power output is found to be proportional to the optical density (N_p), photon reservoir volume (V_p) and optical efficiency (η_o) as seen in the following equation [8].

$$P_{ld} = \eta_o h\nu \frac{N_p V_p}{\tau_p} \tag{3.25}$$

The following block diagram summarizes the model that was developed with the system output and differential equations. It should be noted that the attenuation from the diode laser's optical fiber is assumed to be zero.

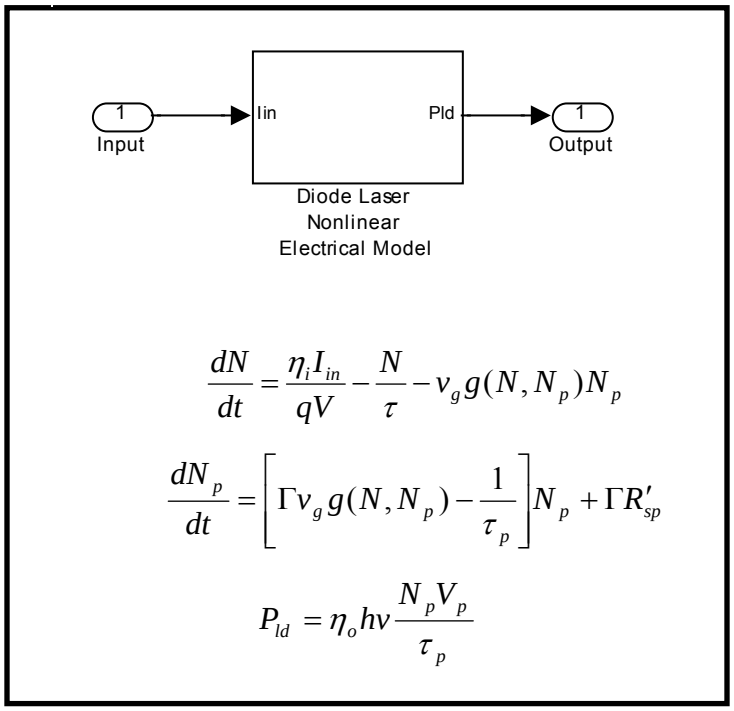

$$\frac{dN}{dt} = \frac{\eta_i I_{in}}{qV} - \frac{N}{\tau} - v_g g(N, N_p) N_p$$

$$\frac{dN_p}{dt} = \left[\Gamma v_g g(N, N_p) - \frac{1}{\tau_p} \right] N_p + \Gamma R'_{sp}$$

$$P_{ld} = \eta_o h\nu \frac{N_p V_p}{\tau_p}$$

Figure 18: Diode Laser Electrical Model block diagram with system equations.

3.3.2 Thermal Model

In the process of developing the thermal model for the diode laser, it was essential that the structure of the diode laser be clearly defined since the thermal model is dependant upon this geometry. The fiber coupled laser diode is packaged in an enclosed metal

housing. After removal of the lid, the internal structure can be defined as seen in Figure 19.

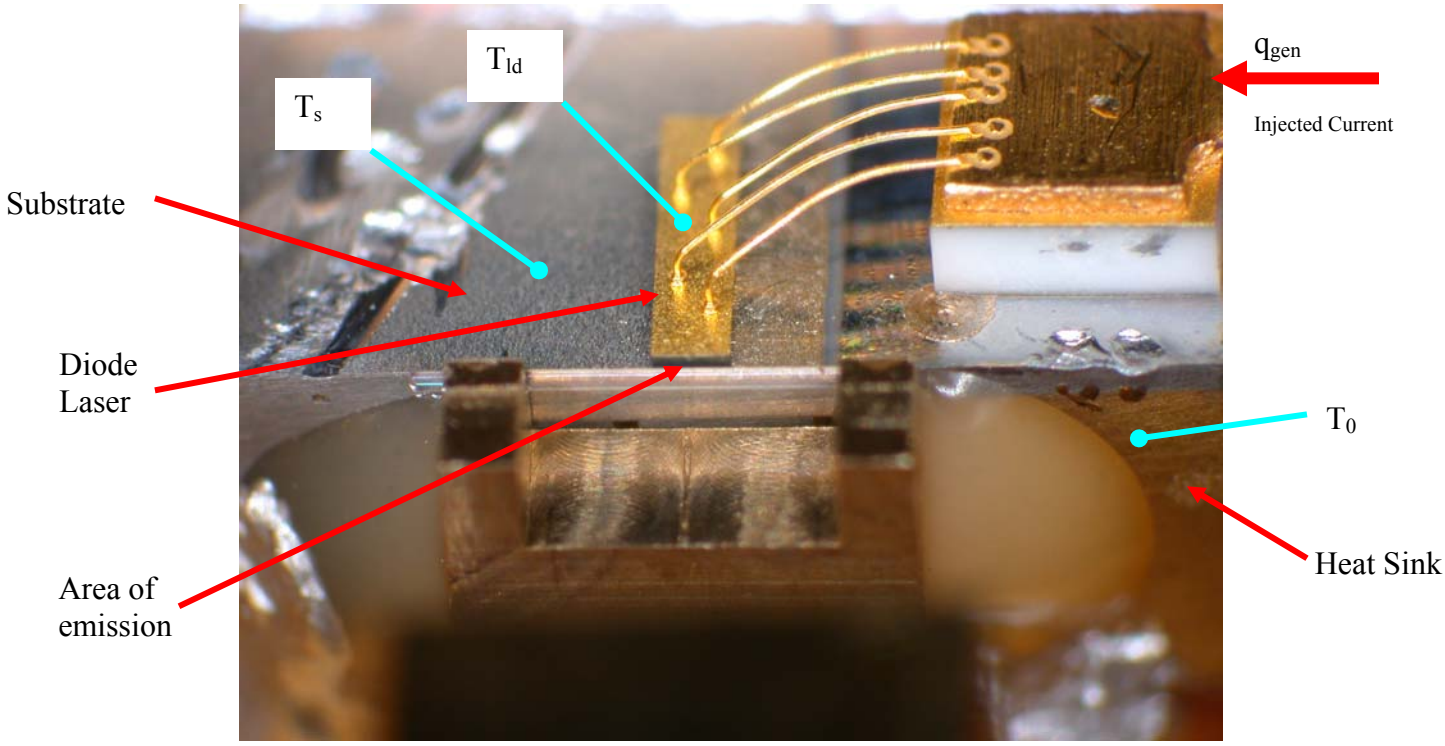

Figure 19: Photograph of the internal diode laser with location for temperature measurement.

In terms of modeling heat flow, the process begins with the injection of current (q_{gen}) to the diode laser. The current flows through the laser and then continues to the substrate. The current then returns back through the copper heat sink. This flow of heat causes the temperature in the materials to increase. A thermal model can now be developed by grouping each material that the current passes through into separate nodes. Figure 20 shows a simplified representation of the diode laser with two nodes for obtaining a thermal model.

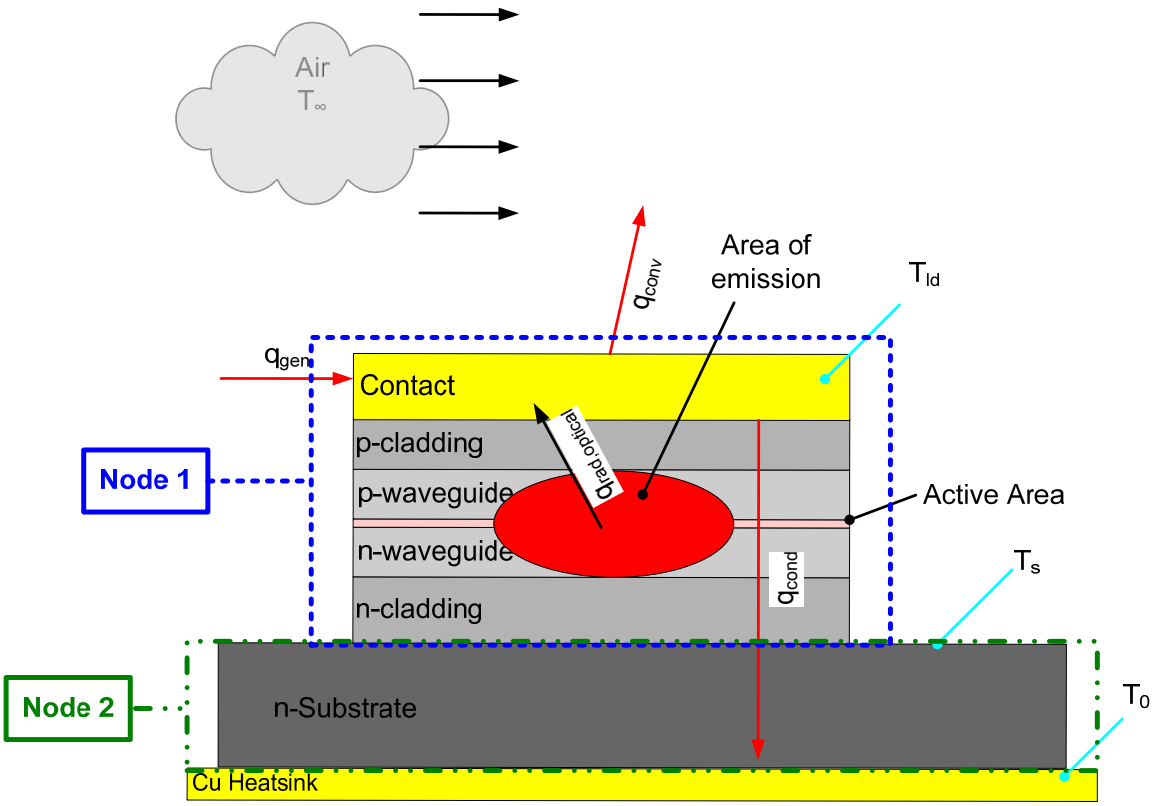

Figure 20: Simplified thermal model of the diode laser.

To reduce the number of differential equations for this system, only two nodes were modeled. Additional nodes can be added as needed to correctly model the system. Node 1 is made up of a system of layered materials but will be modeled as a single material since the thermal properties of the materials are very similar. Node 2 is made up of the substrate material. The following list of assumptions was used to develop the thermal model:

1. The temperature at any time (t) in the material is uniform.
2. One-dimensional heat transfer is used since the heat transfer from sides of the chip is negligible.
3. The diode laser has constant material properties.
4. The temperature of the heat sink (T_0) is equal to the ambient air temperature (T_∞).

The thermal model will begin by using the First Law of Thermodynamics. Recalling Eq. (3.17), the rate of change of the temperature will be determined at a time instant. Again we have:

$$\dot{E}_{st} = \dot{E}_{in} - \dot{E}_{out} + \dot{E}_{g} \tag{3.26}$$

For Node 1, input thermal energy rate ($\dot{E}_{in}$) is not present in this node and therefore the above equation can be rewritten as:

$$\dot{E}_{st} = \dot{E}_{g} - \dot{E}_{out} \tag{3.27}$$

Stored thermal energy rate ($\dot{E}_{st}$) is the thermal energy storage due to the temperature change. It is equal to [4]:

$$\dot{E}_{st} = \frac{dU^{t}}{dt} = \frac{d}{dt}\left(\rho c V_{ld} T_{ld}\right) = \frac{dT_{ld}}{dt} C_{ld} \tag{3.28}$$

ρ is the mass density, c is the specific heat, and V_{ld} is the volume and T_{ld} is the temperature of the laser. The product of the terms ρ, c, and V, are often defined as the thermal capacitance or heat capacity of a specific material denoted as "C". The internal thermal energy rate generation term ($\dot{E}_{g}$) is the input power from the laser diode driver less the contribution due to the electrical resistance (R_{cable}) of the input cable defined as:

$$\dot{E}_{g} = q_{gen} = P_{in} = I_{in} V_{ld} - I_{in}^{2} R_{cable} \tag{3.29}$$

I_{in} is the input applied laser diode current and V_{ld} is the output bias voltage across the anode and cathode. Heating occurs when an electrical current passes through a conductor. The output thermal energy rate term ($\dot{E}_{out}$) is the energy outflow due to

convection, conduction, and thermal radiation from Node 1. The resultant optical power from the active area ($q_{rad,optical}$) is also included and is the output diode laser power (P_{ld}).

Using Eqs.(3.15), (3.12), and (3.8) the output thermal energy rate term can be found to be,

$$\begin{aligned} \dot{E}_{out} &= q_{conv} + q_{cond} + q_{rad} + q_{rad,optical} \\ \dot{E}_{out} &= \lambda_{1,conv}(T_{ld} - T_{\infty}) + \lambda_{1,cond}(\Delta T_1) + h_r A(T_{abs} - T_{sur}) + P_{ld} \end{aligned} \tag{3.30}$$

The output thermal energy rate can be simplified with the assumption that heat loss from q_{conv} and q_{rad} are insignificant. The thermal radiation emitted by surfaces and the surrounding are negligible since the product of the Stefan-Boltzman constant and emissivity are rather small as compared to emitted energy by a blackbody which is an ideal radiator. The emissivity of copper is about 0.03 and the emissive power from this material is about 32 times less than that of the blackbody. Losses due to convection can also be disregarded due to the small volume of the laser bar. With these assumptions, Eq. (3.30) can be rewritten as:

$$\dot{E}_{out} = \lambda_{1,cond}(\Delta T_1) + P_{ld} \tag{3.31}$$

A differential equation that describes Node 1 can be defined by substituting in Eqs. (3.28), (3.29), and (3.31) into Eq. (3.27) to obtain the following heat rate equation.

$$C_{ld}\left(\frac{dT_{ld}}{dt}\right) = -\left[\lambda_{1,cond}\right]\Delta T_1 + P_{in} - P_{ld} \tag{3.32}$$

Defining ΔT_1 as the temperature difference between the diode laser (T_{ld}) and substrate (T_s) temperature, dividing across by the diode laser thermal capacitance (C_{ld}), and

defining the difference between the input power (P_{in}) and output optical power (P_{ld}) as the total power (P_{total}), the heat rate equation for Node 1 is:

$$\frac{dT_{ld}}{dt} = \left[\frac{-\lambda_{1,cond}}{C_{ld}}\right]T_{ld} + \left[\frac{\lambda_{1,cond}}{C_{ld}}\right]T_s + \left[\frac{1}{C_{ld}}\right]P_{total} \tag{3.33}$$

A similar procedure will be followed to obtain the heat rate equation for Node 2. The internal thermal energy rate generation term ($\dot{E}_g$) is not present in this node since there is no conversion from internal to thermal energy. Therefore, Eq. (3.17) can be rewritten as:

$$\dot{E}_{st} = \dot{E}_{in} - \dot{E}_{out} \tag{3.34}$$

The input thermal energy rate ($\dot{E}_{in}$) is the output thermal energy heat rate ($\dot{E}_{out}$) Eq. (3.31) from Node 1 less the output emitted power (P_{ld}) from the active area since it does not add any thermal energy to Node 2.

$$\dot{E}_{in} = \lambda_{1,cond}(\Delta T_1) \tag{3.35}$$

The stored thermal energy rate ($\dot{E}_{st}$) is the thermal energy storage due to the temperature change and is previously defined in Eq. (3.28) except that V_s is the volume and T_s is the temperature of the substrate, and C_s is the substrate thermal capacitance where:

$$\dot{E}_{st} = \frac{dU^t}{dt} = \frac{d}{dt}\left(\rho c V_s T_s\right) = \frac{dT_s}{dt}C_s \tag{3.36}$$

The output thermal energy rate term ($\dot{E}_{out}$) is the energy outflow due to convection, conduction, and thermal radiation from Node 2. Using Eqs. (3.15), (3.12), and (3.8) the output thermal energy rate term can be found to be,

$$\begin{aligned} \dot{E}_{out} &= q_{conv} + q_{cond} + q_{rad} \\ \dot{E}_{out} &= \lambda_{2,conv}(T_s - T_\infty) + \lambda_{2,cond}(\Delta T_2) + h_r A(T_{abs} - T_{sur}) \end{aligned} \tag{3.37}$$

This term can also be simplified with the assumption that q_{conv} and q_{rad} are insignificant. The thermal radiation emitted by surfaces and the surrounding are negligible since the emissivity is rather small as in the previous case for Node 1. Losses due to convection can also be disregarded due to the small volume of the substrate. With these assumptions and defining ΔT_2 as the temperature difference between the substrate (T_s) and heat sink (T_0) temperature, Eq. (3.37) can be rewritten as:

$$\dot{E}_{out} = \lambda_{2,cond}(\Delta T_2) = \lambda_{2,cond}(T_s - T_0) \tag{3.38}$$

The differential equation that describes Node 2 can be defined by substituting in Eqs. (3.36), (3.35), and (3.38) into Eq. (3.34) to obtain the following heat rate equation.

$$C_s\left(\frac{dT_s}{dt}\right) = \lambda_{1,cond}(T_{ld} - T_s) - \lambda_{2,cond}(T_s - T_0) \tag{3.39}$$

ΔT_1 is the temperature difference between the diode laser (T_{ld}) and substrate (T_s) temperature. Dividing across by the substrate thermal capacitance (C_s), the heat rate equation for Node 2 is:

$$\frac{dT_s}{dt} = \left[\frac{\lambda_{1,cond}}{C_s}\right]T_{ld} + \left[\frac{(-\lambda_{1,cond} - \lambda_{2,cond})}{C_s}\right]T_s + \frac{\lambda_{2,cond}T_0}{C_s} \tag{3.40}$$

In summary, the heat balance equations of a diode laser is the thermal response due to the input power (P_{in}) which causes conductive heat flow within the materials. The temperature of each material is dependant on its ability to store and conduct heat. The block diagram and system equations are shown in Figure 21.

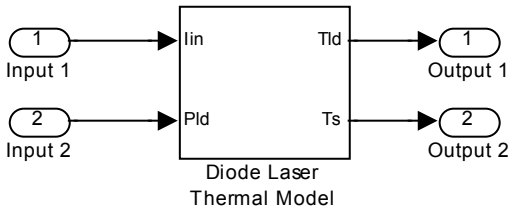

$$\frac{dT_{ld}}{dt} = \left[\frac{-\lambda_{1,cond}}{C_{ld}}\right]T_{ld} + \left[\frac{\lambda_{1,cond}}{C_{ld}}\right]T_s + \left[\frac{1}{C_{ld}}\right]P_{total} \qquad (3.41a)$$

$$\frac{dT_s}{dt} = \left[\frac{\lambda_{1,cond}}{C_s}\right]T_{ld} + \left[\frac{(-\lambda_{1,cond} - \lambda_{2,cond})}{C_s}\right]T_s + \frac{\lambda_{2,cond}T_0}{C_s} \qquad (3.41b)$$

$$\text{Output} = T_{ld} \qquad (3.42)$$

Figure 21: Diode laser thermal model block diagram with system equations.

3.4 Miniature Photovoltaic Array

The Miniature Photovoltaic Array (MPA) or Series Connected Photovoltaic Array (SCPA) is a silicon device that generates current when illuminated by a light source. It is constructed of 2400 photocells connected in series. The cells are laid out in a circular geometry as Figure 23 illustrates. Each cell as seen in Figure 22 will generate current (I_l) when illuminated by a light source.

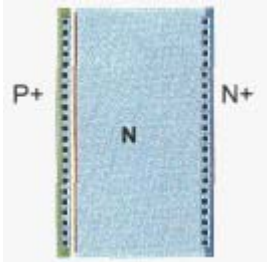

Figure 22: Top view of a single cell of the MPA.

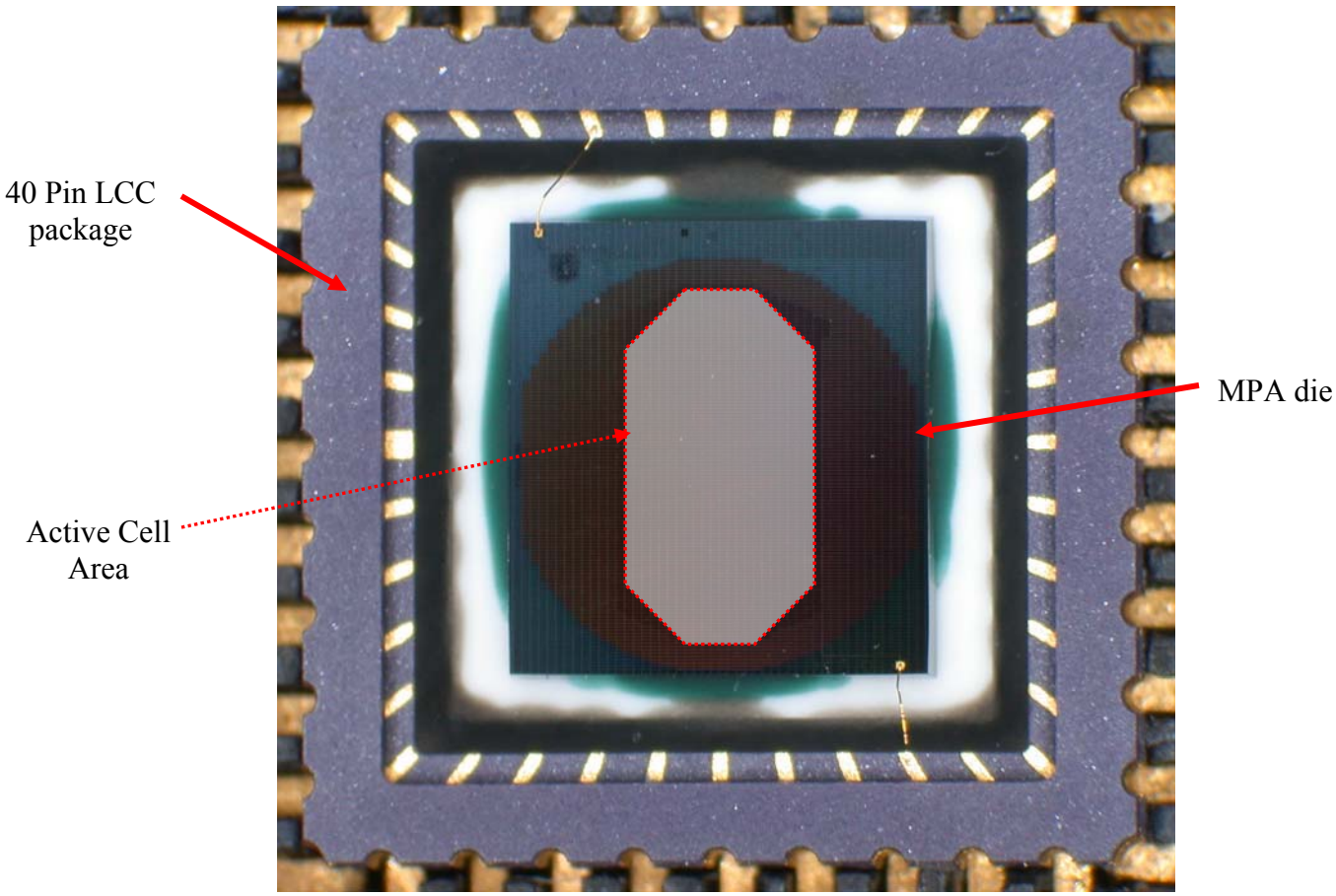

Figure 23: Photograph of a 2400 cell MPA. This MPA is capable of generating about 1.7kV.

The total amount of current generated through the system is dependant on the cell with the least amount of illumination. The series connection permits high voltage output (V_{hv}) from the MPA. Sandia National Laboratories' Microelectronics Development Lab (MDL) manufactures the MPA by using Silicon-On-Insulator (SOI) technology [9].

In general, the photovoltaic cells are made up of a semiconductor material in which impurities are added in a process called doping. This is the same process that is used for all semiconductor manufacturing. When doped with certain materials, the semiconductor becomes either N-type or P-type. N-type material has an incidence of free electrons,

whereas P-type material has free holes. In order to get a material to conduct current, electrons need to move from one area to an open hole. When the P-type and N-type materials are put together, an electric field is created to allow electrons to flow from the P to the N side only. Then when light in the form of photons of distinct energies hit the semiconductor material, its' energy frees electron-hole pairs. When this happens near the electric field, the free electron will move to the N side. This creates an imbalance and the electron wants to return to the original stable state. If we provide a pathway for the electron in the form of electrical wires, the movement of electrons provides a current for the system. The electrical field produces a typical voltage of about 1V; resulting in power for a given circuit. The electron movement continues as long as photons are bombarding the semiconductor material.

During device characterization two devices were damaged due to high voltage breakdown when tested on a curve tracer. These devices worked at 1600V dc levels but when tested with a ±1600V AC voltage they were damaged. Large currents are created when the high voltage signal arcs or breaksdown to a return path. These currents destroy the internal metalized structure of the MPA. Fluorinert liquid was then used to provide additional insulation to prevent the high voltage from arcing when characterized on the curve tracer.

3.4.1 Electrical Model

The electrical model is found by representing the single photocell as an equivalent circuit. It is often modeled as a current source in parallel with a diode as shown in Figure 24.

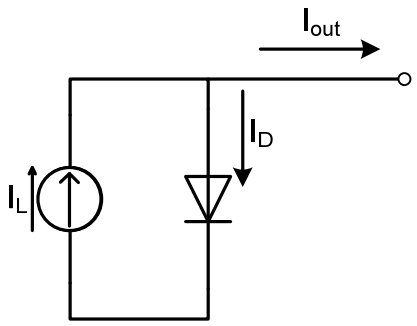

Figure 24: Equivalent circuit of a single photocell.

The Shockley ideal diode equation is used to describe the ideal diode in either forward or reverse bias. This equation is as follows,

$$I_D = I_o\left(e^{\frac{eV_d}{nkT}} - 1\right) \tag{3.43}$$

I_o is the reverse saturation current, e is the electron charge, V_d is the voltage across the diode, n is the diode quality factor, k is Boltzmann's constant, and T is the absolute temperature measured in Kelvin. The output current of an ideal photocell is then the difference between the illumination (I_L) and diode current (I_D).

$$I_{OUT} = I_L - I_D \tag{3.44}$$

This equation can be rewritten to include Eq. (3.43). The following equation is then realized:

$$I_{OUT} = I_L - I_O\left(e^{\frac{eV}{nkT}} - 1\right) \tag{3.45}$$

As previously described, each photocell is connected in series and the equivalent circuit can be made.

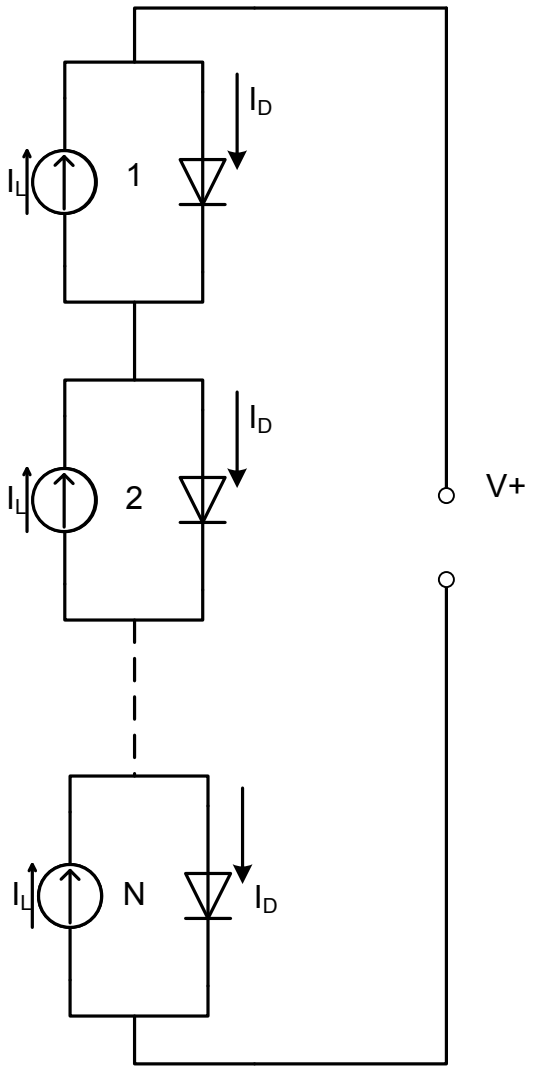

Figure 25: Equivalent series connected circuit of the MPA. N in this case is 2400 cells.

The output current (I_{out}) can then be calculated by the following equation [9]. It is assumed that each N number of cells has identical diode junctions that are each uniformly optically illuminated.

$$I_{OUT} = I_L - I_O\left(e^{\frac{eV}{NnkT}} - 1\right) \tag{3.46}$$

N is the number of photocells in series. With the addition of some parallel resistance (R_p) of the device, the above equation will yield to the following equation [9].

$$I_{OUT} = I_L - I_O\left(e^{\frac{eV_{hv}}{NnkT_{pv}}} - 1\right) - \frac{V_{hv}}{R_p} \tag{3.47}$$

The above equation models the SCPA. During the initial testing of the actual device, temperature was found to play in important role in the output response of the component. Temperature variation causes the illumination current (I_l), reverse saturation current (I_0), and parallel resistance (R_p) to change. The illumination current increases very slightly as the temperature increases. The parallel resistance decreases slightly as temperature increases. Temperature plays a greater effect on the reverse saturation current. As the temperature increases, I_0 will also increase. From the p-n junction physics Eq. (3.48) can be obtained that relates temperature to I_0 [21].

$$I_0 = K_1 T^3 e^{\frac{-qV_g}{kT}} \tag{3.48}$$

K_1 is a constant that is specific to each device and V_g is the bandgap voltage. The parameters in exponent can be lumped together to form Eq. (3.49).

$$I_0 = K_1 T^3 e^{\frac{K_2}{T}} \tag{3.49}$$

K_1 and K_2 are device specific constants that will be determined by curve fitting experimental data. Eq. (3.50) is the final equation that includes the temperature effects of the diode current (I_D).

$$I_{OUT} = I_L - K_1 T_{pv}^{\ 3} e^{\frac{K_2}{T_{pv}}}\left(e^{\frac{eV_{hv}}{NnkT_{pv}}} - 1\right) - \frac{V_{hv}}{R_p} \tag{3.50}$$

Temperature effects of I_L and R_p were not included in the final model because the effects are typically small. Future modeling may include the temperature variation for these

parameters. The illumination current (I_L) is then derived from the I-V curve and is dependant on the illumination power source.

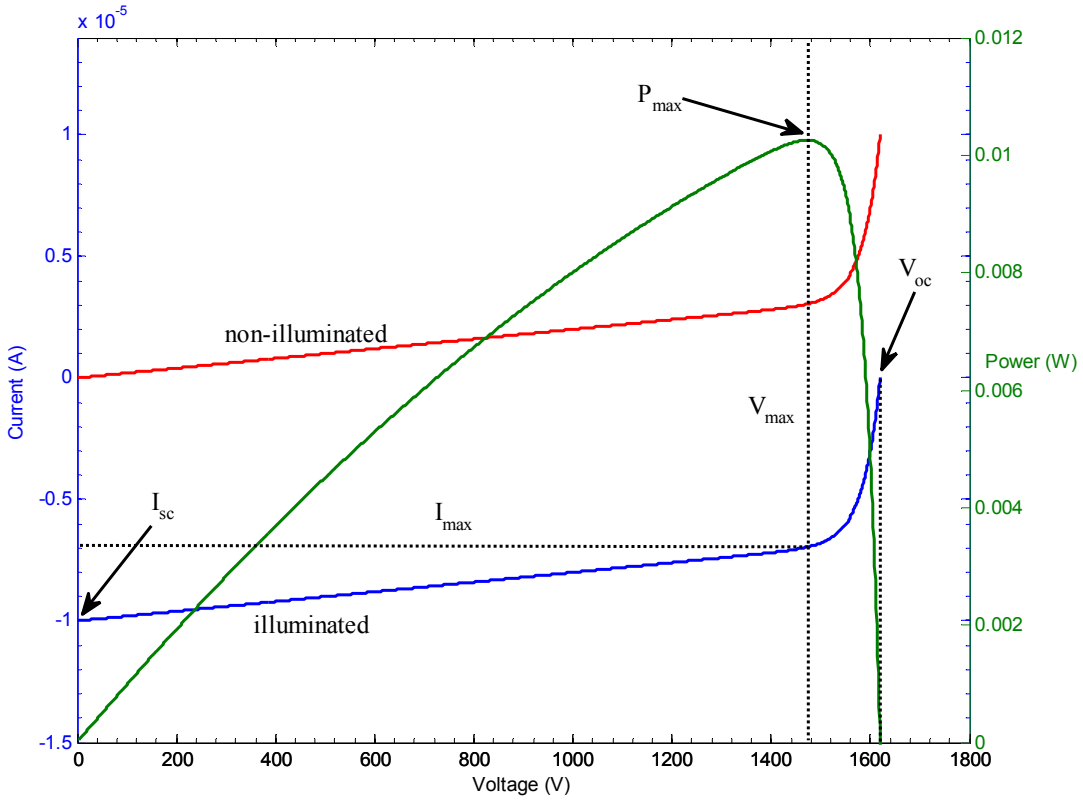

Figure 26: Typical IV curve of an illuminated MPA.

From analysis of MPA I-V and power curves, a general trend can be realized. As Figure 26 shows, short circuit current (I_{sc}) occurs at the point where the output voltage is 0. Here, the short circuit current is equal to the illumination current (I_l). The open circuit voltage (V_{oc}) results when the MPA is connected to a high impedance or open circuit node. The output current is equal to zero, meaning that the illumination current is flowing through all the diodes. The resultant output voltage is the sum of the series diode voltage drops of the entire array. This will be the maximum output voltage of the circuit. In the actual system operation, a high voltage capacitor in parallel with a large resistance

resistor is connected across V+ and is used to store the energy obtained from the conversion of optical (electromagnetic) energy. The green curve in Figure 26 is the current-voltage product of the IV curve. There is a point in the knee where the product of IV is at a maximum value and this is the maximum power (P_{max}) of the device.

The block diagram of the photovoltaic is illustrated in Figure 27 and shows that there are three dynamic variables controlling the output current of this device.

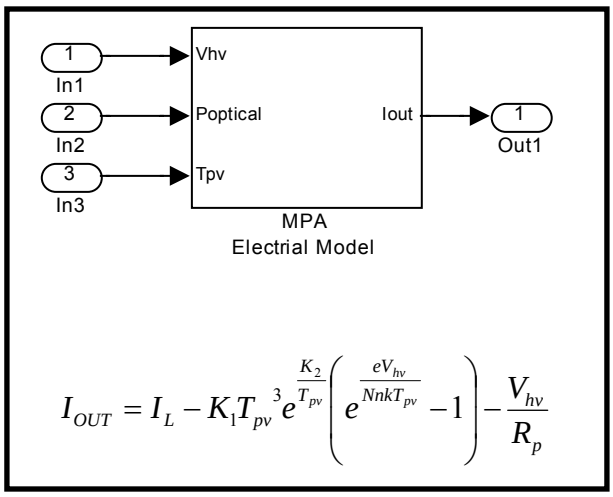

Figure 27: MPA electrical model block diagram with system equation.

3.4.2 Thermal Model

The general derivation of the thermal model follows a similar procedure defined by the development of the diode laser thermal model. The MPC die is mounted in a 40 pin Kyocera leadless chip carrier (LCC). First, the metal ring around the package is removed to minimize potential for high voltage breakdown. The die is then attached with nonconductive die attach adhesive to the ceramic substrate. See Figures 28 and 29.

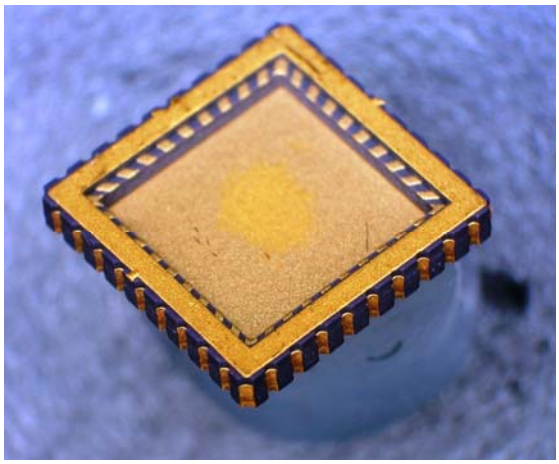

Figure 28: Bare Kyocera 40 pin LCC package. Note: Metal ring around top of package is removed prior to use.

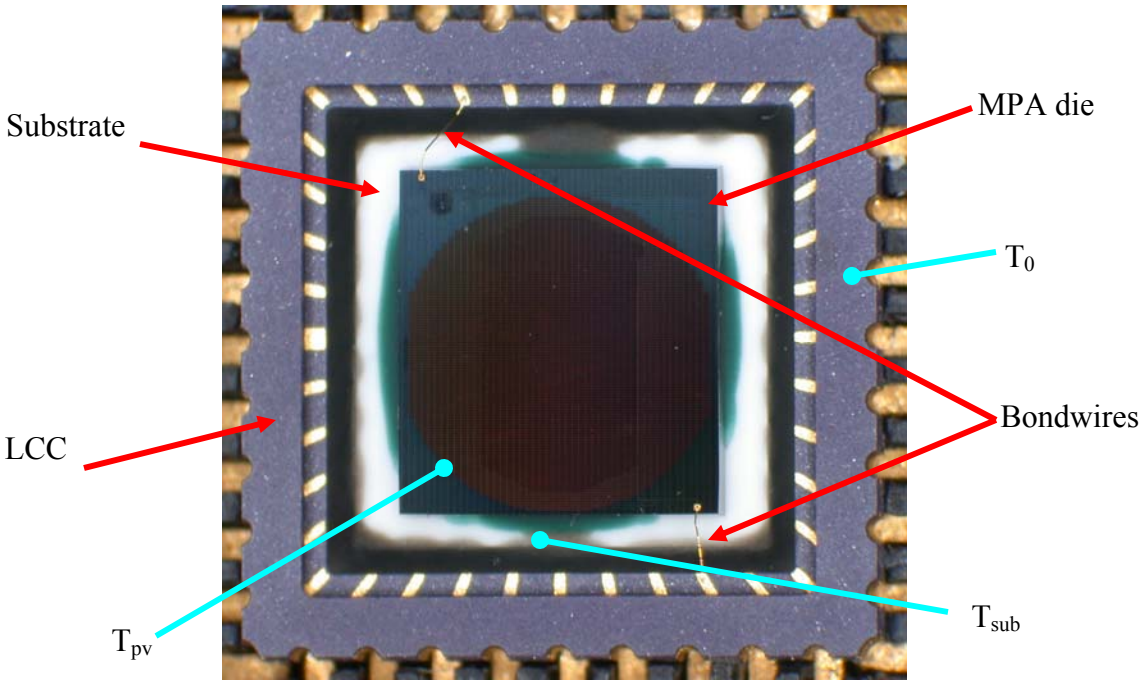

Figure 29: Top view of a packaged MPA die with temperature measurement points.

Two bondwires are used to connect to the anode and cathode. Epoxy is then added to passivate the metal lines that follow the perimeter of the device, bond pads, and die sidewall of the device from high voltage potentials. A special LCC chip carrier socket is used to connect to the device.

Thermal heat transfer begins when the die is illuminated by an optical source. A portion of illuminated power is absorbed by the device and the rest is reflected. A temperature change then results and the heat flows through the MPA die, substrate, and finally the ceramic LCC package. The packaged assembly was then divided into two nodes and the following simplified representation of the packaged MPA was developed.

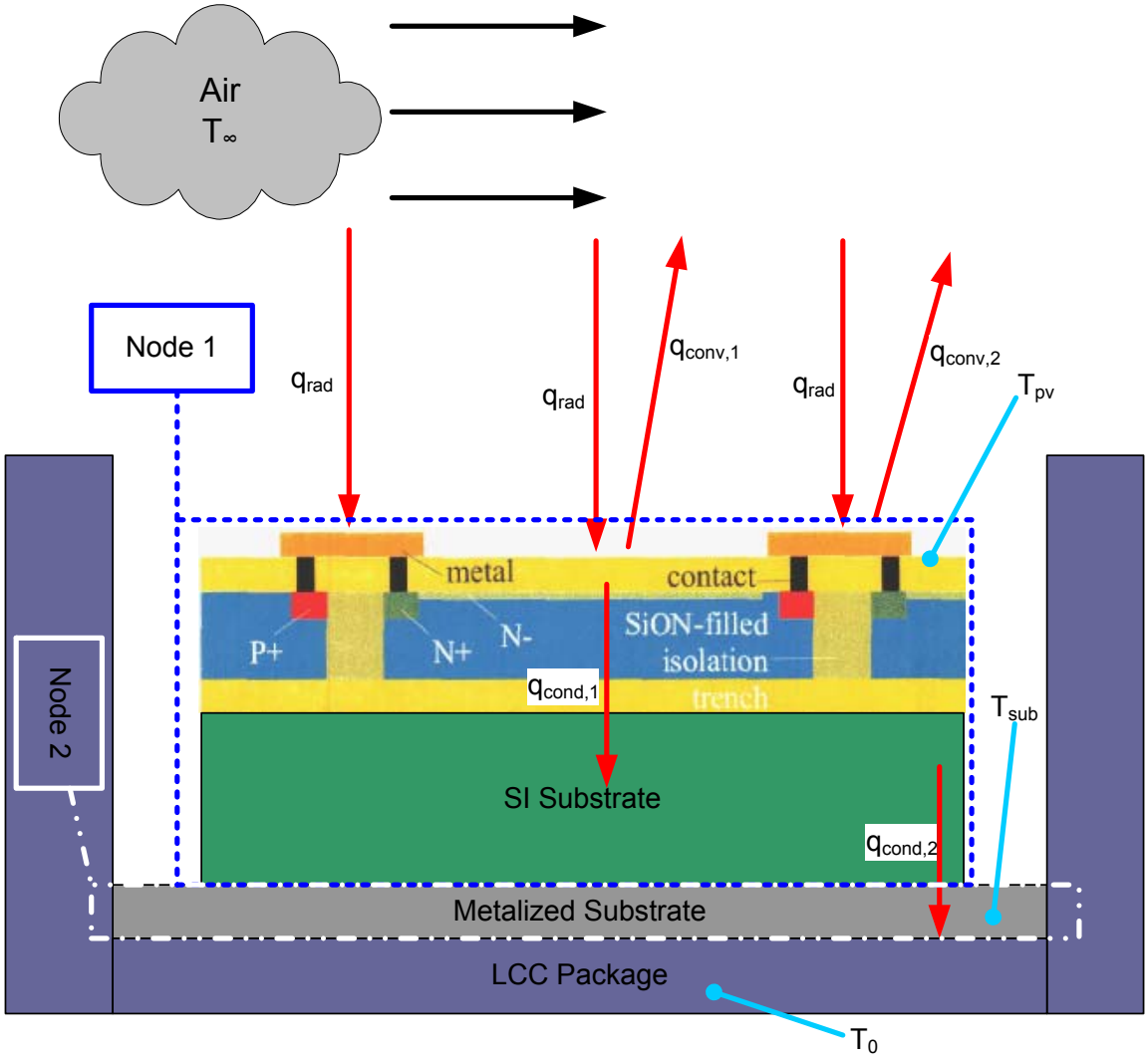

Figure 30: Side view of simplified thermal model for the MPA device mounted to a 40 pin LCC package.

To reduce the number of differential equations for this system, only two nodes were analyzed. Node 1 is the entire layered structure of the MPA die. Node 2 is the metalized substrate material. The following was assumed when developing the thermal model:

1. The temperature at any time (t) in the material is uniform.
2. One-dimensional heat transfer is used since the heat transfer from sides of the chip is negligible.
3. The material properties are constant.
4. The temperature of the LCC package (T_0) will be modeled as being equal to the ambient air temperature (T_∞). This assumption is valid when the MPA is used in its final configuration. Creating another node that includes the convection heat losses of the package can be added to the model if the device is not thermally connected to a large heat sink.

The thermal model will begin by using the First Law of Thermodynamics. Recalling Eq. (3.17), the rate of change of the temperature for the node will be determined at a time instant:

$$\dot{E}_{st} = \dot{E}_{in} - \dot{E}_{out} + \dot{E}_g \tag{3.51}$$

The internal thermal energy rate generation term ($\dot{E}_g$) will be assumed to be negligible since the generated illuminating current (I_L) is small. At maximum input power and at 1 V, the internal power will be less than 70 uW. At $P_{max,}$ as seen in Figure 26, the internal power will be less than 60 mW at full illumination power. Therefore, Eq. (3.51) can be rewritten as:

$$\dot{E}_{st} = \dot{E}_{in} - \dot{E}_{out} \tag{3.52}$$

The input thermal energy rate ($\dot{E}_{in}$) is the amount of energy absorbed by the device from optical radiation (P_{ld}) of the diode laser.

$$\dot{E}_{in} = \left(1 - R_{mat}(\lambda)\right) P_{ld} \tag{3.53}$$

$R_{mat}(\lambda)$ is the reflectivity of a material at a particular frequency. In this case $R_{mat}(\lambda)$ will be the outer Si oxide layer at 810 nm. $R_{mat}(\lambda)$ will be obtained experimentally by using a spectrophotometer that will determine amount of reflection at a given wavelength. Stored thermal energy rate ($\dot{E}_{st}$) is the thermal energy storage due to the temperature change. It is equal to [4]:

$$\dot{E}_{st} = \frac{dU^t}{dt} = \frac{d}{dt}\left(\rho c V_{pv} T_{pv}\right) = \frac{dT_{pv}}{dt} C_{pv} \tag{3.54}$$

Where ρ is the mass density, c is the specific heat, V_{pv} is the volume and T_{pv} is the temperature of the MPA die. The output thermal energy rate term ($\dot{E}_{out}$) is the energy outflow due to convection, conduction, and thermal radiation from Node 1. Using Eqs. (3.15), (3.12), and (3.8) the output thermal energy rate term can be found to be,

$$\begin{aligned} \dot{E}_{out} &= q_{conv} + q_{cond} + q_{rad} \\ \dot{E}_{out} &= \lambda_{a,conv}(T_{pv} - T_{\infty}) + \lambda_{a,cond}(\Delta T_a) + h_r A(T_{abs} - T_{sur}) \end{aligned} \tag{3.55}$$

The term $\lambda_{a,cond}$ represents the thermal conductance between the MPA die and substrate and the term $\lambda_{a,conv}$ represents the thermal conductance for convection between the MPA die and ambient air. Assuming that q_{conv} and q_{rad} provide an insignificant amount of heat transfer $\dot{E}_{out}$ can be further simplified. With these assumptions, Eq. (3.55) can be rewritten as:

$$\dot{E}_{out} = \lambda_{a,cond}(\Delta T_a) \tag{3.56}$$

A differential equation that describes Node 1 can be defined by substituting in Eq. (3.54), (3.56), and (3.53) into Eq. (3.52) to obtain the following heat rate equation.

$$C_{pv}\left(\frac{dT_{pv}}{dt}\right) = -\left[\lambda_{a,cond}\right]\Delta T_a + \left[1 - R_{mat}(\lambda)\right]P_{ld} \tag{3.57}$$

Defining ΔT_a as the temperature difference between the MPA (T_{pv}) and substrate (T_{sub}) and by dividing across the photovoltaic thermal capacitance (C_{pv}), the heat rate equation for Node 1 is:

$$\frac{dT_{pv}}{dt} = \left[\frac{-\lambda_{a,cond}}{C_{pv}}\right]T_{pv} + \left[\frac{\lambda_{a,cond}}{C_{pv}}\right]T_{sub} + \left[\frac{(1 - R_{mat}(\lambda))}{C_{pv}}\right]P_{ld} \tag{3.58}$$

A similar procedure will be followed to obtain the heat rate equation for Node 2. The internal thermal energy rate generation term ($\dot{E}_g$) is not present in this node since there is no conversion from internal to thermal energy. Therefore, Eq. (3.51) can be rewritten as:

$$\dot{E}_{st} = \dot{E}_{in} - \dot{E}_{out} \tag{3.59}$$

The input thermal energy rate ($\dot{E}_{in}$) is the output thermal energy heat rate ($\dot{E}_{out}$) as defined in Eq. (3.56) from Node 1.

$$\dot{E}_{in} = \lambda_{a,cond}(\Delta T_a) \tag{3.60}$$

The stored thermal energy rate ($\dot{E}_{st}$) is the thermal energy storage due to the temperature change and is previously defined in Eq. (3.28) except that V_{sub} is the volume and T_{sub} is the temperature of the ceramic substrate, and C_{sub} is the ceramic substrate thermal capacitance where:

$$\dot{E}_{st} = \frac{dU^t}{dt} = \frac{d}{dt}\left(\rho c V_{sub} T_{pv}\right) = \frac{dT_{sub}}{dt} C_{sub} \tag{3.61}$$

The output thermal energy rate term ($\dot{E}_{out}$) is the energy outflow due to convection, conduction, and thermal radiation from Node 2. Using Eqs. (3.15), (3.12), and (3.8) the output thermal energy rate term can be found to be,

$$\begin{aligned} \dot{E}_{out} &= q_{conv} + q_{cond} + q_{rad} \\ \dot{E}_{out} &= \lambda_{b,conv}(T_{sub} - T_{\infty}) + \lambda_{b,cond}(\Delta T_b) + h_r A(T_{abs} - T_{sur}) \end{aligned} \tag{3.62}$$

This term can also be simplified with the assumption that q_{conv} and q_{rad} are insignificant due to the small physical size of the device. With these assumptions and defining ΔT_b as the temperature difference between the ceramic substrate (T_{sub}) and LCC package (T_0) temperature, Eq. (3.62) can be rewritten as:

$$\dot{E}_{out} = \lambda_{b,cond}(\Delta T_b) = \lambda_{b,cond}(T_{sub} - T_0) \tag{3.63}$$

The differential equation that describes Node 2 can be defined by substituting in Eqs (3.61), (3.60), and (3.63) into Eq. (3.59) to obtain the following heat rate equation.

$$C_{sub}\left(\frac{dT_{sub}}{dt}\right) = \lambda_{a,cond}(T_{pv} - T_{sub}) - \lambda_{b,cond}(T_{sub} - T_0) \tag{3.64}$$

Dividing across by the ceramic substrate thermal capacitance (C_{sub}), the heat rate equation for Node 2 is:

$$\frac{dT_{sub}}{dt} = \left[\frac{\lambda_{a,cond}}{C_{sub}}\right]T_{pv} + \left[\frac{(-\lambda_{a,cond} - \lambda_{b,cond})}{C_{sub}}\right]T_{sub} + \frac{\lambda_{b,cond}T_0}{C_{sub}} \tag{3.65}$$

In summary, the heat balance equations of the MPA is the thermal response due to the absorbed input power (P_{ld}) which causes conductive heat flow within the materials. The temperature of each material is dependant on its ability to store and conduct heat. The block diagram and system equations are shown in Figure 31.

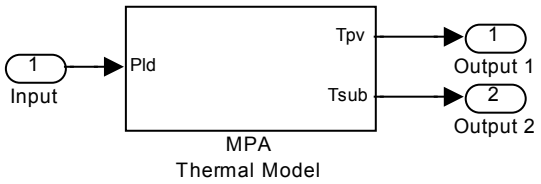

$$\frac{dT_{pv}}{dt} = \left[\frac{-\lambda_{a,cond}}{C_{pv}}\right]T_{pv} + \left[\frac{\lambda_{a,cond}}{C_{pv}}\right]T_{sub} + \left[\frac{(1-R_{mat}(\lambda))}{C_{pv}}\right]P_{pv} \qquad (3.66a)$$

$$\frac{dT_{sub}}{dt} = \left[\frac{\lambda_{a,cond}}{C_{sub}}\right]T_{pv} + \left[\frac{(-\lambda_{a,cond} - \lambda_{b,cond})}{C_{sub}}\right]T_{sub} + \frac{\lambda_{b,cond}T_0}{C_{sub}} \qquad (3.66b)$$

$$\text{Output} = T_{pv} \qquad (3.67)$$

Figure 31: MPA thermal model block diagram with system equations.

3.5 High Voltage CDU

The actual CDU schematic is shown by Figure 32. I_{out} is the output current provided by the MPA during illumination and is depicted as a current source. This current source charges the high voltage capacitor (C_{hv}) and is used to store the energy. The resistors provide a monitoring reference voltage ($V_{hv(1000:1)}$ and V_{ref}) and a pathway to ground for safety. The switch and detonator are used when the trigger signal is given and the capacitor energy is dumped into the detonator. When this occurs, a large current pulse is generated and sent through to activate the detonator.

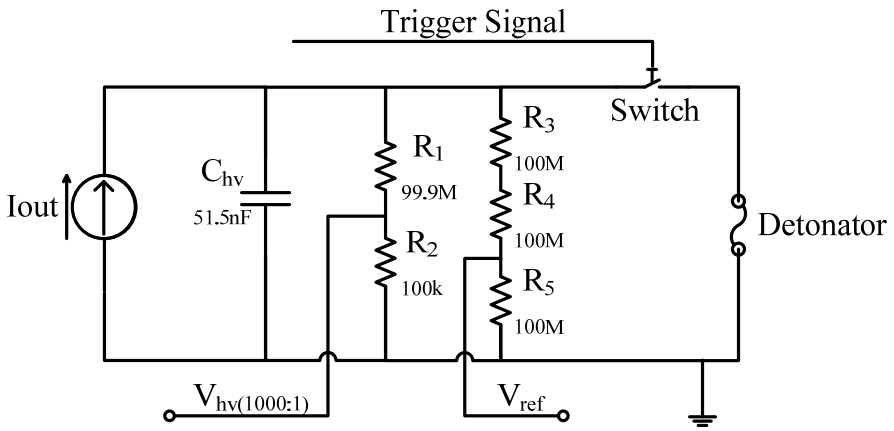

Figure 32: Schematic of the high voltage CDU used in the optical powered firing set.

3.5.1 Electrical Model

The electrical model of the CDU will not include the switch and detonator since they will not be evaluated as part of the control system. They do not affect the electrical characteristics since the switch is open during voltage charging. The series and parallel resistors will be lumped together as a single parallel resistance (R_p) as shown in Figure 33. The input is the current (I_{out}) provided by the MPA and the output is the high voltage (V_{hv}) across C_{hv} and R_P. The transfer function will be obtained by modeling this circuit in the frequency domain.

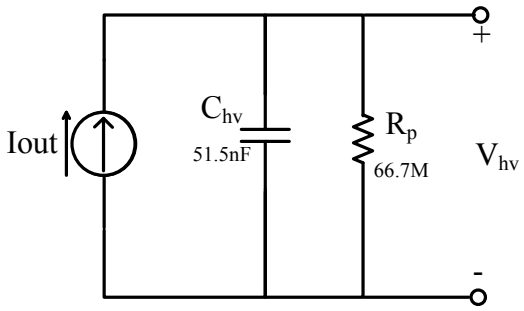

Figure 33: Simplified high voltage CDU schematic.

In this analysis, the Laplace transform is taken for each circuit element to allow the impedance to be calculated for each element. Ordinary circuit analysis techniques are

then used to obtain the transfer function and zero initial conditions are assumed for the passive components. The impedance for a capacitor is [14]:

$$Z_2 = \frac{1}{Cs} \tag{3.68}$$

The impedance (Z_1) for a resistor is R. The Laplace transform of each element for the circuit is shown on the Figure 34.

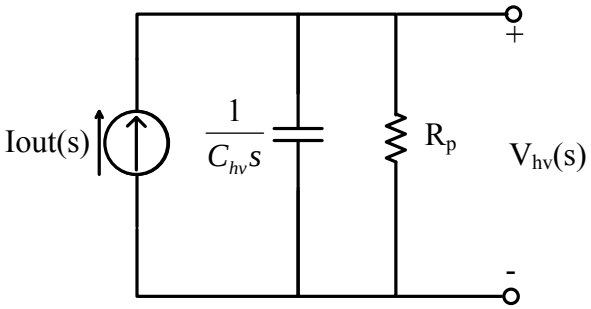

Figure 34: Laplace transform of simplified high voltage CDU model with impedances of the passive components.

The parallel combination of the capacitor and resistor can be lumped together as the total impedance of the circuit (Z_t). The total impedance calculation for two circuit impedances is the product of the two individual impedances divided by their sum. In equation form:

$$Z_t = \frac{Z_1 Z_2}{Z_1 + Z_2} \tag{3.69}$$

For this circuit the total impedance is:

$$Z_t = \frac{R_p \dfrac{1}{C_{HV}s}}{R_p + \dfrac{1}{C_{HV}s}} \tag{3.70}$$

From Figure 35, the output voltage is simply the product of the input current and total impedance.

$$V_c(s) = I_{sp}(s)Z_t \tag{3.71}$$

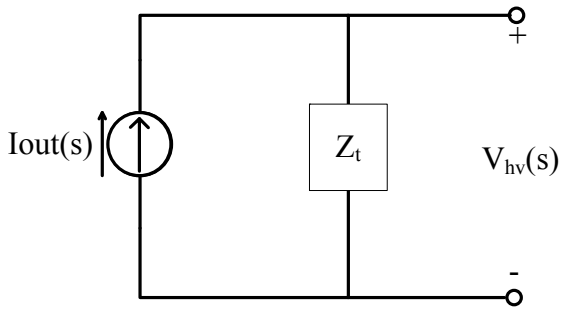

Figure 35: Simplified schematic of the CDU model with total impedance.

The transfer function is the output divided by the input. Therefore, the total impedance is the transfer function. After simplifying Eq. (3.70) the following is obtained and the block diagram is shown in Figure 36.

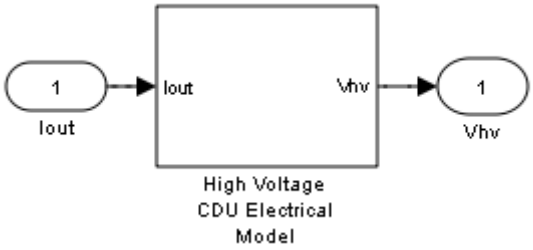

$$G(s) = \frac{V_c(s)}{I_{sp}(s)} = \frac{\dfrac{1}{C_{HV}}}{\left(s + \dfrac{1}{R_p C_{HV}}\right)} \tag{3.72}$$

Figure 36: High voltage CDU block diagram with transfer function.

3.6 Diode Laser Driver Current Source

A precision current source was used to provide the necessary current to the diode laser. An ILX Lightwave, model LDX-3565 instrument was chosen. This device is able to

output up to 6 A and allow analog modulation through voltage control. The user's guide specified the transfer function for modulation of 600 mA/V which was used in the model and is shown in Figure 37.

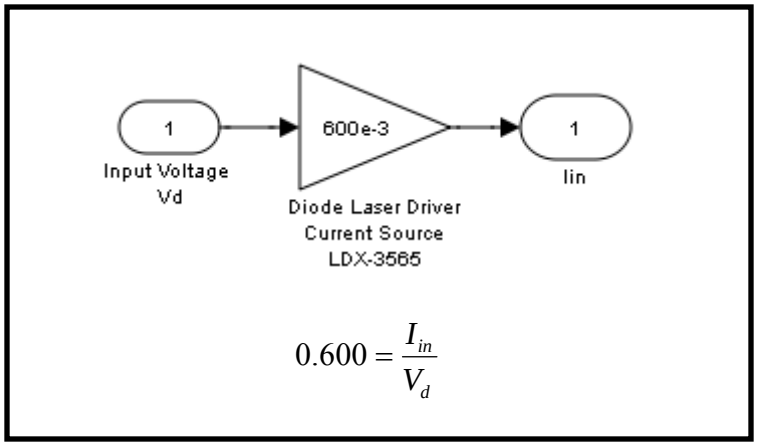

$$0.600 = \frac{I_{in}}{V_d}$$

Figure 37: Current source for the diode laser block diagram and transfer function.

4. MODELING VERIFICATION WITH EXPERIMENTAL DATA

The completed set of models for the optically powered firing set were each implemented in a numeric solver and then compared to actual test data to verify that the model is representative of the component. MATLAB was first used to solve the ordinary differential equations (ODE) using an ODE solver and the results were used to verify that the basic mathematical structure was correct. These models were then used to build individual blocks in Simulink. Simulink provides an environment to model physical systems with the connection of standard Simulink blocks. Some of the model's unknown parameters were then tuned to fit actual test data. After the individual blocks were complete, they were connected together to build the entire plant.

4.1 Diode Laser

Three diode lasers were used to gather data for validation. They were JUM 3000_105_20 with serial number R00354_04 and JOLD-3-BAFC-11 with serial numbers EK-08211 and EK-08207. The first device was made by Jenoptik and the second two are made by Unique Mode. Unique Mode was purchased by Jenoptik group's Laser&Optik division in 2006 and since then they have changed their name to Jenoptik unique-mode GmbH. They are all identical in terms of geometry and output. Diode laser power curves were taken for each device since that is the most fundamental characteristic of device performance and operation. All optical output test data was measured from a Scientech AC 2501H Power Head and a Scientech Vector D200 power meter. An ILX Lightwave LDX-3565 Precision Current Source was used as the input source. The JUM-3000_105_20 diode laser was initially used to set up the prototype optically powered firing set before it was damaged from a high input current pulse. Serial number EK-

08211 was then used for all further testing and EK-08207 was a backup. All data measured and compared to the simulated model is from serial number EK-08211. Figure 38, (a) and (b) shows the diode laser Simulink models used in the model verification.

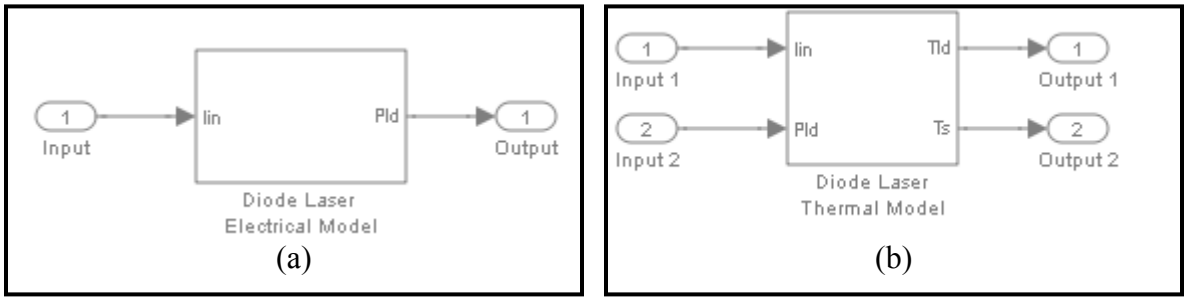

Figure 38: Diode laser models used in verification. (a)electrical model and (b) is the thermal model.

4.1.1 Electrical Model

The set of ODE's from Eq. (3.24) cannot be solved analytically and must use a numerical method to solve. MATLAB's ordinary differential equation solver, which uses a Runge-Kutta method (ODE45), was used. Since the parameters of the 3W laser diode were not yet known, a set of predefined parameters listed in Table 5 were obtained [8]. These parameters were derived from an InGaAs/GaAs Fabry-Perot diode laser and used in the testing of the diode laser electrical model.

Parameter	Description	Value	Units
η_i	injection efficiency	0.8	none
q	electron charge	1.60E-19	C
V	volume of carrier reservoir (active area)	4.00E-12	cm^3
τ	differential carrier lifetime	2.71E-09	s
v_g	group velocity	7.14E+09	cm/s
Γ	confinement factor	3.20E-02	none
V_p	volume of photon reservoir	1.25E-10	cm^3
τ_p	differential photon lifetime	2.77E-12	s
η_o	optical efficiency of laser	0.45	none
R'_{sp}	spontaneous emission rate into 1 optical mode	1.02E+23	cm^{-3}/s
g_o	empirical gain coefficient	1800	1/cm
N_s	gain linearity parameter	-4.00E+17	$1/cm^3$
N_{tr}	transparency carrier density	1.80E+18	$1/cm^3$
hv	energy per photon at desired wavelength	2.03E-10	J/photon
d	thickness	80A	m
w	width	2u	m
L_a	Active section length	250u	m
L	Length for photons	250u	m

Table 5: Parameters of the electrical model for an InGaAs/GaAs diode laser [8].

The numerical calculation results as seen on Figures 39, 40, and 41, match the characteristic large signal modulation output [8]. A step input was applied to the model. Steady state response was also performed on the output power and photon density with given parameters and returned a percent error of 0.079% and 0.6293% respectively.

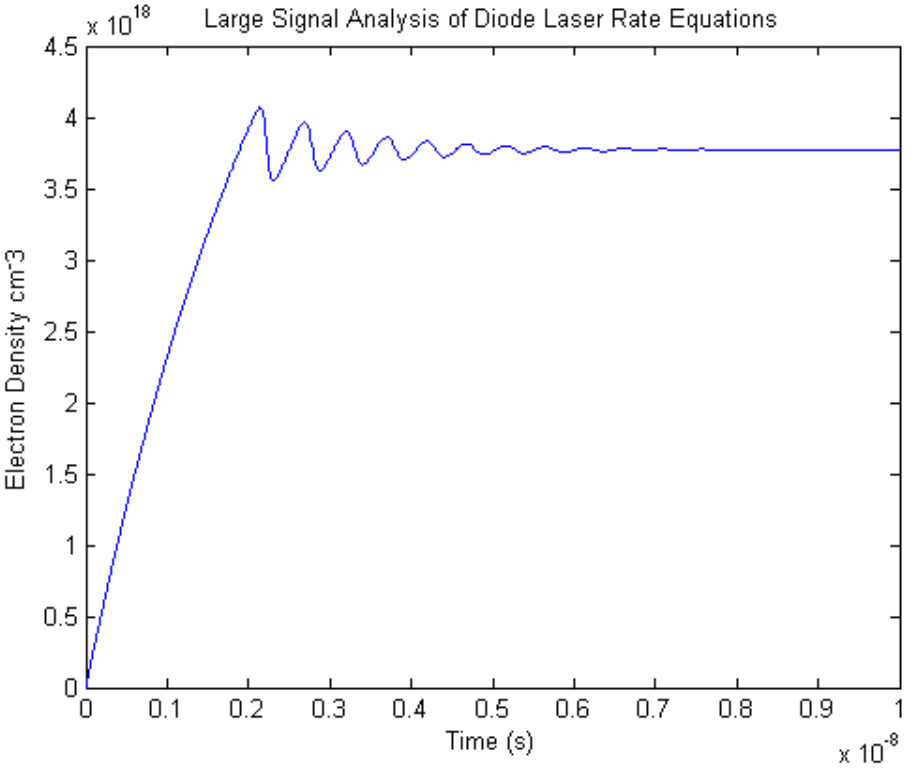

Figure 39: Electron Density (N) of an InGaAs/GaAs Fabry-Perot Laser.

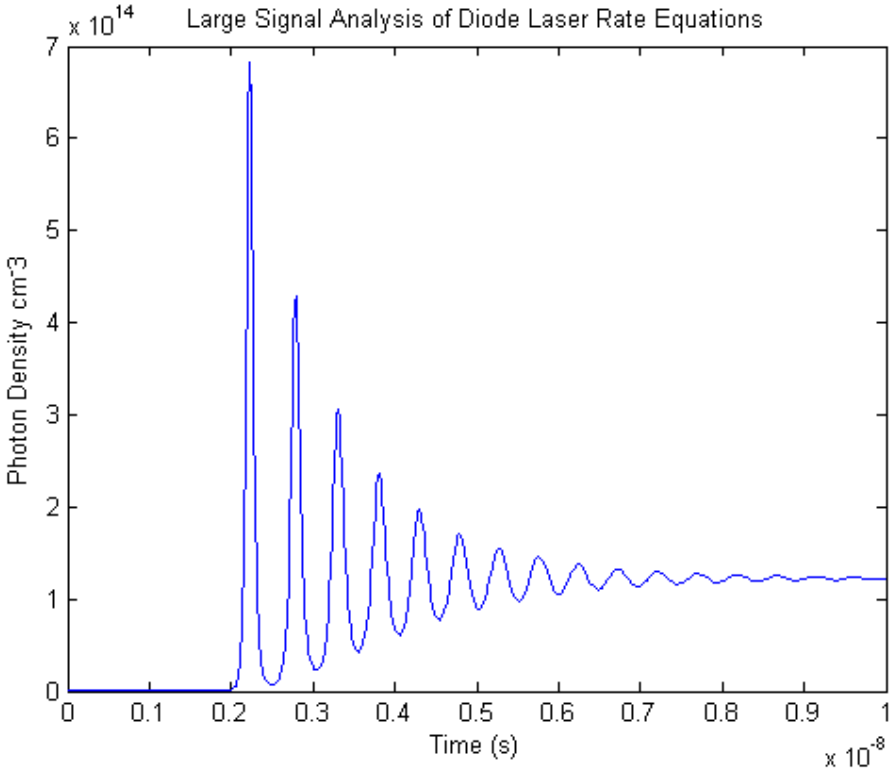

Figure 40: Photon Density (N_p) of an InGaAs/GaAs Fabry-Perot Laser.

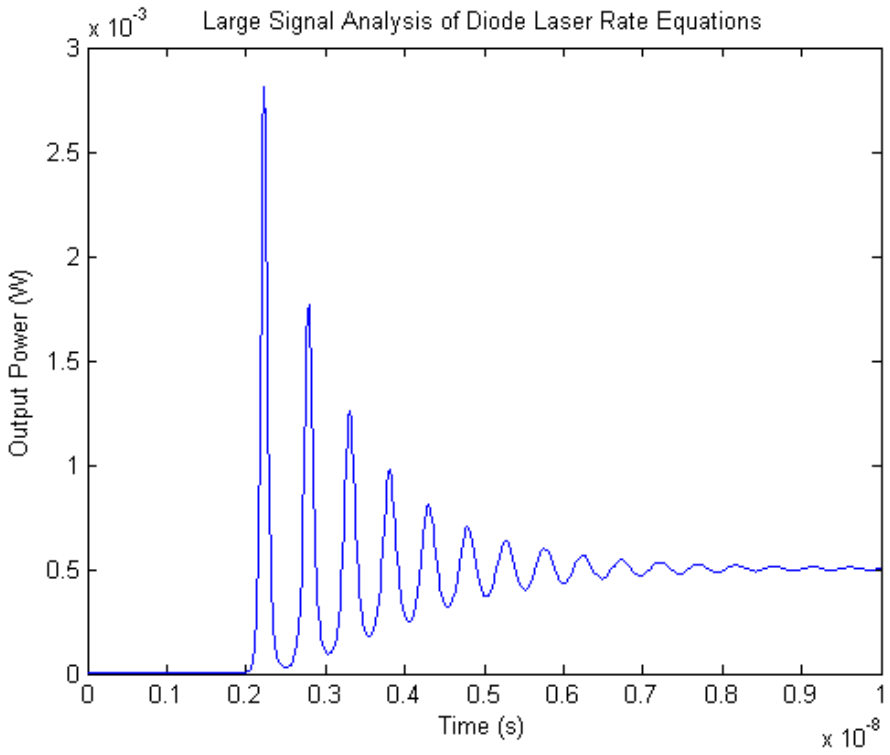

Figure 41: Optical output power for an InGaAs/GaAs Fabry-Perot Laser.

The small error proved that the electrical model from a steady state point of view is accurate. From Figures 39, 40, and 41, the carrier density initially increases as the carrier begins to fill. A small amount of photon density happens due to spontaneous emission, but the majority of the photon density output happens when the carrier reservoir reaches its threshold level. At this point stimulated emission is dominating, thus a large and rapid increase in photon emission occur as seen around 2 nsec in Figure 40. When the photon emission transpires, the carrier density will decrease slightly because charge is lost in the process of stimulated emission. With the decrease in carrier density below threshold, photon density output rapidly decreases which then allows the carrier density to build back up. This process repeats and is called frequency chirping [8]. Frequency chirping happens for a short amount of time until a steady state condition results. Direct

experimental measurement of the electron density and photon density in the time regimes presented in Figures 39, 40, and 41 could not be completed since these measurements are uncommon and require expensive and specialized systems to measure.

4.1.1.1 Calculation and Estimation of Electrical Model Parameters

Parameters listed in Table 3 need to be determined since they are specific to the diode laser that is used for experimental data. Some parameters that can be calculated from data and measurements include threshold current (I_{th}), differential quantum efficiency (η_d), mirror loss (α_m), and mean mirror reflectivity (R). Parameters such as net internal optical loss $\langle \alpha_i \rangle$ and injection efficiency (η_i) can only be measured by using multiple lasers with varying lengths [8]. Therefore, only a limited number of parameters can be calculated and the rest will be estimated and then tuned to fit the experimental data.

A power-current (P-I) curve is first obtained from the diode laser to determine the experimental threshold current (I_{th}) which occurs when stimulated emission dominates over spontaneous emission for the P-I curve as shown in Figure 44. This happens at the knee of the curve. The slope of the P-I curve after the threshold current is used to determine η_d which is the number of photons out per electron and leads to

$$\eta_d = \left(\frac{q}{h\nu}\right)\frac{\Delta P_o}{\Delta I} \tag{4.1}$$

q is the charge of a electron, hv is the energy per photon, and $\frac{\Delta P_o}{\Delta I}$ is the slope of the curve. The energy per photon is defined as

$$h\nu = \frac{hc}{\lambda} \tag{4.2}$$

h is Planck's constant, c is the speed of light, and λ the laser operational wavelength. The injection and optical efficiency are also related to the differential efficiency by

$$\eta_d = \eta_i \eta_o \tag{4.3}$$

Volumes of the carrier (V) and photon reservoir (V_p) are then found by measuring the dimensions of the laser diode bar as seen in Figure 16. Additionally, Γ is

$$\Gamma = \frac{V}{V_p} \tag{4.4}$$

The remaining parameters cannot be determined from measuring a single packaged diode laser and therefore the values were estimated and then tuned as necessary when comparing the simulated to experimental data. The parameters η_i and η_o were obtained from characteristic data for Large Optical Cavity (LOC) AlGaAs diode laser structures [10]. These values were used as they are a close match to the actual experimental diode lasers. The gain coefficient (g_o) and the two linearity gain parameters (N_{tr} , N_s) were obtained from curve fits as defined in [8] since an analysis of the gain curves were not part of this design. The photon differential lifetime (τ_p) and Spontaneous Emission Rate (R'_{sp}) parameters were unknown and estimated from a list of common parameters for In-Plane Lasers [8]. Photon differential lifetime (τ_p) is photon losses that are due to optical absorption and do not affect large signal output diode lasers. Furthermore, the R'_{sp} is typically small for power diode lasers so these values are not important driving characteristics of the devices since they typically have low spontaneous-emission factors [10]. After a few iterations of running the model in Simulink and comparing to experimental data, the following parameters listed in Table 6 were obtained.

Parameter	Description	Value	Units
η_i	injection efficiency	0.8	none
q	electron charge	1.60E-19	C
V	volume of carrier reservoir (active area)	6.48E-07	cm^3
τ	differential carrier lifetime	2.28E-06	s
v_g	group velocity	7.14E+09	cm/s
Γ	confinement factor	1.30E-02	none
V_p	volume of photon reservoir	4.97E-05	cm^3
τ_p	differential photon lifetime	2.77E-12	s
η_o	optical efficiency of laser	0.673	none
R'_{sp}	spontaneous emission rate into 1 optical mode	1.00E-24	cm^{-3}/s
g_o	empirical gain coefficient	1800	1/cm
N_s	gain linearity parameter	-4.00E+17	$1/cm^3$
N_{tr}	transparency carrier density	1.80E+18	$1/cm^3$
hv	energy per photon at desired wavelength	2.45E-19	J/photon
d	thickness	6.00E-05	m
w	width	460u	m
L_a	Active section length	1800u	m
L	Length for photons	1800u	m

Table 6: Parameters of the electrical model for a JOLD-3-BAFC-11 S/N#: EK-08211 diode laser.

4.1.1.2 Electrical Model Verification

Simulated optical output power was obtained from the model by entering 53 separate current values into the Simulink Diode Laser Electrical Model and running for one second. The model uses an ode23s solver which is a solver for stiff problems since the solution to the model becomes stiff as it approaches the steady state. These values were then compared to the experimental optical output data as illustrated in Figure 42. The fundamental characteristic power curve for both the experimental and simulated data are a close match. The maximum deviation between the two curves is 0.098 W at 2700 mA which corresponds to a 5.6% error.

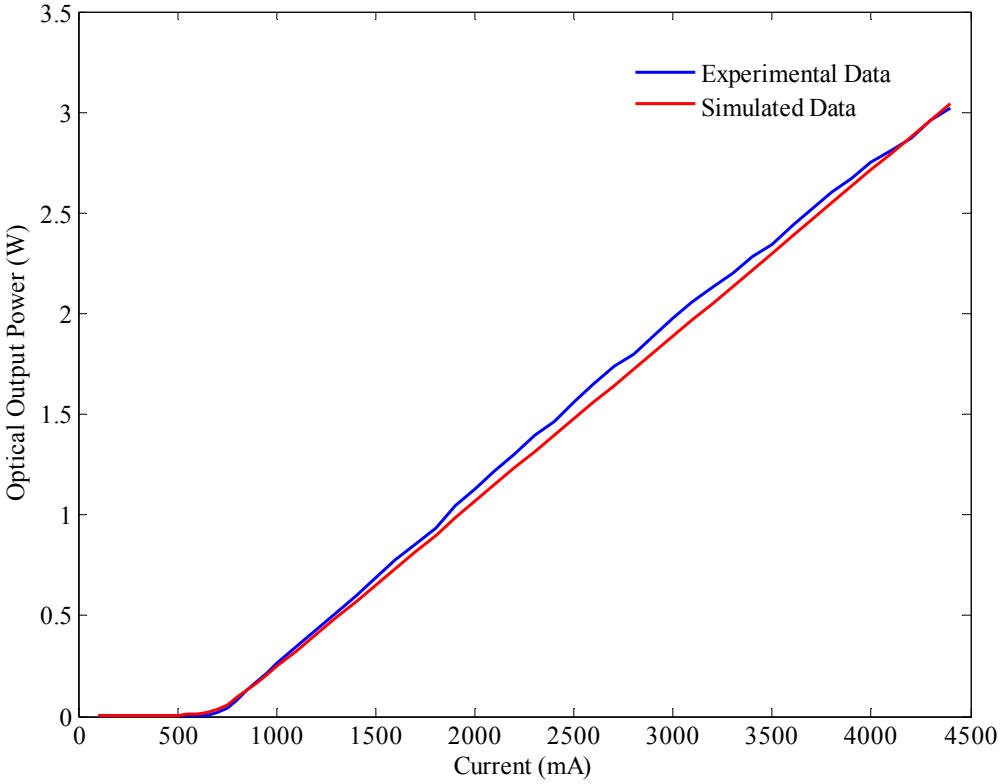

Figure 42: Simulated and experimental output power versus current for the JOLD-3-BAFC-11 (S/N#: EK-08211) diode laser.

A step response analysis could not be conducted due to the electrical limitations of the diode laser current driver. The fastest rise time for the current pulse was about 150ns and most of the frequency chirping characteristics happens within 10ns. Equally, an accurate turn on delay comparison could not be conducted because of hardware limitations. Since the diode laser is used in a constant width (CW) mode, these parameters do not affect the final output of the system. A ramp pulse was then used to test the input response and Figure 43 illustrates the result.

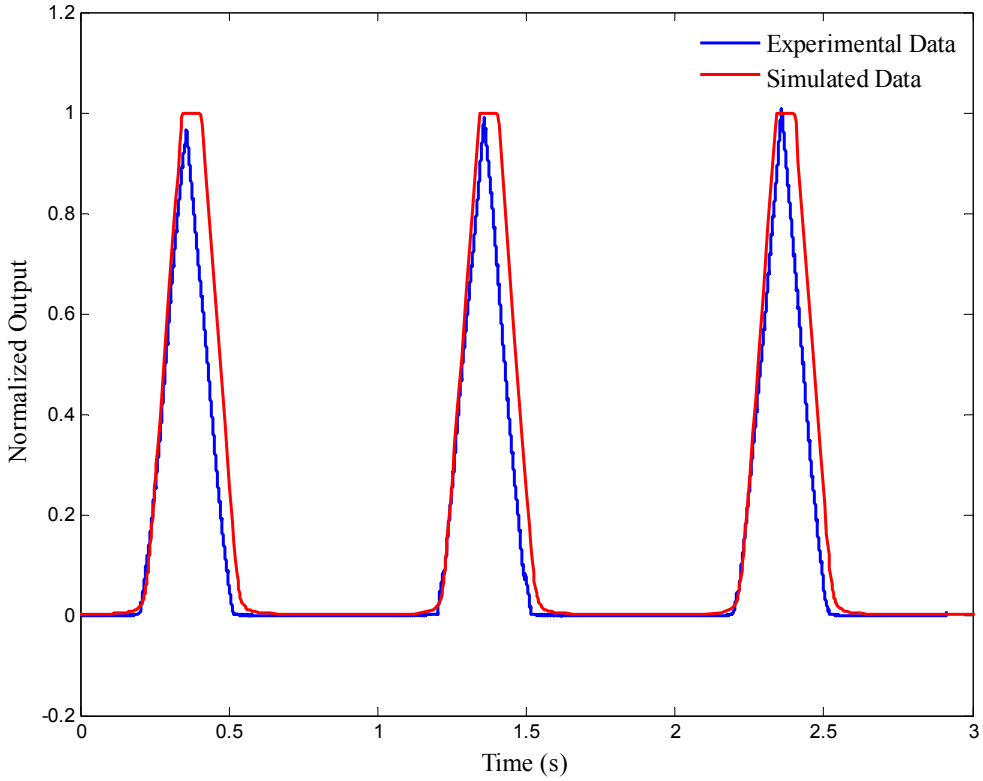

Figure 43: Input response of simulated and experimental output data when the diode laser is driven by a ramp current pulse. A det210 photodiode was used to capture the optical output. The output was normalized to provide easy comparison since the photodiode data was not converted to output optical power.

From Figure 43, the initial rise time matches well and the only deviation is the point at which the output begins to fall off. This is due to the difference between the experimental and simulated input current waveform. The simulated input current waveform was estimated from the values of the function generator and experimental output current response. Therefore, it can be determined that the input response characteristics of the model and experimental data closely match. The data from the power curve and input response show that the electrical model represents the data reasonably well.

4.1.2 Steady State Response

The rate equations can also be used to calculate the steady state electrical/optical output characteristic of diode lasers. When the laser diode is operating in the steady state mode the carrier and optical densities do not change, which allows:

$$\frac{dN}{dt} = 0 \; and \; \frac{dN_p}{dt} = 0 \tag{4.5}$$

The output response will be vastly different depending on the input current since the carrier density needs to be large enough to allow for stimulated emission. The level at which this occurs is called threshold current (I_{th}) as shown in Figure 44. Therefore, steady state response can be broken down into two groups: 1) input current less than the threshold current and 2) input current greater than the threshold current.

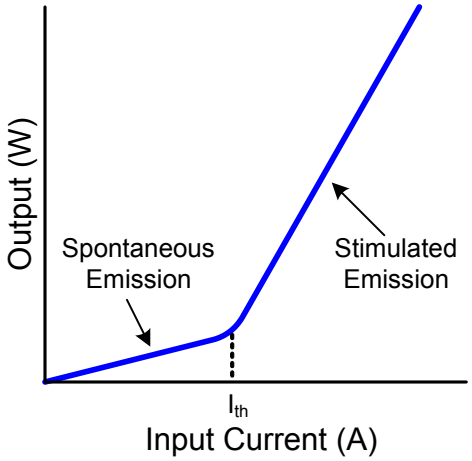

Note: Spontaneous emission output is exaggerated to show the transition to stimulated emission

Figure 44: Typical PI curve for a diode laser.

1) Input current greater than threshold current ($I > I_{th}$).

   By rearranging the rate equations when the input current is above threshold (I_{th}) an equation for photon density can be realized [10,8].

$$N_p = \frac{\eta_i (I - I_{th})}{q v_g g_{th} V} \qquad (I > I_{th}) \tag{4.6}$$

With these conditions, the carrier (N) and photon (N_p) densities can be found. For a general diode laser, the photons leaving through the mirrors equal the laser output. This output is the stored optical energy (E_{os}) in the cavity and the energy loss of the mirrors ($\frac{1}{\tau_m}$) is the following where [8]:

$$E_{os} = N_p h\nu V_p \tag{4.7}$$

$$v_g \alpha_m = \frac{1}{\tau_m} \tag{4.8}$$

$$P_o = E_{os} \frac{1}{\tau_m} \tag{4.9}$$

The output power can be solved with a few substitutions to form Eq. (4.10). This equation illustrates that input current is proportional to the output. The term η_d is the differential efficiency and is the differential increase in diode laser emitted photons per time divided by differential increase of input carriers per time. The term hv is the energy per photon. The output power is therefore:

$$P_o = \eta_d \frac{h\nu}{q}\left(I - I_{th}\right) \tag{4.10}$$

2) Input current is less then the threshold current ($I < I_{th}$)

In this state stimulated emission does not occur, therefore N_p from Eq.(3.24b) can be found [8]:

$$N_p = \Gamma B_{sp} R_{sp} \tau_p \qquad (I < I_{th}) \tag{4.11}$$

The output power is then found to be:

$$P_o = \eta_r \eta_i \left(\frac{\alpha_m}{\langle \alpha_i \rangle + \alpha_m} \right) \frac{h\nu}{q} \beta_{sp} I \tag{4.12}$$

The power curve in Figure 42 shows the comparison between the steady state response of the diode laser model and experimental data. The optical power meter displays the steady state output and the simulated data was obtained at its steady state value. Therefore, the steady state response between the model and experimental data are similar.

4.1.3 Thermal Model

Output optical power (P_{ld}) and input current (I_{in}) are the two inputs to the thermal model. The model also needs the input voltage to determine the input power (P_{in}). Since the I-V characteristic curve for a typical diode laser is linear for currents above the threshold level, a linear equation was used in the model to predict the voltage level. A voltage measurement was taken with a calibrated Fluke 189 DMM from different input current levels and a VI characteristic curve was obtained as shown in Figure 45. A linear equation was obtained from curve fitting the data: The slope was adjusted to allow for the x variables to be in amps instead of milli-amps. The fitted line had an R^2 value of 0.9986 showing goodness of the curve fit. This voltage estimation is only for values above the threshold current level of 700mA. The normal operation of the diode laser is always above threshold current, therefore the linear estimation is valid.

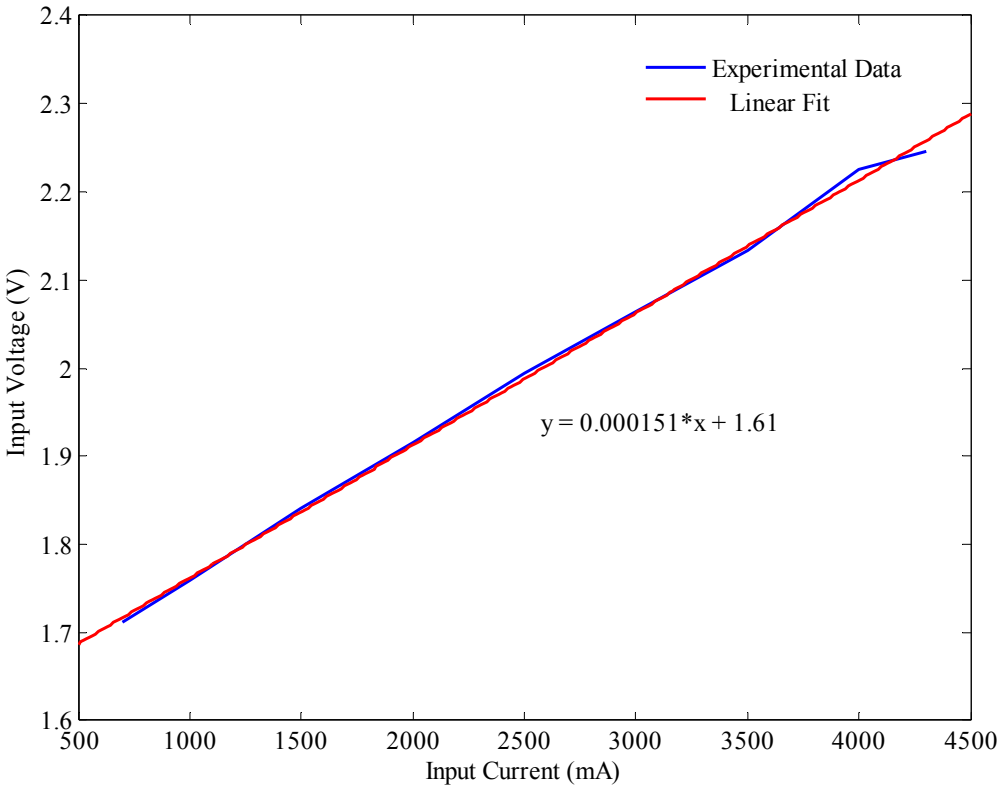

Figure 45: Experimental VI curve for the diode laser when using the ILX 3565 precision current source.

The experimental diode lasers are fully enclosed therefore the lid had to be removed to allow access to place micro miniature thermocouples to the device. Two thermocouples were used to measure the temperature of the laser diode bar (T_{ld}) and the temperature of the substrate (T_s). Omega® fine wire thermocouples were chosen for their small size and availability. A small amount of epoxy was placed on the thermocouple to ensure direct contact with the surface at all times. Figures 46 and 47 show the actual experimental setup and Figure 47 shows the placement of the thermocouples.

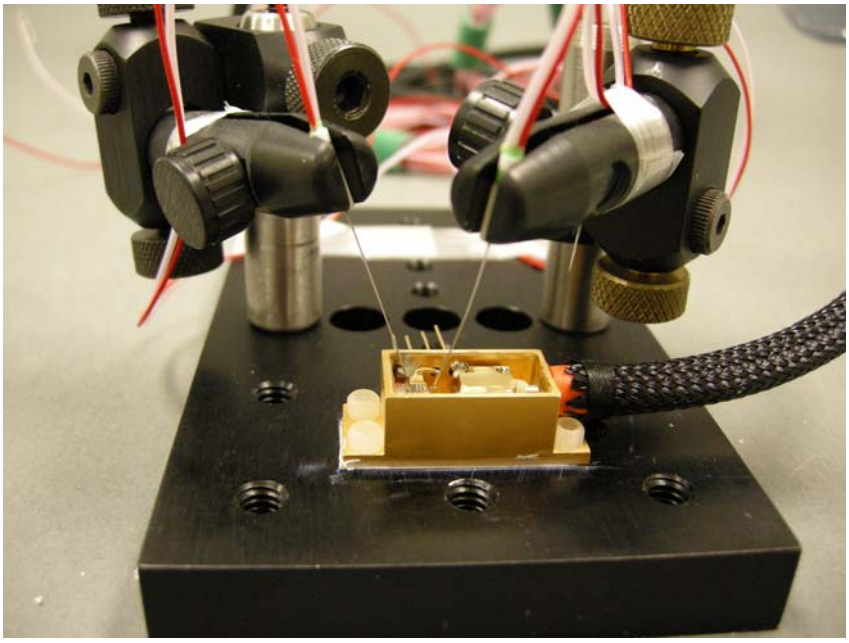

Figure 46: Side view of the diode laser with 2 thermocouples used to measure T_{ld} and T_s.

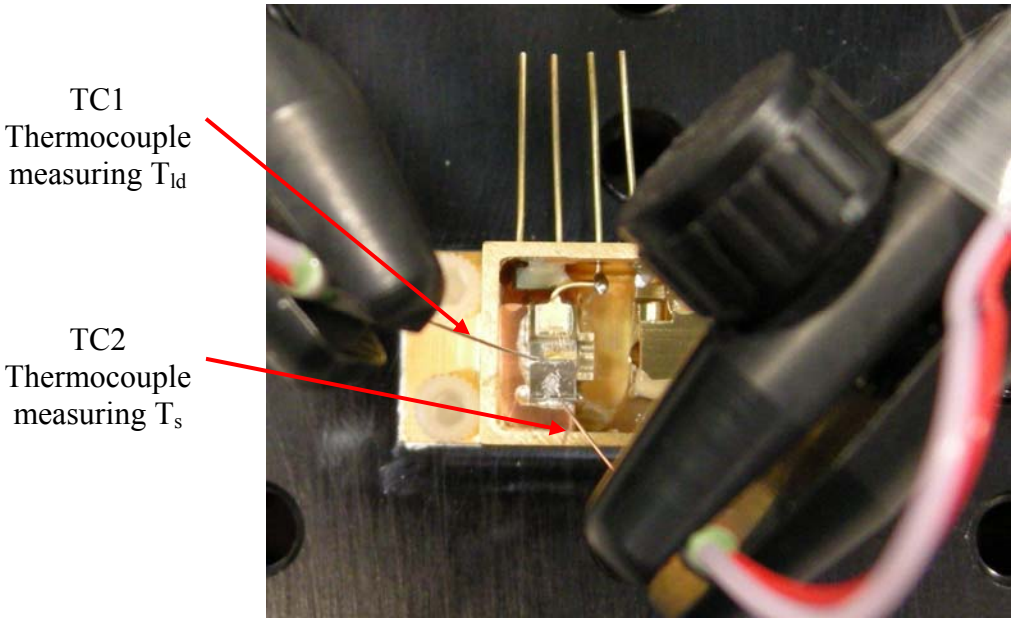

Figure 47: Top view of diode laser with 2 thermocouples used to measure T_{ld} and T_s.

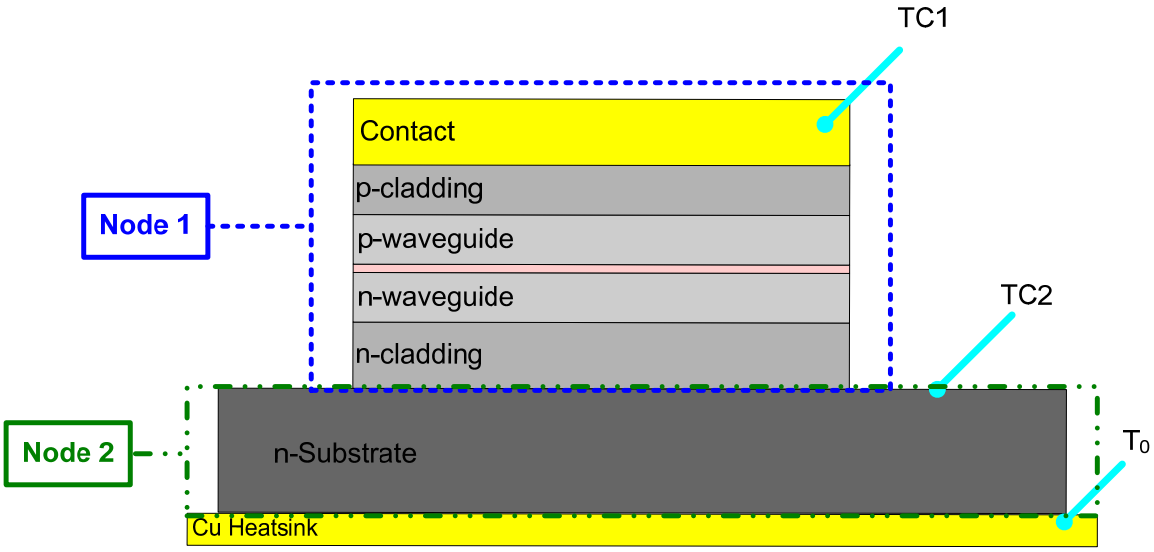

Figure 48: Schematic view of the location of thermal probes used to measure temperature of the diode laser. The heatsink or T_0 temperature is assumed to be at constant room temperature.

Thermocouple Name	Measurement Description	Measurement Type
TC1	Laser Diode Bar Temperature (T_{ld})	K
TC2	Substrate Temperature (T_s)	K

Table 7: Thermocouple measurement details for the diode laser.

Table 7 defines the thermocouple details used in the experiment. Several calibrated Fluke 189 DMM's were used to acquire temperature measurements and set to record every second.

4.1.4.1 Calculation and Estimation of Thermal Model Parameters

The first parameter of the thermal model that can be calculated from experimental temperature data is the thermal conductance of Node 1. A resistance measurement on the precision current source output cable was made on a calibrated Valhalla Scientific Inc. Model 4100 ATC Digital Ohmmeter to include the power loss of the cabling. Eleven input current values were injected into the diode lasers for about 200 seconds and

temperature data was gathered. The temperature output for each input level had the characteristic heating curve, steady state condition, and cooling curve as seen in Figure 49.

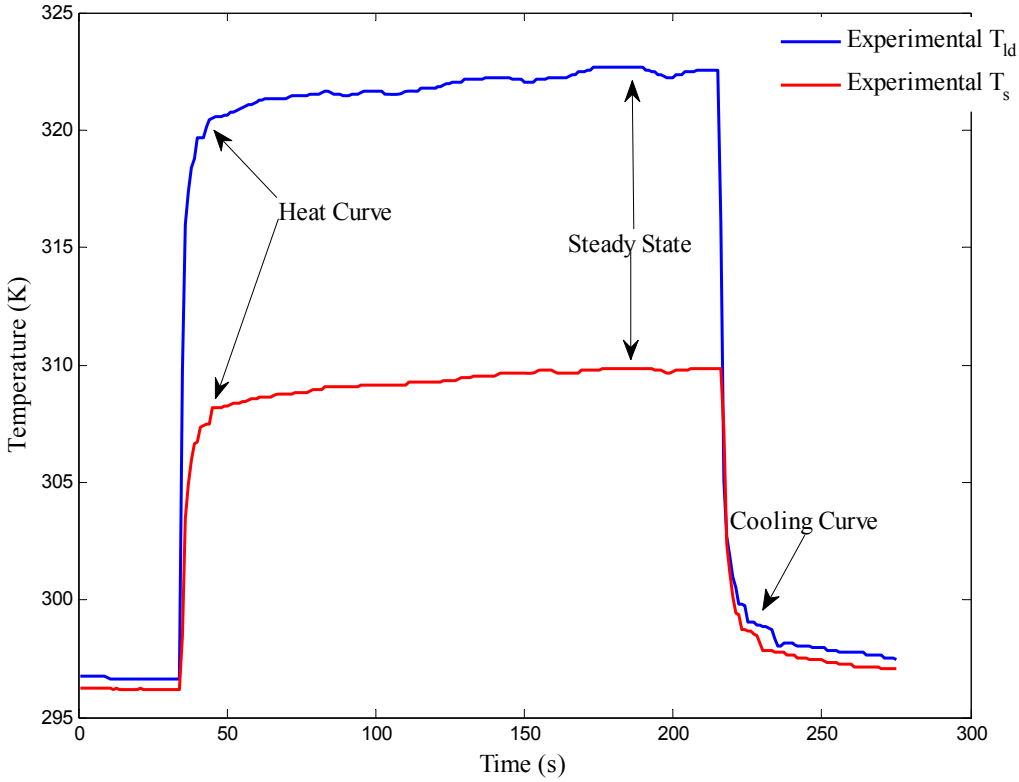

Figure 49: Experimental heat curves for the diode laser at 4300mA input current.

The steady state temperature for each measurement was found and the temperature difference versus thermal power was plotted to obtain the estimated conductance of Node 1. Thermal conductance is found to be:

$$\frac{1}{\lambda_{1,cond}} = \frac{\Delta T}{P} \tag{4.13}$$

ΔT is the difference between the laser diode bar temperature (T_{ld}) and the substrate temperature (T_s) and P is the thermal power. A curve fit of the data was conducted, as

seen in Figure 50. The reciprocal of the slope is the thermal conductance for Node 1 and was calculated to be 0.292 (W/K).

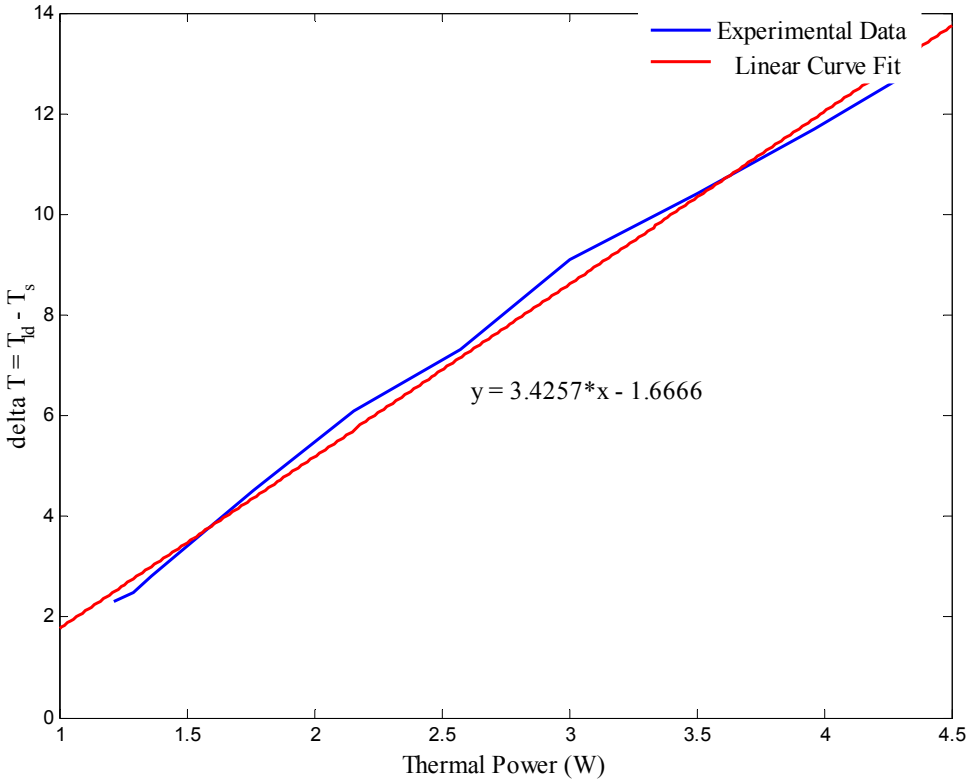

Figure 50: Experimental thermal conductance curve for the diode laser.

The three additional parameters of the heat rate equation cannot be experimentally calculated. The thermal power to Node 2 cannot be measured, therefore the thermal impedance of the substrate material ($\lambda_{2,cond}$) cannot be calculated. It was assumed that this value would be less than the thermal impedance of the laser diode bar ($\lambda_{1,cond}$) since the thermal power to the substrate is greatly reduced. The initial thermal capacitance values were obtained from the work done on distributed feedback semiconductor laser diodes [2]. The model was simulated and the parameters were tuned to fit the experimental data. In the tuning process, the adjustment of the thermal impedance was

inversely proportional to the output temperature and the thermal capacitance values controlled the rise time of the temperature. Table 8 shows the initial and final tuned values.

Parameter	Description	Initial value	Final Tuned Value	Units
$\lambda_{1,cond}$	thermal conductance between laser and substrate	0.292	0.36	W/K
$\lambda_{2,cond}$	thermal conductance between substrate and heat sink	0.192	0.34	W/K
C_{ld}	thermal capacitance of laser [C]	0.1396	0.3	J/K
C_s	thermal capacitance of substrate [C]	0.1819	0.5	J/K

Table 8: Thermal parameters for the JOLD-3-BAFC-11, serial number: EK-08211 diode laser.

4.1.4.2 Thermal Model Verification

Multiple values of current and power were injected into the diode laser model and simulated output data was gathered. Figure 51, (a) and (b), shows a sampling of the simulated and experimental temperature curves of the laser and substrate for two different input current conditions. It is important to point out that there is a slight positive slope on the experimental temperature curves due to the fact that the heat sink temperature was assumed to be room temperature. In reality, a small amount of heating occurs to the heat sink. This characteristic could be removed during the experimental testing if the diode laser was attached to a surface with constant temperature such as a Peltier cooler. The heat model could also be adjusted to include a third node to account for this increase in temperature.

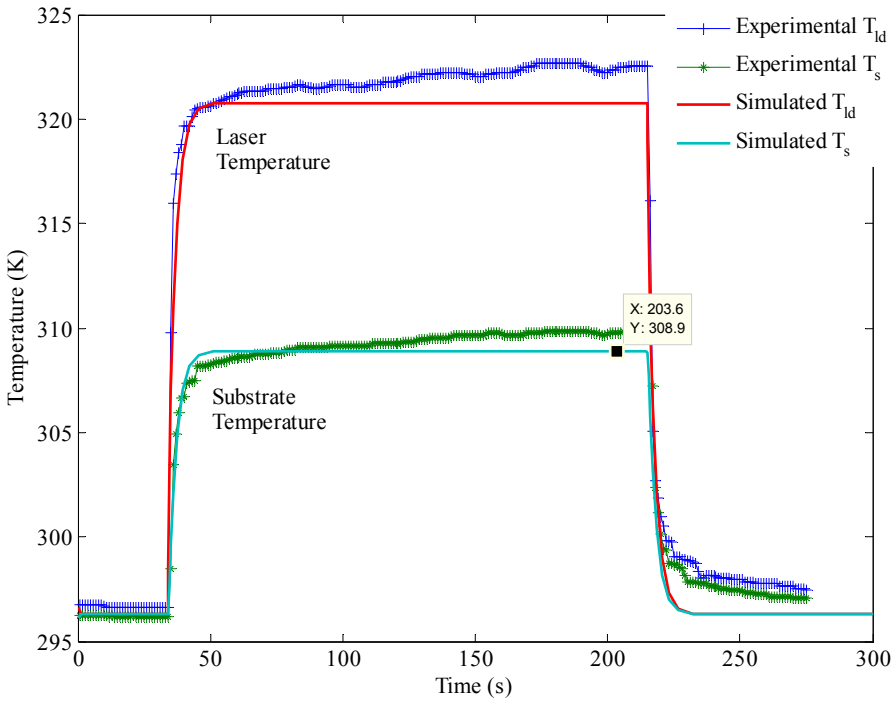

(a)

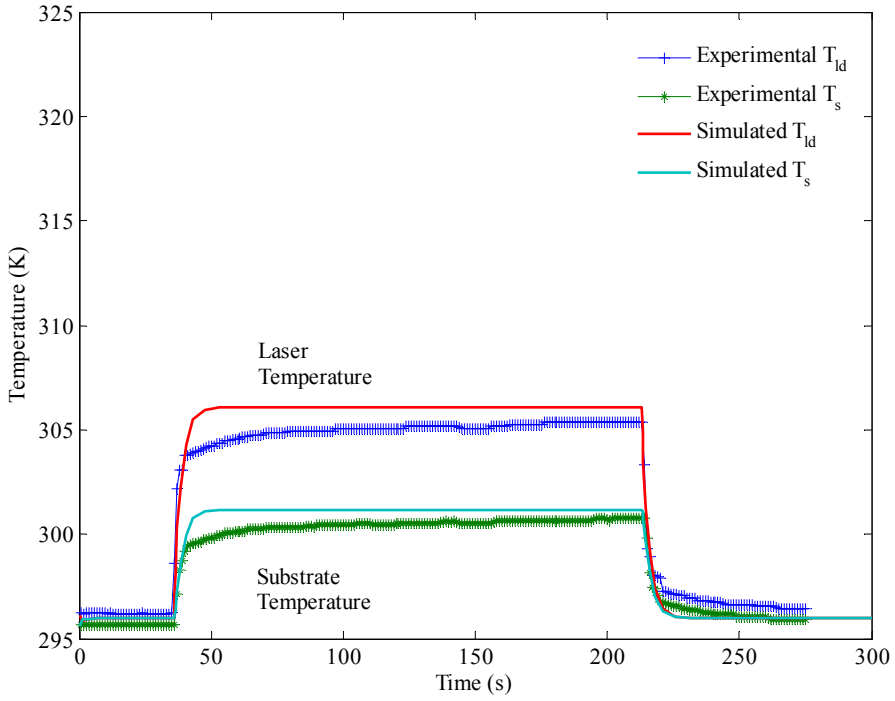

(b)

Figure 51: Simulated and experimental temperature data of the diode laser. (a) 4300 mA and (b) 1500 mA of injected current to the diode laser.

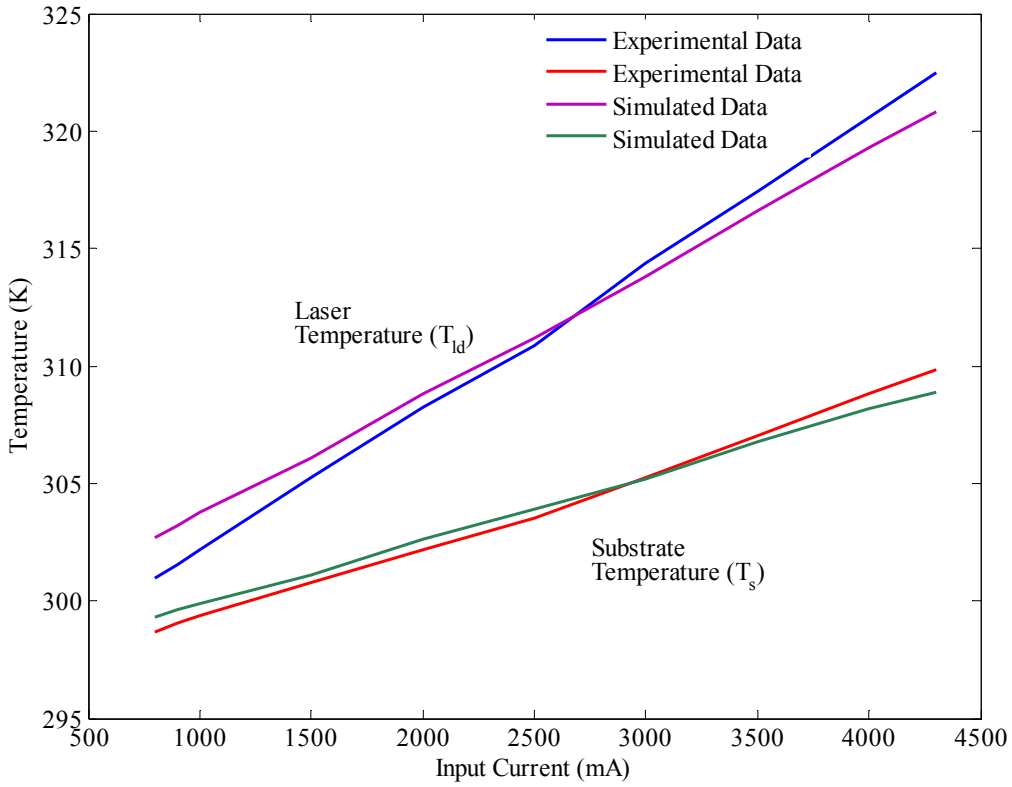

Figure 52: Temperature profile comparison of the simulated and experimental data for the diode laser.

From the above temperature profile, the simulated temperature curves closely match the experimental data. The temperature values were obtained at the steady state conditions from the experimental and simulated heat curves. The laser temperature (T_{ld}) had the largest difference of 1.8 K at 800mA input current and the substrate temperature had a 0.9 K difference at 4300mA input current. Further refinement of the diode laser thermal model parameters could allow the error to decrease but the results obtained were acceptable. An analysis of the cooling portion of the curve was not conducted but the data between the simulated and experimental data show a slight difference. This is most likely due to the admission of convection heating in the thermal model.

4.2 Miniature Photovoltaic Array (MPA)

A total of four 5mm MPA's, units X1, X2, X3, X4, were built for evaluation and testing. The MPA must be actively aligned to the optical connector in order to have the entire semi-circular array illuminated which allows the MPA to provide maximum illumination current. This is accomplished by connecting a 10kΩ resistor across the anode and cathode and measuring the resultant voltage drop. The output voltage increases as the illumination current increases. The optical connector is attached to a micropositioning stage and the MPA is firmly attached to the optical table. Each axis of the stage is then adjusted to get the highest voltage. This process is repeated until the voltage is at its maximum level. The optical connector is then optically aligned to the MPA device. The Simulink models used for verification for the MPA are shown on Figure 53.

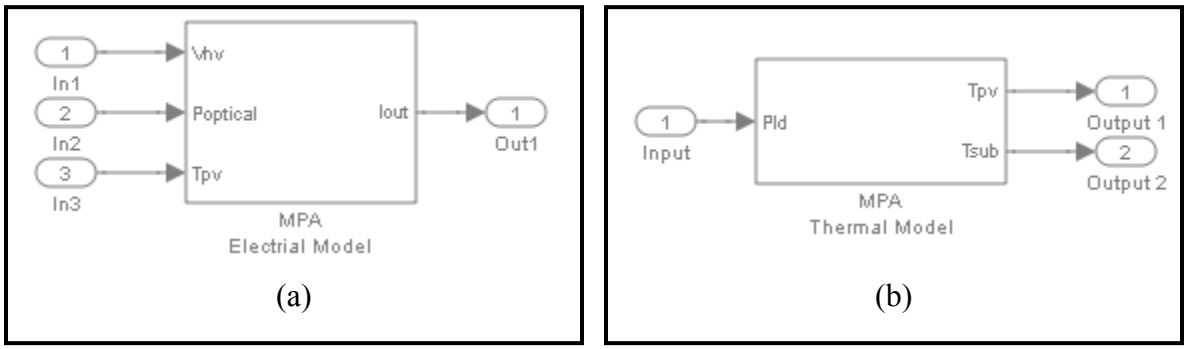

Figure 53: MPA models used in verification. (a) electrical model and (b) thermal model.

4.2.1 Electrical Model

A non-illuminated IV characteristic curve is first obtained to make sure that the device is operating correctly. A Tektronix 370B curve tracer was used for all characterization data. A typical waveform is shown in Figure 54. When the device is illuminated, the curve will initially shift the IV curve down by the illumination current.

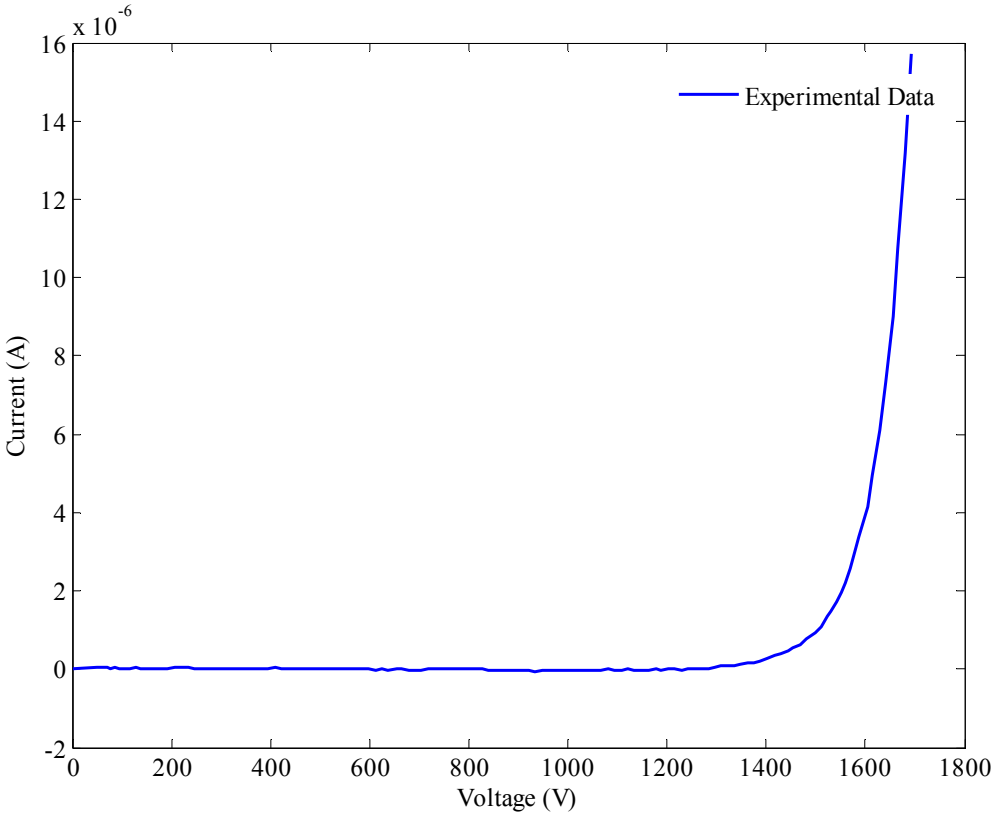

Figure 54: Experimental non-illuminated IV curve for a typical MPA device.

4.2.1.1 Calculation and Estimation of Electrical Model Parameters

The illuminated IV curves are more difficult to obtain since illuminating the device causes a positive voltage to develop. One way around this is to change the sweeping polarity from DC to AC. In this mode, ±1600 V is swept to the collector output at about 60 Hz. A collector compensation knob is then used to try to match up the sweeping curves. Repeatable measurements are difficult to attain since thermal heat to the MPA causes the output current (I_{out}) and output voltage to decrease. The illumination IV data curve is fit to the characteristic equation that did not include the temperature variation of I_0 and is able to provide the reverse saturation current (I_o), the diode quality factor (n), and the parallel resistance (R_p) of the device. Since it was difficult to obtain repeatable

measurements of the device throughout the different illumination levels, a single reading at 4300mA was used to provide the initial parameters for the characteristic equation and is shown on Figure 55.

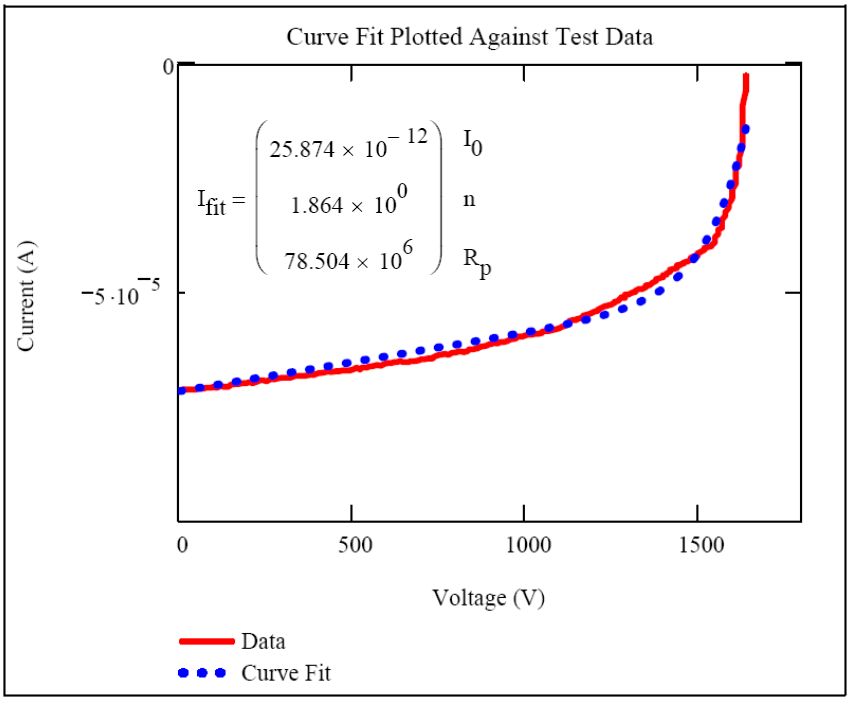

Figure 55: IV data of MPA unit X2 when illuminated with 2.96W. Data is curve fitted to the characteristic MPA equation.

Parameter	Description	Initial value	Final Tuned Value	Final Tuned Value with Temperature included in model	Units
Io	Reverse Saturation Current	2.57E-11	1.59E-11	NA	A
n	Diode Quality Factor	1.864	1.94	0.7	none
Rp	Parallel Resistance	7.85E+07	1.00E+09	1.00E+09	Ω

Table 9: Parameters of the characteristic equation for MPA unit X2 without temperature variation of I_0.

Table 9 lists the parameters of the characteristic equation from the curve fit and the final tuned values. The final parallel resistance term is two orders of magnitude larger than the

calculated value since the curve tracer inserts a parallel resistor across its connection to the device which decreases the estimated parallel resistance.

The characteristic equation for the MPA also contains the illumination current (I_l) variable that is a function of the input optical power. Illumination current experimental data was obtained by quickly illuminating the device at different levels and recording the current output when the collector voltage on the curve tracer is set at 0V. A plot of the illumination current versus the output optical power resulted in a linear curve as seen in Figure 56. The curve fit produces a linear equation that can be used to find the illumination current for a given optical power. This fit provided a goodness of fit R^2 value of 0.9985. Illumination current is dependent upon the uniformity of the illumination. Each current generator or cell is connected in series, therefore it requires a uniform flux density over the area contained by the cells. Consequently the illumination profile will change for each time the system is actively aligned. An analysis of the variation of illumination output in different alignment conditions was not conducted since the system was aligned and all experimental measurements were then taken. A variation of temperature analysis was also not completed since temperature has a minor effect on the illumination current [21].

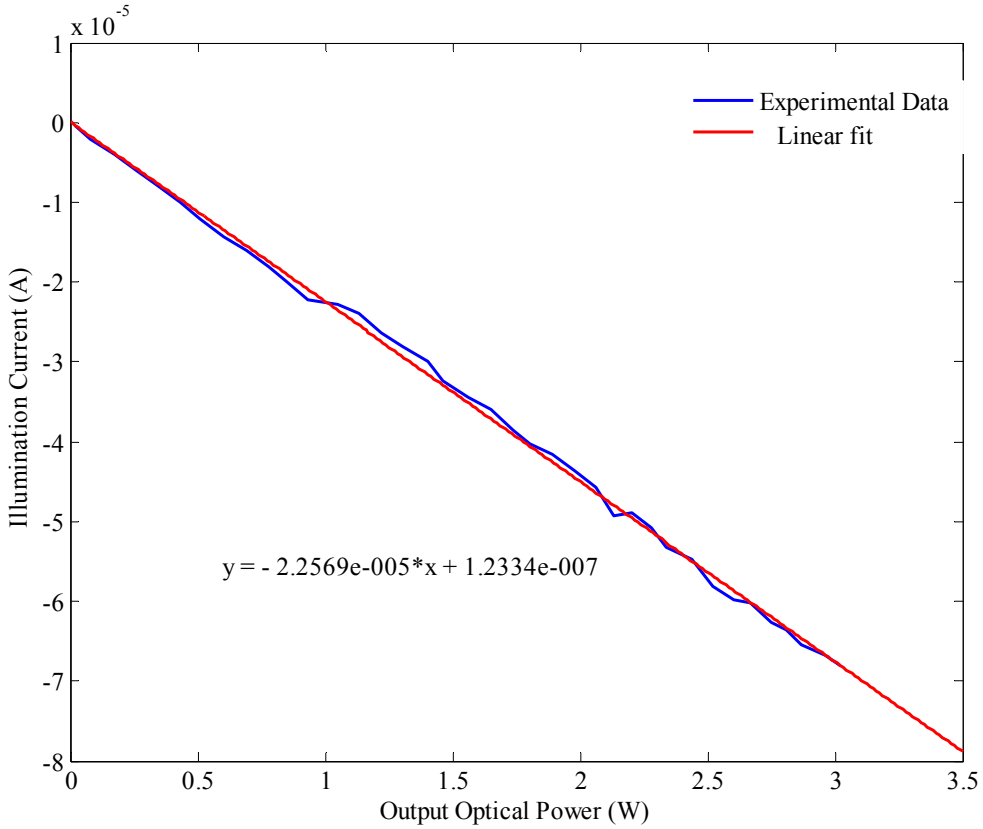

Figure 56: Characteristic illumination curve for MPA unit X2. The device is illuminated by JOLD-3-BAFC-11 S/N#: EK 08211.

4.2.1.2 Electrical Model Verification

Once all the parameters were included in the model, a 2.96 W constant was inserted for $P_{optical}$ and a ramp signal of 0 to 1800 V was used for V_{hv} input. Figure 57 shows the resultant output compared to the experimental data. There is a vertical shift between the two data sets and this is due to the adjustment of the collector compensation knob. The short circuit current (I_{sc}) values are off by 4.9 uA and are within reason. The initial slope of the curves match well and the open circuit voltage (V_{oc}) where $I_{out} = 0$, has a 22 V difference. Overall, the model data followed the general trend of the experimental data and was further verified when the CDU was added to the system as shown in chapter 4.3.

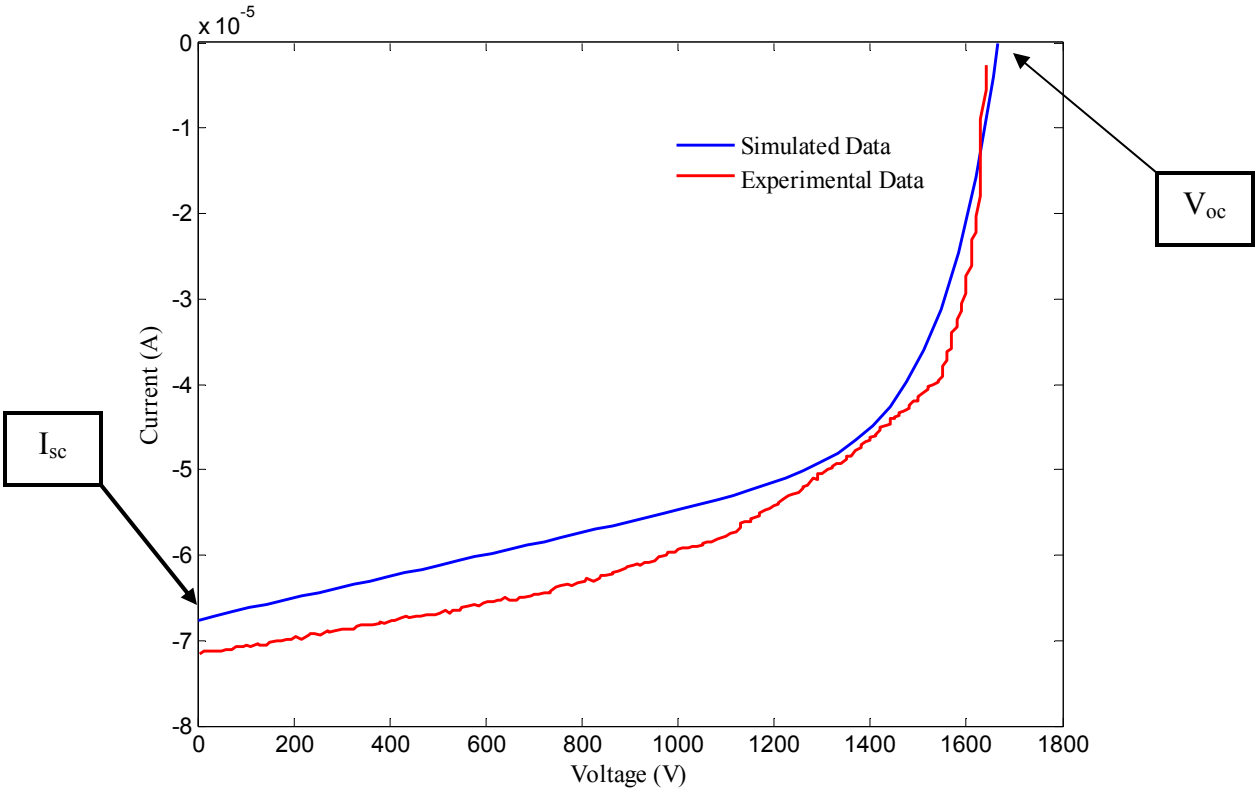

Figure 57: Experimental illuminated IV curve. MPA unit X2 is illuminated with 2.96W (4300mA input current).

4.2.2 Thermal Model

The characteristic thermal model equations are closely related to the model defined for the diode laser. One major difference is the input thermal power results from the power of the optical illumination. The reflectivity $R_{mat}(\lambda)$ of the device at the diode laser operating wavelength is needed since the thermal power is equal to the absorbed illumination power. The surface material of the MPA was not a homogenous material, therefore a reflectance measurement was taken. A Cary spectrophotometer was used to measure the reflectance. The sample was run across 700 nm to 900 nm wavelengths and the resultant data is shown in Figure 58. At 810nm, 30.92% of the input signal was reflected back. This value is proportional to the amount of thermal power absorbed into

the device. Future thermal consideration may look at operating the illumination device at different wavelengths to minimize absorbed thermal power.

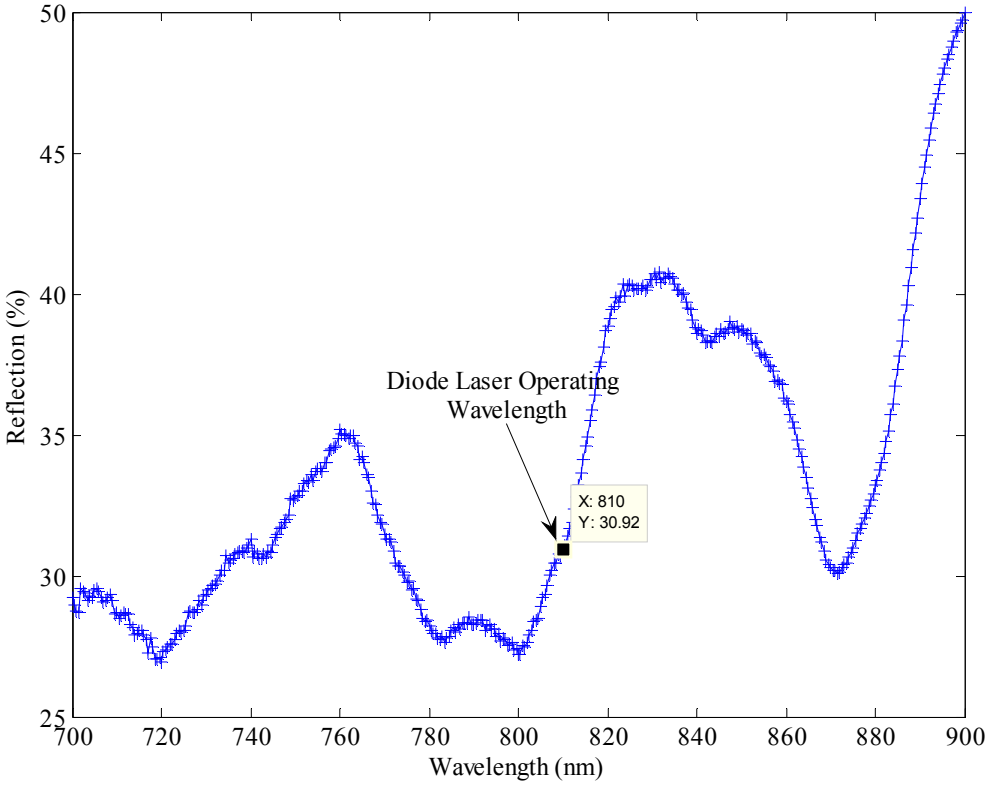

Figure 58: Experimental reflectance measurement of the MPA unit X2.

Two thermocouples were used to measure the temperature of the MPA (T_{pv}) and of the metalized substrate (T_{sub}). Omega® fine wire thermocouples of type K were used and placed during the building process when epoxy was used to passivate the metal lines, bond pads, and die sidewall. The epoxy was used to keep the thermocouple from moving and to keep contact with the measurement surface. Figures 59 and 60 illustrate the actual locations of the temperature probes. The temperature probe, which measures the MPA surface temperature, was placed just outside of the working cells so that the device could

still be functional. Calibrated Fluke 189 DMM's were used to collect all temperature measurements and sampled in one second intervals.

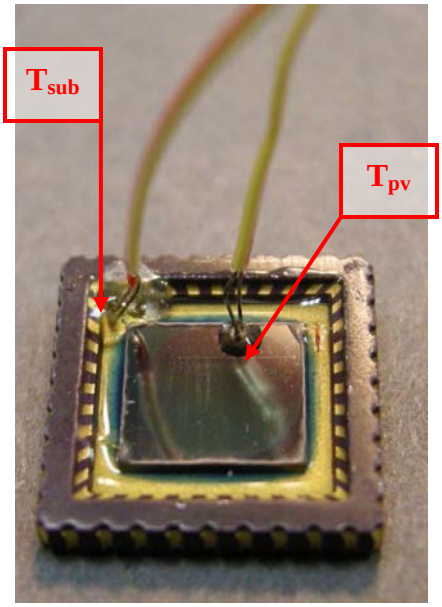

Figure 59: Experimental setup of MPA unit X3 with thermocouples used to measure the MPA die temperature (T_{pv}) and the substrate temperature (T_{sub}).

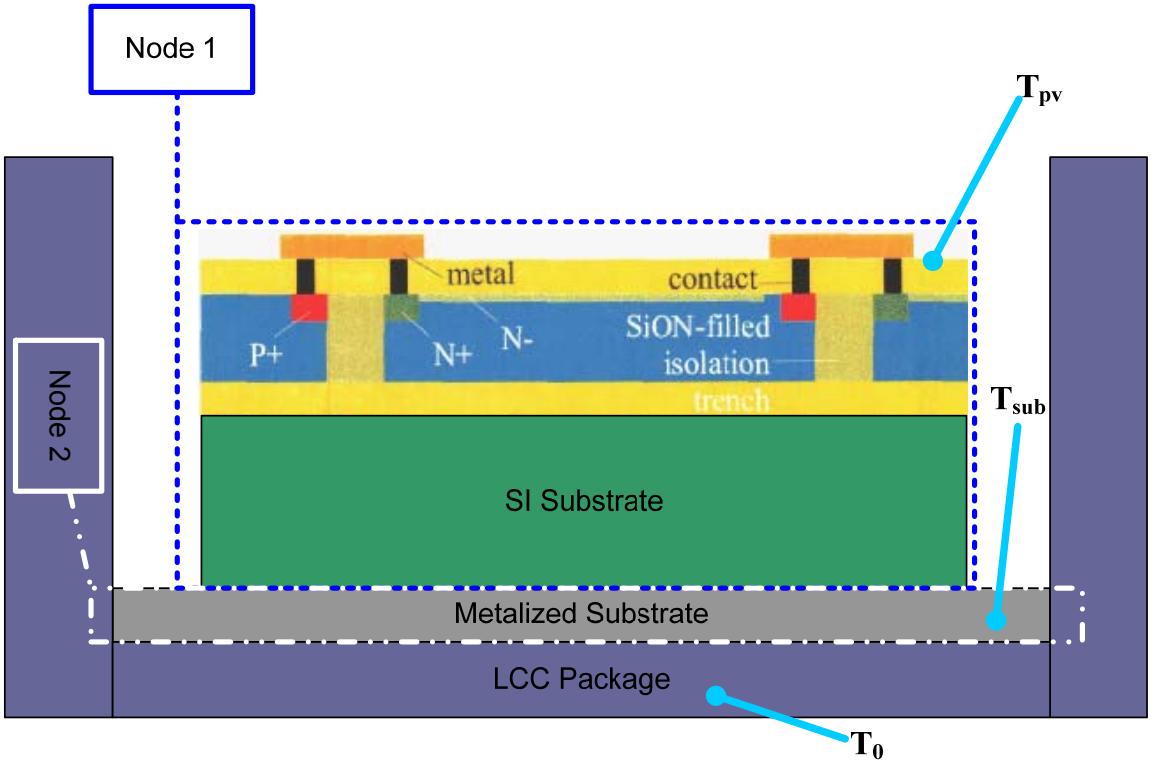

Figure 60: Location of temperature probes used to measure the temperature of the MPA.

4.2.2.1 Calculation and Estimation of Thermal Model Parameters

The thermal conductance of Node 1 can be calculated with the experimental temperature data. The MPA was tested with eleven different optical power levels that lasted about three minutes for each test. Data was first gathered for 30 seconds to capture the initial temperature and the device was then illuminated. After the specified time, illumination was removed and data was taken for an additional two minutes to capture the cooling curve. Input levels above 2.75 W lasted only for 1.5 minutes due to excessive heating of the device. At 2.96 W, the MPA reached a temperature of 435 K (324.41 F) just after 100 seconds. The temperature output again had the typical heating and cooling curve. As previously mentioned in Chapter 3, a steady state condition did not occur since the device was tested in a configuration that did not allow the device to be connected to a heat sink. Therefore, the heating continued to increase as seen in Figure 61.

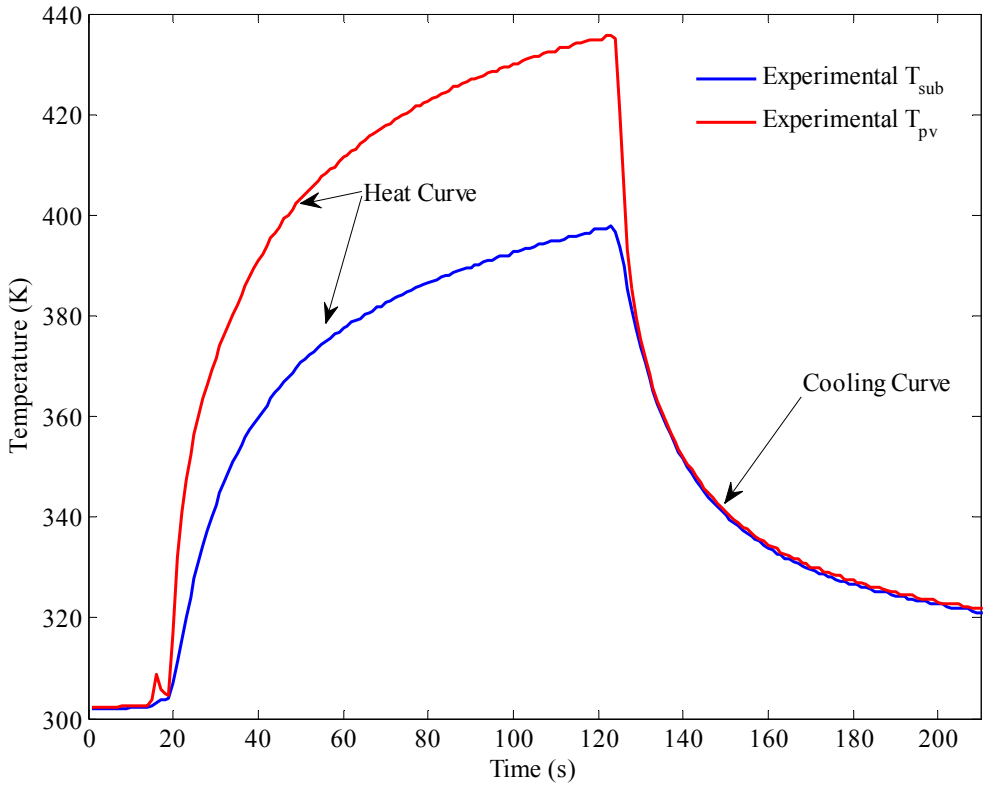

Figure 61: Experimental heat curves of MPA unit X3 when illuminated with 2.96W of optical power.

In the final geometry, the MPA will be connected to a large ceramic substrate or heat sink. Therefore, the temperature output will be similar to the heat curves obtained for the diode laser thermal model, except for a magnitude difference. In Figure 61, there is an initial spike that can be seen on the red (T_{pv}) curve just before 20 seconds. This phenomenon is due to the current driver turning off initially after it injected current into the diode laser. After a few seconds it turned back on and this occurred for injected currents above 2.5 Amps.

The experimental thermal conductance equation was previously examined in Eq. (4.13). The temperature difference between the MPA temperature (T_{pv}) and metalized substrate

temperature (T_{sub}) was taken from the experimental data. Since a steady state condition did not exist the temperature at 100s was used. A curve fit of the data was prepared and the reciprocal of the slope is the estimated thermal conductance between Node 1 and Node 2 as seen in Figure 62. The thermal conductance was calculated to be 0.0571 (W/K). The curve fit had a goodness of fit R^2 value of 0.9863.

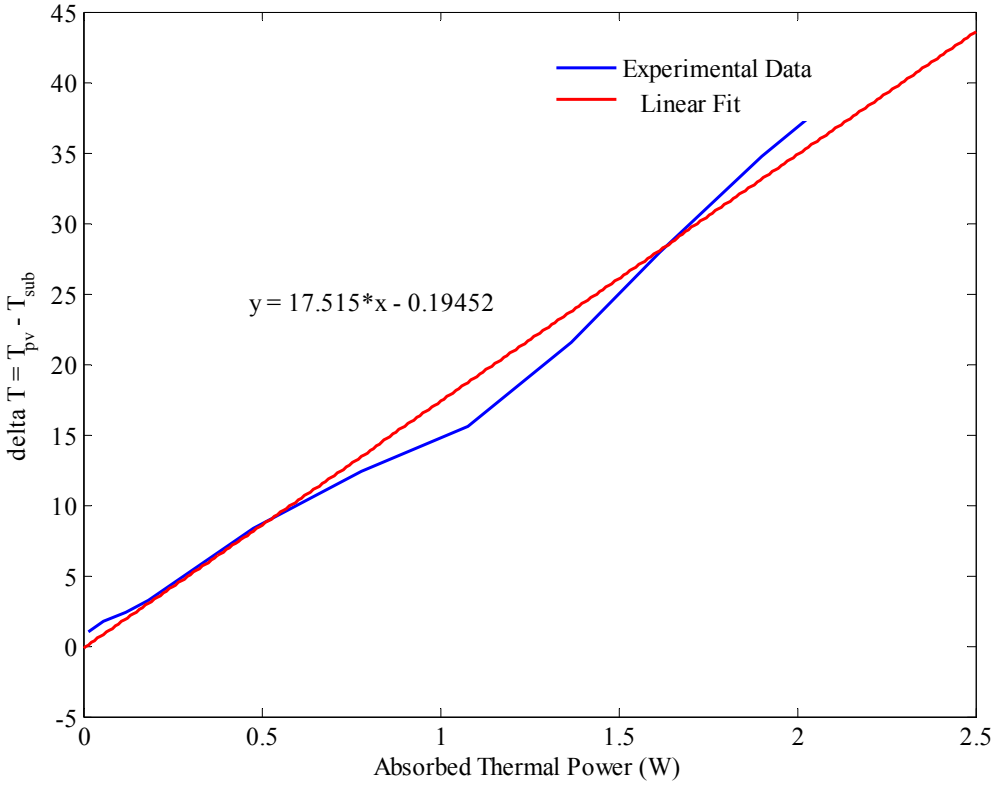

Figure 62: Experimental thermal conductance curve for MPA unit X3.

Similar measurements cannot be experimentally obtained for the other three parameters of the thermal model. Similar assumptions were made on these parameters as were defined in the diode laser thermal model. The initial thermal capacitance values were again obtained from the work done on semiconductor laser measurements [2]. These parameters were used and adjusted in the model simulation. The adjustment of the

thermal conductance was inversely proportional to the output temperature and the thermal capacitance values controlled the rise time of the temperature curve. Initial and final tuned values are shown in Table 10.

Parameter	Description	Initial value	Final Tuned Value	Units
$\lambda_{a,cond}$	thermal conductance between MPA die and metalized substrate	0.0571	0.058	W/K
$\lambda_{b,cond}$	thermal conductance between metalized substrate and package	0.0471	0.029	W/K
C_{pv}	thermal capacitance of MPA die	0.1396	0.11	J/K
C_{sub}	thermal capacitance of substrate	0.1819	0.2	J/K

Table 10: MPA unit X3 parameters for the 2-node thermal model.

4.2.2.2 Thermal Model Verification

The simulated and experimental temperature curves can be seen in Figure 63, (a) and (b). The simulated temperature curves show a steady state value after about 60 seconds. Since the original model assumed that the LCC package temperature stays at a constant room temperature, the deviation is apparent in the model. The deviation from the steady state could be removed if the experimental setup allowed the LCC package to be connected to a heat sink. Additionally, if the MPA is not connected to a heat sink where the assumption of constant temperature is not valid, another node could be added to the thermal model so that the temperature of the package could be determined. A 3-Node thermal model was completed to show that the model can be flexible enough to account for different geometry conditions. Figure 64 shows the 2-Node and 3-Node simulated data. The 2-Node model will be used for all further analysis since the experimental and simulated data match well for 30 seconds which will meet the maximum requirement of providing a regulated output voltage for 30 seconds.

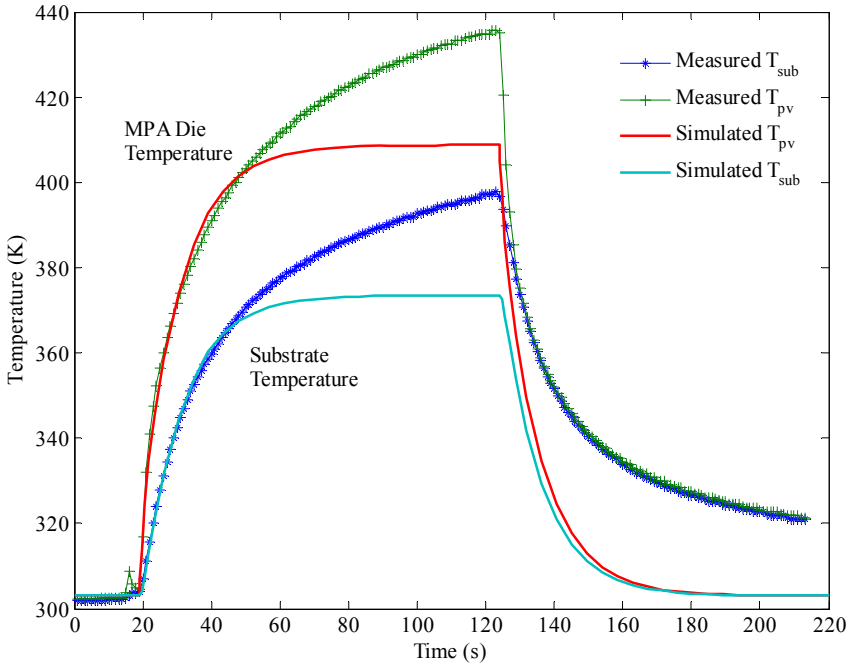

(a)

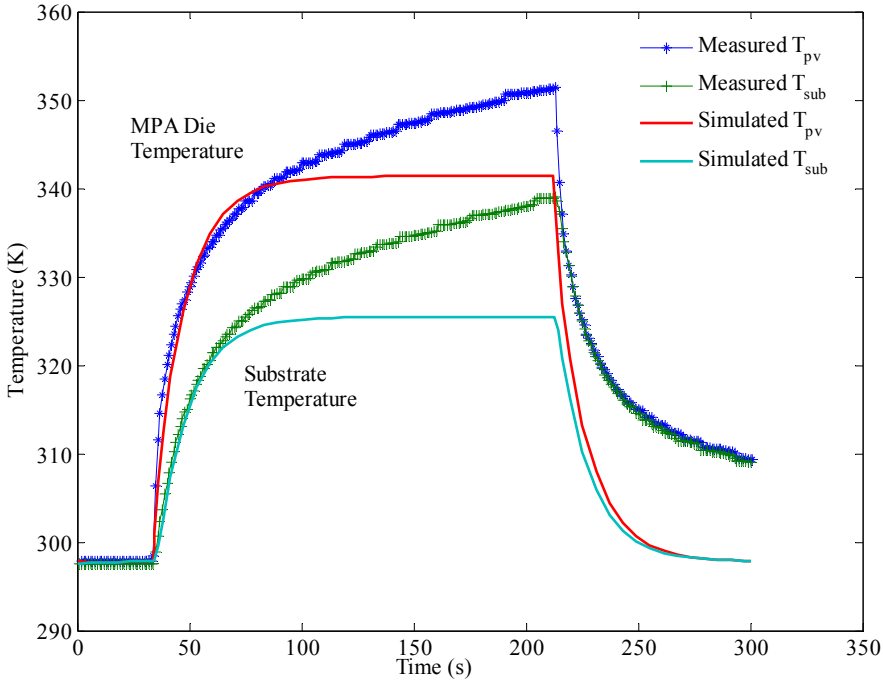

(b)

Figure 63: Simulated and experimental temperature data of the MPA unit X3. (a) 2.96 W and (b) 1.13 W of injected optical power to device.

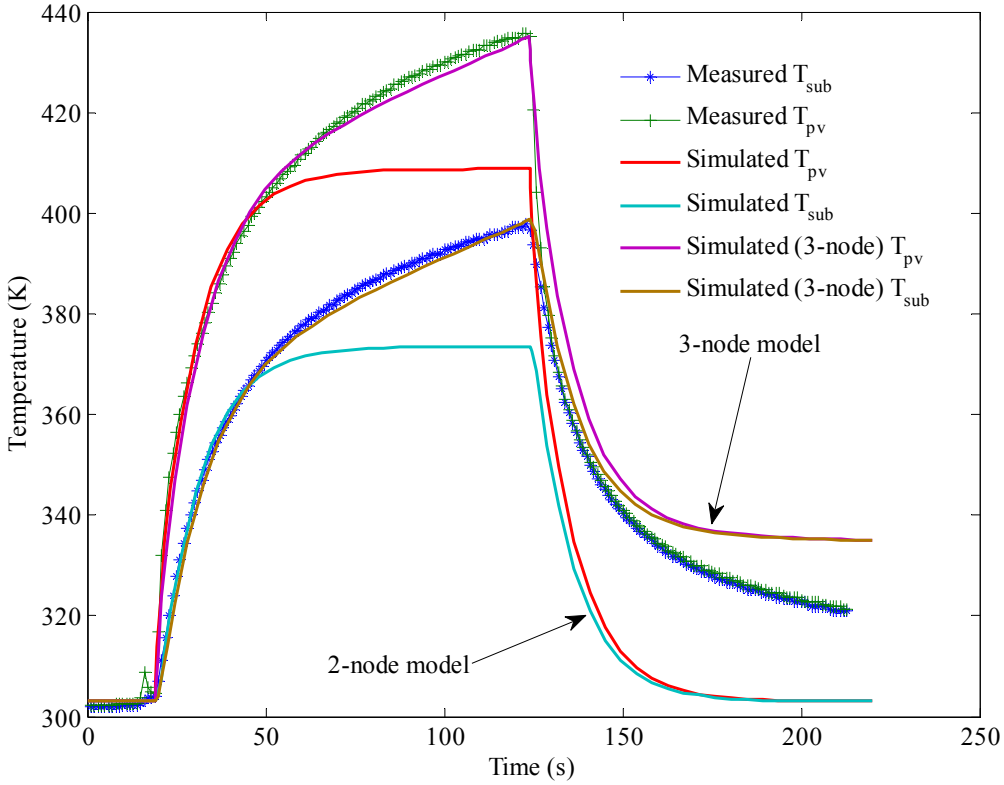

Figure 64: Simulated and experimental temperature data MPA unit X3 showing the difference between 2-Node and 3-Node thermal model.

The temperature profiles from Figures 63 and 64 show that the model closely follows the heating curve of the experimental data. Furthermore, if the geometry of the design dictates that the assumption of device temperature being fairly constant is inaccurate, the model can be adjusted to more accurately predict the actual output. Optimization of the model parameters would also decrease the deviation and errors.

4.3 High Voltage CDU

A printed wiring board (PWB) was designed to mount the CDU components as shown in Figure 32, except for the high voltage capacitor. Additionally, it contained a socket to accept the MPA devices for testing. Two separate sets of parallel resistors were used. One resistor network provided a 1000:1 signal so that the high voltage could be safely

measured. The other resistor provided a 2.5 V signal when the high voltage is at 1500V. The 2.5 V signal was designed to be compatible with a 3.3 V Analog to Digital Converter (ADC) that was present on a microprocessor. Further connection to the high voltage capacitor would be accomplished via two wires. These wires connect directly to the high voltage capacitor mounted on a strip line cable. The cable also contained a high voltage switch and detonator. Figure 65 illustrates the High Voltage CDU connections.

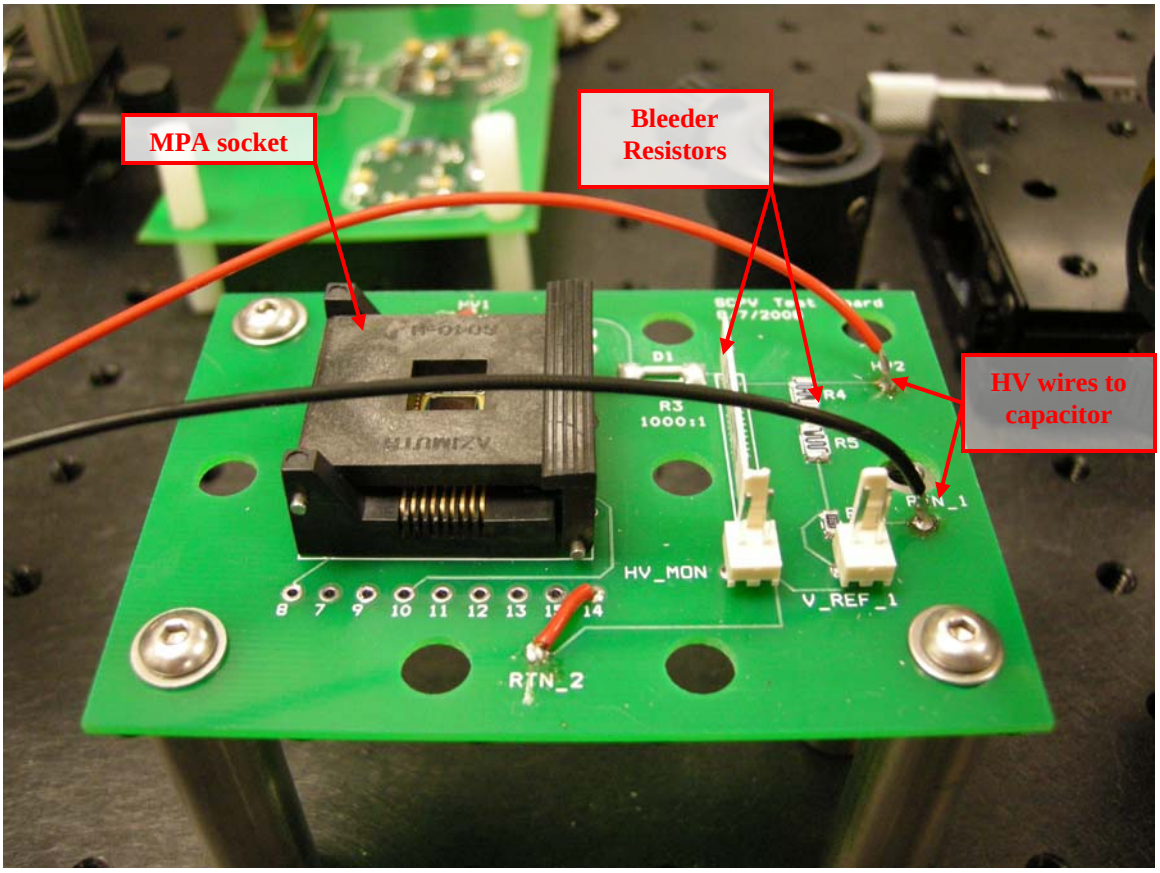

Figure 65: Photograph of the CDU test board for the optical powered firing set.

4.3.1 Electrical Model Verification

Experimental data of the High Voltage CDU subsystem could not be obtained since a specialized high voltage current generator was needed. Therefore the MPA was

connected to the CDU and 38 different levels of optical illumination were injected. Figure 66 shows the model that was used for this verification analysis.

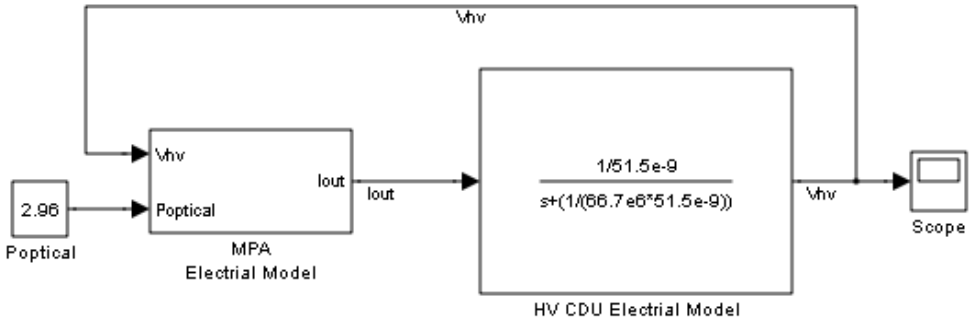

Figure 66: MPA model connected to the HV CDU model used for verification of the CDU model.

Figure 67 shows a sampling of the experimental and simulated high voltage output data from the CDU. From the experimental data, the charge time is a function of illuminated input power. At 2.96 W, the CDU will charge to 1560 V in about 1.7 seconds. Input optical power below 1.22 W will take more than 20 seconds to reach 1500 V. At input values above 1.22 W, the output voltage begins to decrease after it reaches the maximum voltage level. This characteristic is a function of heating that occurs to the MPA device. The reverse saturation (I_0) current increases and reverse diode (I_d) currents decrease as temperature increases. The other parameters will also change with temperature, but the two current values are the most significant. This effect causes the resultant output voltage to decrease with increasing temperature. K_1 and K_2 of the MPA characteristic equation were determined by curve fitting to the V_{hv} output data. The values of K_1 and K_2 are 0.014 and -18221.0 respectively.

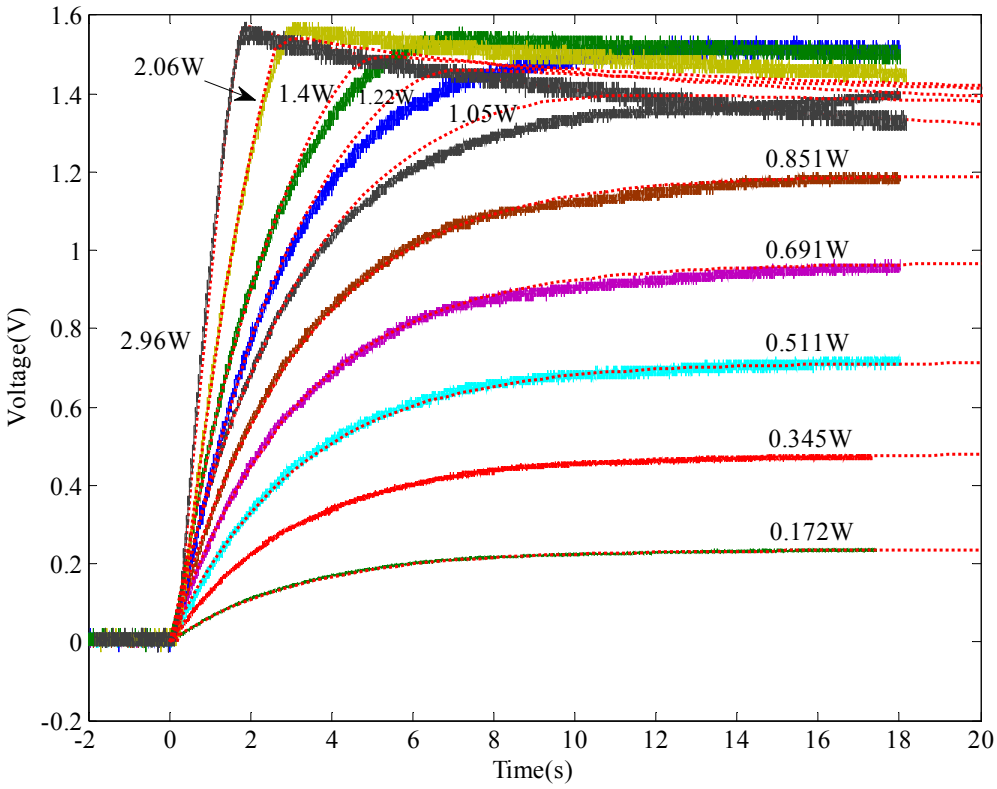

Figure 67: Optical powered firing set V_{hv} output data. Different illumination powers were used. The red dotted line is the simulated output from the electrical model.

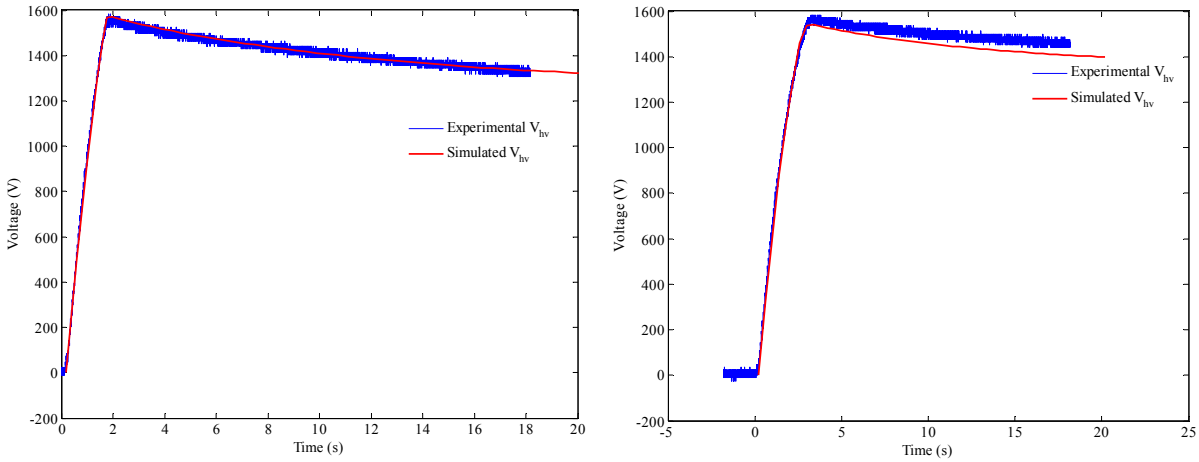

Figure 68: High voltage output (V_{hv}) of optical powered firing set. Optical illumination of (a) 2.98 W and (b) 1.98 W to MPA.

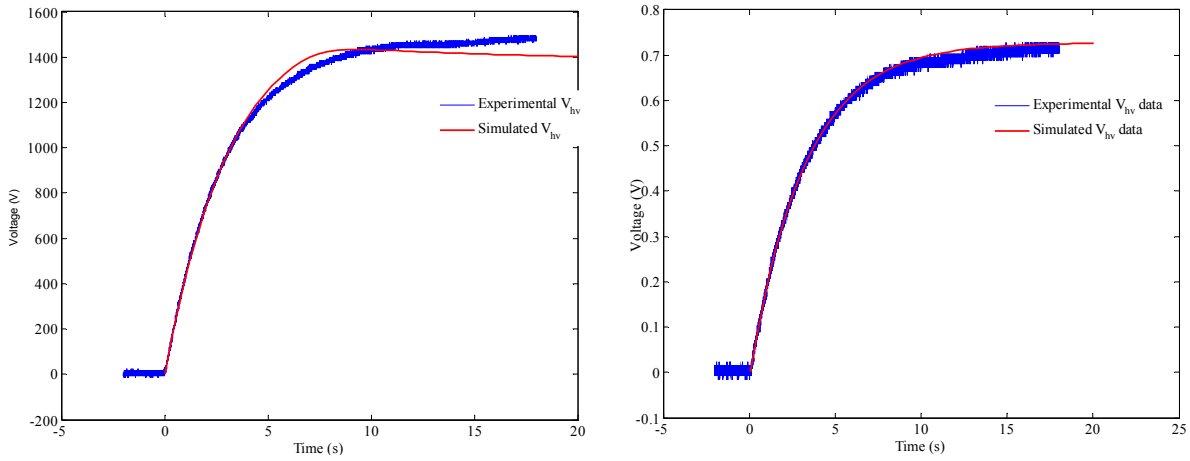

(a) (b)

Figure 69: High voltage output (V_{hv}) of optical firing set. Optical illumination of (a) 1.13 W and (b) 0.51 W to the MPA.

From Figures 67, 68, and 69, the simulated and experimental data match well. There is a small amount of deviation of about 54 V in output voltage at 1.98 W as seen in Figure 68(b). Figures 68(a) and 69(b) are almost an exact match. Figure 69(a) shows a little variation at about five seconds where the simulated voltage increases by 46 V and is probably due to a temperature effect not being taken into account in the MPA electrical model. Overall the CDU electrical model accurately predicts the actual experimental system over a wide range of input conditions.

5. CONTROL SOLUTION

Once each subsystem was verified and compared to experimental data, the analysis and design of the optically powered firing set could begin. Some of the models developed for the optically powered firing set were nonlinear differential equations. In this situation it is common for the designer to linearize the models around a particular solution so that the transfer functions and state equations could be easily found. MATLAB and Simulink, computer based programs that can solve nonlinear ODE's because they use numerical methods for solving, were used to simulate the model in the control solution. Therefore, it was deemed unnecessary to linearize these functions. Future analysis and design may include linearizing the nonlinear subsystem equations.

5.1 Total Modeled System – Initial Response

Each subsystem was connected together as shown in Figure 70. This figure is the block diagram subsystem model that is built in Simulink. The input and output signals are the input voltage to the LDX-3565 current source and the high voltage monitor respectively.

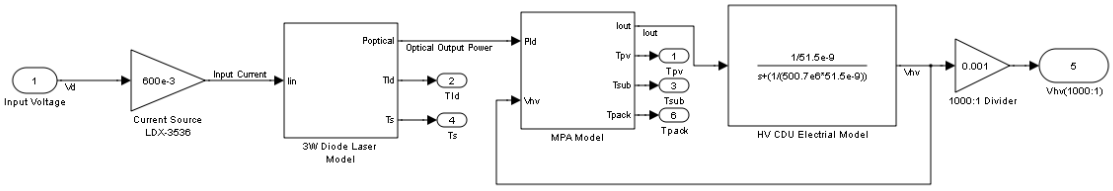

Figure 70: Modeled optically powered firing set subsystem.

The input voltage to the LDX-3565 controls the output current from the device. The output current (I_{in}) is then fed to the 3W laser diode model which generates an optical output ($P_{optical}$). This optical output power is then fed to the MPA model and is used to generate the output current (I_{out}). The output current is then fed into the HV CDU

electrical model where it uses a transfer function to output high voltage (V_{hv}). The signal is then put through an amplifier with a gain of 0.001 to simulate a 1000:1 divider resistor, which is the final measured state of the optically powered firing set. It should also be noted that the high voltage (V_{hv}) output from the HV CDU electrical model is fed back to the MPA model since it is a dynamic variable in the MPA model system equations. The optically powered firing set plant is modeled as a single block by creating a subsystem of Figure 70 and is shown in Figure 71.

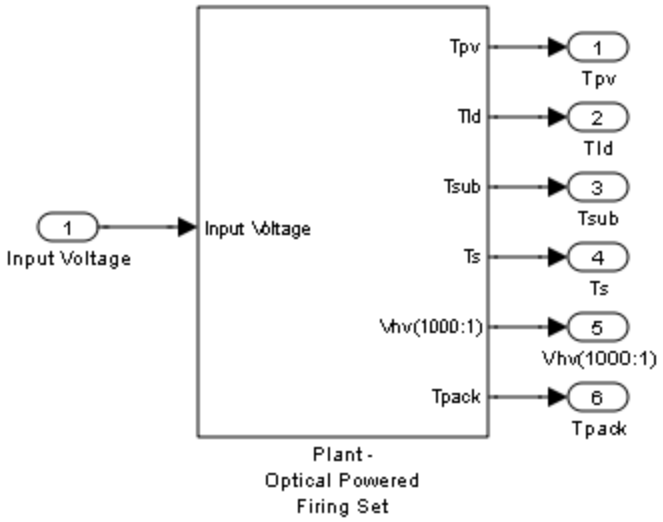

Figure 71: Optically powered firing set plant as modeled in Simulink.

The Optically Powered Firing Set plant was used in the control system analysis and design. The plant has a single input of voltage and six outputs. The outputs include a high voltage monitor ($V_{hv(1000:1)}$) and temperatures of the diode laser (T_{ld}), diode laser substrate (T_s), MPA die (T_{pv}), MPA substrate (T_{sub}), and MPA package (T_{pack}). T_{pack} is only relevant when the 3-Node thermal model is used for the MPA. A check was completed to see if the response specifications and performance requirements could be met by only making a simple adjustment to the system input. From experimental data it

was known that a step input of about 2100 mA injected into the diode laser, would provide an output of about 1510 V, however, it would take over 10 seconds to reach that level. The optically powered firing set plant was simulated with 3.5 V which corresponds to 2100 mA of injected input current to the diode laser and the simulated output states of the optical powered firing set are shown on Figure 72. Since the voltage rise time was off by about five seconds the total parallel resistance of the CDU (Rp) from Figure 34 was increased. Rp is not defined by the system requirements and can be varied.

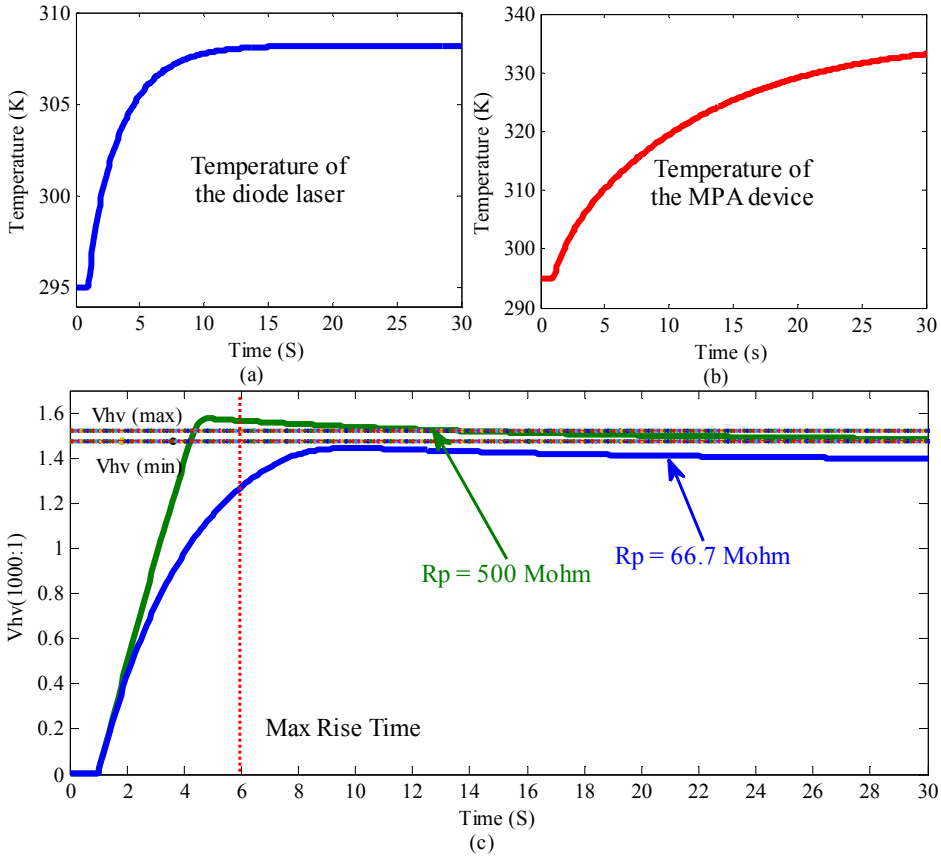

Figure 72: Simulated open loop output from the optical powered firing set at 3.5 V input. (a) is the temperature of the diode laser (b) is the temperature of the MPA (c) is the output high voltage monitor V_{hv} of the model.

From Figure 72, red dotted lines are used to indicate limits imposed by the system requirements. The thermal temperature curves show some heating in both devices. After

30 seconds a temperature of 308 K (95 F) for the diode laser and 333.2 K (140 F) for the MPA were estimated. In Figure 72(c), the output voltage when R_p is 66.7 MΩ does not meet the max rise time or regulated voltage level requirements. The output voltage when R_p is 500 MΩ does meet the max rise time requirement, but is fails to meet the regulated voltage level requirement. The input was further adjusted but the output state would not meet all the system requirements. A closed loop feedback control system was then investigated.

5.2 PID Controller

A closed loop control system is needed to keep the output state at a desired level in spite of any disturbances or other variations made to the plant. Typically a feedback signal is used to measure the output state and is fed back to a controller. A closed loop control system with a feedback signal is called a feedback control system and is represented in Figure 73.

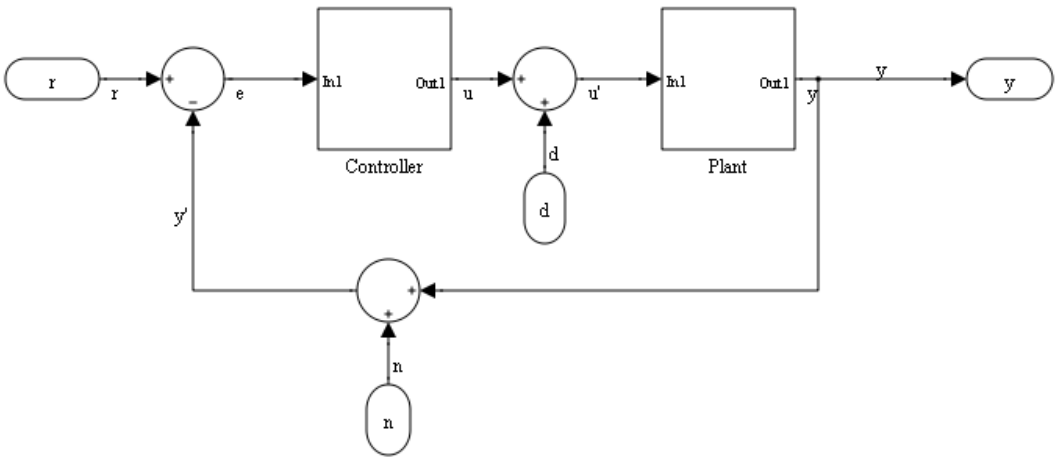

Figure 73: Block diagram of a closed loop feedback control system.

In Figure 73, *r* is the reference signal, *e* is the error signal, *u* is the input control variable, *y* is the output signal, *n* is the measurement noise signal, and *d* is the load disturbance

signal. The terms *y' and u'* are the output and input signals with the addition of the disturbance signals. The error signal is the reference signal minus the output signal ($e = r - y$).

A Proportional-plus-Integral-plus-Derivative (PID) controller was chosen due to its easy implementation on the nonlinear plant and its ability to adjust both the transient and steady-state response. Moreover, Simulink has a predefined PID block that allows a user to input the three PID parameters. A PID controller is three separate controllers - proportional, integral, and derivative - which are summed together in the proper manner as seen in the Figure 74. This controller is displayed in a parallel structure.

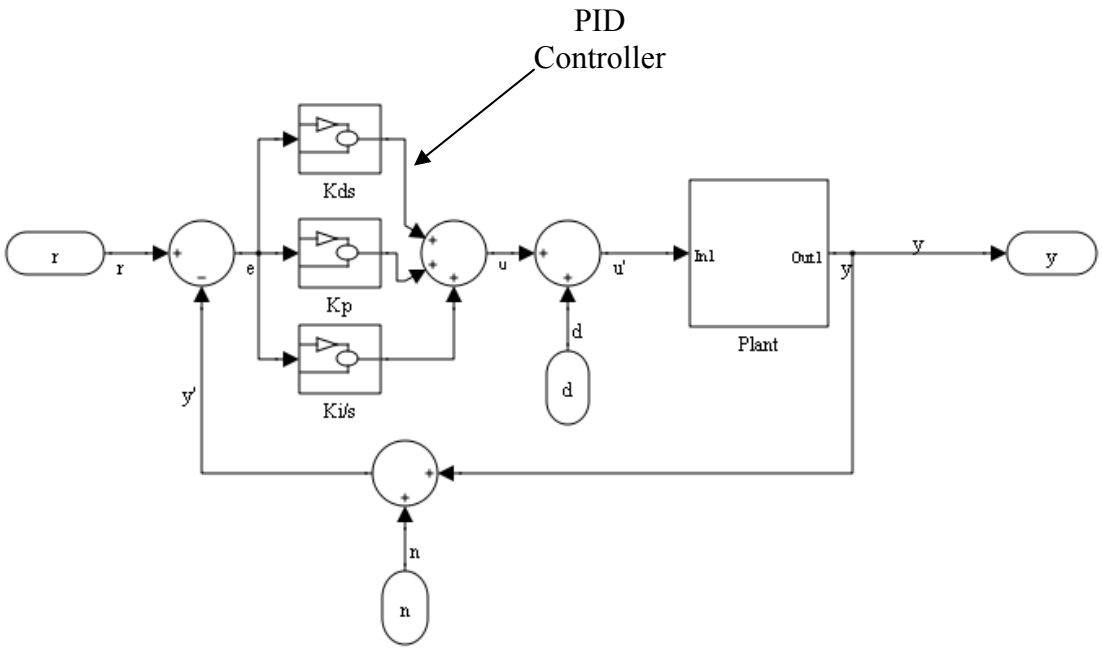

Figure 74: Block diagram of closed loop feedback control system with a PID controller.

Kp, Kd, and Ki, are three tunable parameters that adjust the controllers transient and steady state response. The PID transfer function is often expressed as shown in Eq. (5.1) [14].

$$C(s) = K_p + \frac{K_i}{s} + K_d s \tag{5.1}$$

K_p is the proportional term, K_i is the integral term, and K_d is the derivative term. If ideal controllers are used, two zeros and a pole are additionally placed at the origin when the system is plotted in the s-plane. One pole and one zero is due to the integral controller and the additional zero is due to the derivative controller. The proportional control action adjusts the control signal in response to the error signal. If the error is large, then a large signal is fed to the plant. Alternatively, if the error is small, a small signal is fed to the plant. The output expression is

$$u(t) = K_p e(t) = K_p\big(r(t) - y(t)\big) \tag{5.2}$$

and the Laplace transform of Eq. (5.2) is the transfer function as defined in Eq. (5.3):

$$C(s) = K_p \tag{5.3}$$

This regulation causes a steady state error in the output. Adding a pole in the case of the single integral controller allows the reduction of the steady state error to approach zero. The output expression of the integral controller is:

$$u(t) = K_i \int_0^t e(\tau) d\tau \tag{5.4}$$

From this expression the output is related to the past values of the error signal (e). The transfer function is the Laplace transform of Eq. (5.4) and is the following:

$$C(s) = \frac{K_i}{s} \tag{5.5}$$

The reduction of error is done through low-frequency compensation. The derivative control action improves the controller transient response since it can anticipate an

incorrect trend in the error signal and appropriately counter it [20]. The output expression is:

$$u(t) = K_d \frac{de(t)}{dt} \tag{5.6}$$

The corresponding transfer function is then the Laplace transform of Eq. (5.6) where:

$$C(s) = K_d s \tag{5.7}$$

Equations (5.3), (5.5), and (5.7) are then combined to form Eq. (5.1) when the PID controller is connected in the parallel fashion of Figure 74. The PID parameters are then selected. The tuning process has been extensively examined and the results are displayed in Table 11 [19,20].

PID Tuning		Transient Response			Steady-State Error	Stability
		Rise time	Settling Time	Overshoot		
Increasing	Kp	Reduces	Slight Increase	Increase	Reduces	Degrade
	Ki	Slight Reduction	Increase	Increase	Large Reduction	Degrade
	Kd	Slight Reduction	Reduces	Reduces	Very slight change	Improve

Table 11: Tuning effect of PID controller terms [19,20].

The PID controller was connected to the optical powered firing set plant and the PID gain values were tuned to meet the requirements. In the selection of the PID values a signal constraint blockset from the Simulink Design Optimization toolbox was used to automatically adjust user specified parameters so that the output response matches the user defined signal constraints. The blockset was setup to only tune the PID gain parameters and the signal was constrained to meet the control system requirements. A

series of simulations were then run while the parameters were automatically tuned. Figure 75 shows the closed loop PID control system.

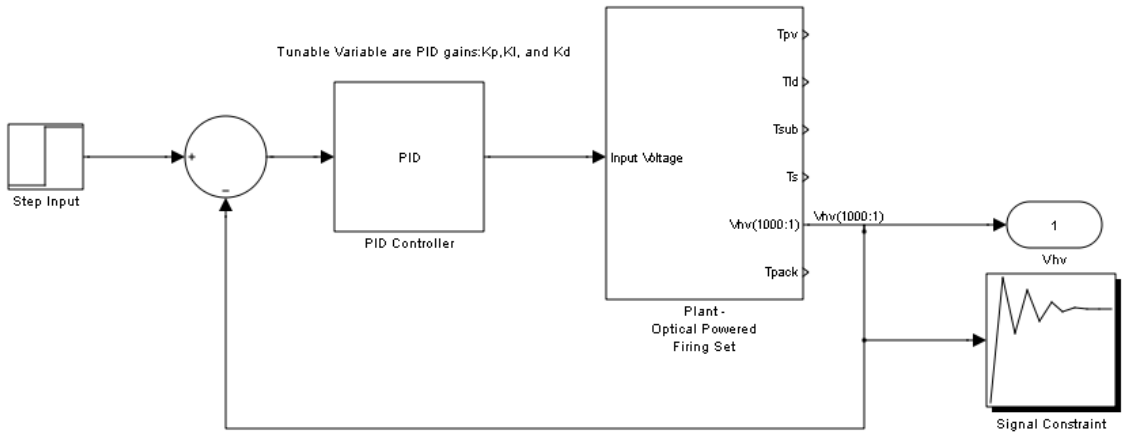

Figure 75: Final control system for the optically powered firing set with PID controller.

The system was simulated and the following signal constraints were placed on the output signal. The maximum voltage was set to 1.525 V and the rise time was set to five seconds. The min voltage for V_{hv} after five seconds was set to 1.475 V. The step input signal was set to a reference level of 1.5V. Figure 76 shows the signal constraint window with multiple simulations and the resultant output state. It should be noted that the derivative term caused the model to converge very slowly - more than two hours for each simulation. Improvement on the overshoot and settling time of the output response was not needed. It was therefore eliminated by setting Kd to zero. The final solution is therefore a PI controller. Also the parallel resistance of the CDU (R_p) was changed to 500 MΩ to allow for quicker charging time.

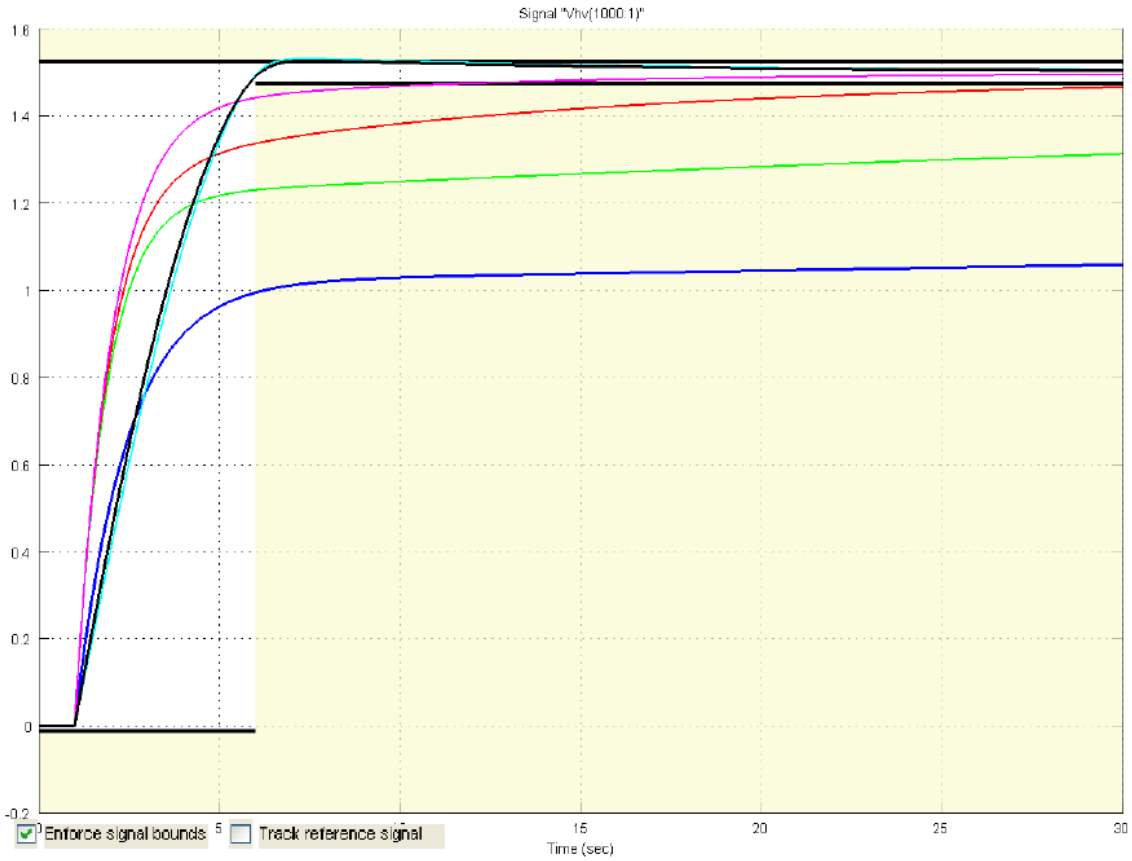

Figure 76: Signal constraint window used in Simulink to determine the PI gains for the controller. Multiple output states are shown and the black curve is the final optimized solution.

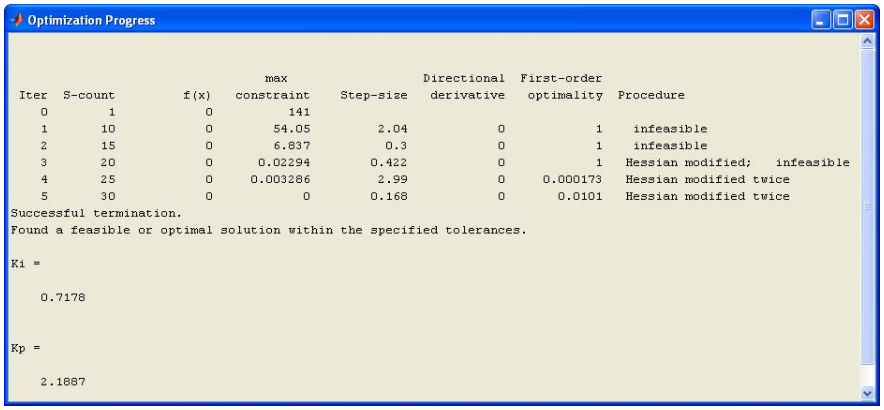

Figure 77: Optimization output window displaying the number of runs and final optimal solution. Final PI values are given.

The final PI values that meet the system requirement are shown on Figure 77. Ki was found to be 0.7178 and Kp is 2.1887. Additional margin in requirements can be obtained

by lowering the system requirements in the signal constraint blockset and obtaining new PI gain values. Figure 78 shows the output states of the PI controlled optically powered firing system.

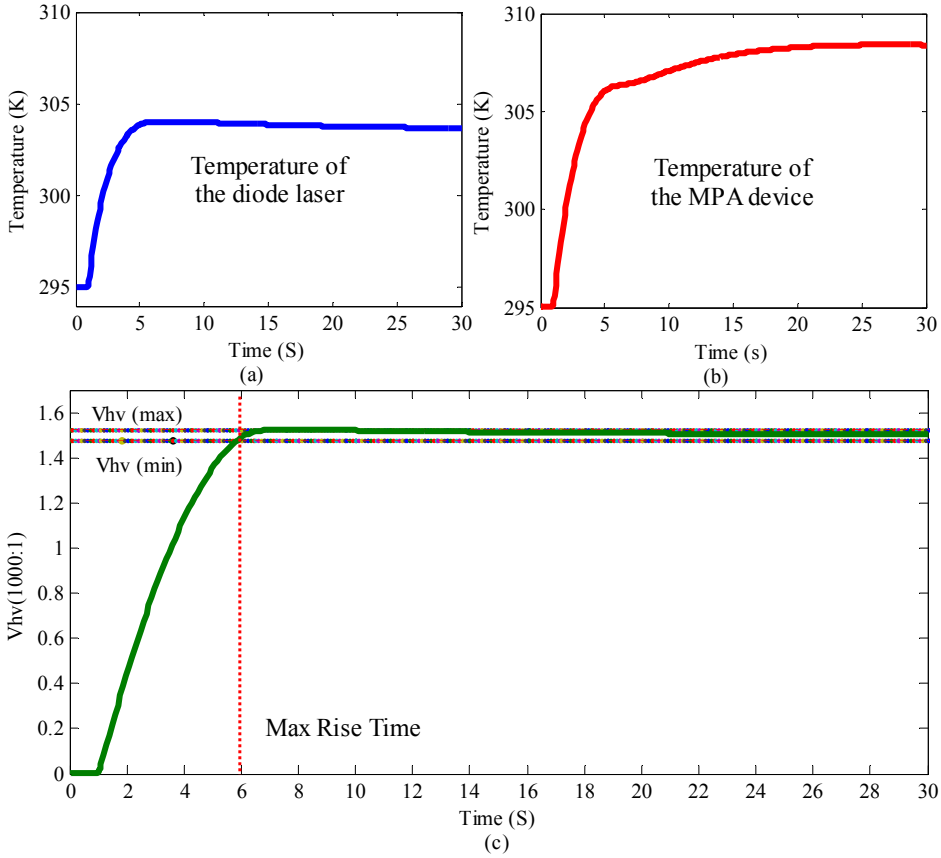

Figure 78: Simulated output voltage state of the closed loop feedback control with PI controller. Voltage reference is set to 1.5 V.

From Figure 78, the temperature of the diode laser has only increased by 8.7 K and the MPA has increased 13.4 K. In comparing to the open loop response of Figure 72, the diode laser temperature decreased by 4.3 K or 4.4% and the MPA temperature decreased by 24.8 K or 7.7%. The high voltage output state had a rise time of 3.7 seconds and a 2% settling time of 4.778 seconds. Table 12 shows the comparison of the initial system requirements and final system transient response values.

	Initial Requirements	Open Loop Response	Final System Response
Rise Time	5	2.633	3.7
Settling Time	NA	9.61	4.778
Max Regulation Votlage	1525	1574*	1525
Min Regulation Voltage	1475	1485	1475
Max Diode Laser Temperature	Minimize	308.2	303.7
Max MPA Temperature	Minimize	333.2	304.8
Adjustable Output	Desired	No*	Yes

* did not meet requirements

Table 12: Initial requirements and transient response of the optically powered firing set.

All requirements were met with the closed loop feedback system with PI controller and the temperature states were less then the open loop response. The final system also had the ability to set the output voltage level by adjusting the step voltage input level.

In order for this system to be realized, embedded microprocessors can be used as the PID controller. The analog feedback signals are converted into discrete digital samples. These samples are used in an embedded algorithm to calculate the PID output (u(t)) to provide compensation. A typical algorithm may calculate the integral by using the trapezoidal integration rule which is a numerical approximation of an integral. The derivative can be found since it is the rate of change of the error. The performance is related to the sampling rate since all the calculations of each term must be complete before the next sample time begins. Therefore it is important to choose a processor that has the necessary speed and available resources to provide control.

6. CONCLUSION

A complete model of an optically powered firing set composed of a diode laser, Miniature Photovoltaic Array (MPA), current generator, and capacitive discharge unit (CDU) was developed in Simulink and MATLAB to allow for simulations. A closed loop feedback control system with a PI controller was then simulated to provide control of the output voltage state and temperature states of the diode laser and MPA. The control system was able to meet the system requirements of setting the high voltage output state to 1500 V and minimizing the temperatures of the diode laser and MPA. The control system also allowed for the adjustment of the output voltage state to be set. Three subsystem components of the optically powered firing set - diode laser, MPA, and CDU - are each separately modeled with adjustments for device parameters. Following the methodology that has been defined in this thesis, the optical powered firing set model can be used for future analysis and design. An optically powered firing set with a closed loop feedback control system can now enable a new set of designs that promise to revolutionize the art.

In retrospect, through the process of developing the model, verifying the model with experiential data, and simulating a control solution, three important lessons were learned.

1) Develop accurate models.

   An accurate model is important in control system design. However, parameters or characteristics of the components can be overlooked when developing a system. A designer needs to include the characteristics that drastically change the output

response. In the optical powered firing set, for example, the MPA electrical response is tied closely with the temperature of the device. If the model did not include this dependency as was first modeled, the finalized control system response would be extremely different. Obtaining a 100% accurate model is ideal, but in the real world it is a compromise between time and accuracy.

2) Analyze and understand experimental data for model validation.

Gathering and understanding data always seems to be difficult when testing new components. There are many testing limitations that depend on test equipment, time frame, money, and lack of knowledge of the device. An experimental setup usually cannot depict real world conditions and therefore the data gathered must be analyzed carefully. In the optical powered firing set, the MPA was connected to the CDU board via a special socket. This connection did not provide the correct heat flow characteristics that the device would normally experience, therefore the experimental data showed excessive heating of the LCC package. Understanding the experimental data can have drastic effects on the comparison of simulated data.

3) Create flexible models.

The flexibility of the thermal model allowed for easy adjustment of the model parameters so that the additional temperature of the MPA package could be determined. The characteristic equation was adjusted and changed in the model to accept the two additional thermal parameters. This allowed for a quick demonstration

of the accuracy of the model since the simulation did not match the experimental data.

Recommendations for further development include model enhancements, experimental setup changes, linearization of the non-linear ODE's, and a study of illumination wavelength changes. Some model enhancements include adding temperature effects to the diode laser electrical/optical model. This can be accomplished by including the temperature to the diode laser rate equations. Additional refinement of the MPA electrical/optical model could include temperature and illumination variations of all the parameters that make up the characteristic equation. More specifically, the illumination current changes slightly with increasing illumination and temperature. Also, parallel resistance will vary with temperature. Adding these variations would create a more complete MPA model. Developing software to produce device specific parameters of the models with experimental data would also aid in creating a more flexible and user friendly model. Some experimental setup changes that would provide more accurate data include adding additional thermocouples for measuring temperatures and changing the mechanical connection of the MPA device. Optimization of illumination wavelength should be carefully studied since a 10% - 20% increase in reflection to the MPA may be possible which lowers the thermal injected power to the device, thus lowering temperature.

Overall, by practically applying control system design principles and simulating a control system, the work of this thesis has provided essential experience in real world control problem design.

REFERENCES

1. AMD, "CPU Thermal Management," Advanced Micro Devices, Publication # 18448, Rev. D, 1995.

2. P. S. Andre, P. Antunes, A. L. J. Teixeira, and J. L.Pinto, "Simplified heat exchange model for semiconductor laser diodes thermal parameters extraction." Laser Physics Letters, vol 2, no. 11, 2005.

3. R. Puchert, A. Barwolff, M. Vob, U. Menzel, J. W. Tomm, and J. Luft, "Transient Thermal Behavior of High Power Diode Laser Arrays," IEEE Transactions on components, packaging, and manufacturing technology, Part A, vol. 23, no. 1, 2000.

4. F. P. Incropera, D.P. DeWitt, T. L. Bergman, and A.S. Lavine, *Fundamentals of Heat and Mass Transfer*, 6th edition, John Wiley & Sons, New York, NY, 2007

5. D. L. Blackburn, "Temperature Measurements of Semiconductor Devices – A review"20th SEMI-THERM Symposium, 2004.

6. D. M. Burns and V. M. Bright, "Optical power induced damage to microelectromechnical mirrors,' Sensors and Actuators A: Physical, vol 70, 1998.

7. D. M. Byrne and B. A. Keating, "A Laser Diode Model Based on Temperature Dependent Rate Equations," IEEE Photonics Technology Letters, vol. 1, no. 11, 1989.

8. L. A. Coldren and S.W. Corzine, *Diode Lasers and Photonic Integrated Circuits*, John Wiley & Sons, New York, NY, 1995.

9. J. Shelton, F. Dickey, W. Thomes "Optically powered firing set using miniature photovoltaic arrays," in Optical Technologies for Arming, Safing, Fuzing, and Firing III, edited by William J. Thomes, Jr., Fred M. Dickey, Proceedings of SPIE Vol. 6662 (SPIE, Bellingham, WA, 2006) 6662-5.

10. R. Diehl, *High-Power Diode Lasers Fundamentals, Technology, Application*, Volume 78, Springer, New York, NY, 2000.

11. G. F. Franklin, J. D. Powell, and M. L. Workman, *Digital Control of Dynamic Systems*, 2nd edition, Addison-Wesley, Reading, MA, 1990.

12. J. Hulett and C. Kelly, "Measuring LED Junction Temperature," Photonics Spectra, pg 73-75, July 2008.

13. Jenoptik, "Semiconductors – From Wafer to Chip," Power Point Presentation, 2008-04-23.

14. N. S. Nise, *Control Systems Engineering*, 3rd edition, John Wiley & Sons, New York, NY, 2000

15. K. P. Pipe and R. J. Ram, "Comprehensive Heat Exchange Model for a Semiconductor for a Semiconductor Laser Diode," IEEE Photonics Technology Letters, vol. 15, no. 4, 2003.

16. B. H. Rose, "GaAs Series Connected Photovoltaic Converters for High Voltage Capacitor Charging Applications," Sandia Report: SAND97-2306, Sandia National Laboratories, Albuquerque, NM, 1997.

17. R. A. Serway, *Physics For Scientists & Engineers with Modern Physics*, 4th edition, Saunders College, Philadelphia, PA, 1996.

18. T. Suhara, *Semiconductor Laser Fundamentals*, Marcel Dekker, New York, NY, 2004.

19. Y. Li, K. H. Ang, G.C.Y. Chong, "PID Control System Analysis and Design," IEEE Control Systems Magazine, vol. 26, no. 1, 2006.

20. A. Visioli, *Practical PID Control*, Springer, London, 2006

21. J.A. Gow, C.D Manning. “Development of a photovoltaic array model for use in power-electronics simulation studies,” IEE Proceedings, vol. 146, no. 2, 1999.